ACS OMEGA

http://pubs.acs.org/journal/acsodf

Review

Advances in Titanium Carbide ($Ti_3C_2T_x$) MXenes and Their Metal–Organic Framework (MOF)-Based Nanotextures for Solar Energy Applications: A Review

Wei Keen Fan, Areen Sherryna, and Muhammad Tahir*

Cite This: *ACS Omega* 2022, 7, 38158–38192

Read Online

ACCESS | Metrics & More | Article Recommendations

ABSTRACT: Introducing new materials with low cost and superior solar harvesting efficiency requires urgent attention to solve energy and environmental challenges. Titanium carbide ($Ti_3C_2T_x$) MXene, a 2D layered material, is a promising solution to solve the issues of existing materials due to their promising conductivity with low cost to function as a cocatalyst/support. On the other hand, metal–organic frameworks (MOFs) are emerging materials due to their high surface area and semiconducting characteristics. Therefore, coupling them would be promising to form composites with higher solar harvesting efficiency. Thus, the main objective of this work to disclose recent development in $Ti_3C_2T_x$-based MOF nanocomposites for energy conversion applications to produce renewable fuels. MOFs can generate photoinduced electron/hole pairs, followed by transfer of electrons to MXenes through Schottky junctions for photoredox reactions. Currently, the principles, fundamentals, and mechanism of photocatalytic systems with construction of Schottky junctions are critically discussed. Then the basics of MOFs are discussed thoroughly in terms of their physical properties, morphologies, optical properties, and derivatives. The synthesis of $Ti_3C_2T_x$ MXenes and their composites with the formation of surface functionals is systematically illustrated. Next, critical discussions are conducted on design considerations and strategies to engineer the morphology of $Ti_3C_2T_x$ MXenes and MOFs. The interfacial/heterojunction modification strategies of $Ti_3C_2T_x$ MXenes and MOFs are then deeply discussed to understand the roles of both materials. Following that, the applications of MXene-mediated MOF nanotextures in view of CO_2 reduction and water splitting for solar fuel production are critically analyzed. Finally, the challenges and a perspective toward the future research of MXene-based MOF composites are disclosed.

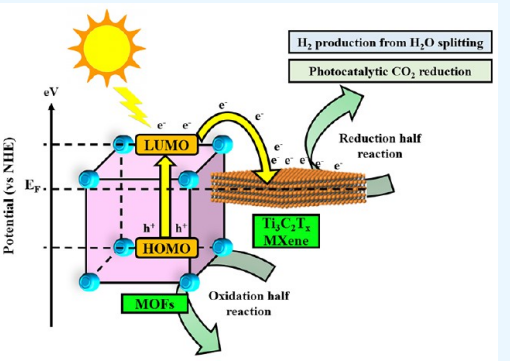

1. INTRODUCTION

In the modern age, the major issues faced by mankind is the energy crisis and the rapid depletion of fossil fuels. There is a growing urgency to look for alternative fuels and energy sources to partially fulfill the increasing energy demand. Thus, researchers are devoted to discovering sustainable technologies to overcome the energy crisis.[1,2] For instance, renewable energy production such as steam reforming for H_2 energy production[3] and CO_2 hydrogenation reactions[4] to produce fuels such as hydrocarbons or alcohols are mature technologies that have already reached commercial scale operations. However, these approaches are highly energy-intensive as they require high thermal energy input to initiate the reactions. In turn, photocatalytic H_2 production and CO_2 reduction are emerging as promising advances in generating fuels and energy as they rely solely on naturally available solar energy to drive the reactions.[5−7] Not only that, abundantly available CO_2 and H_2O function as low-cost feed stocks for the photocatalytic reactions. Hence, solar-driven CO_2 reduction and water splitting is an up-and-coming approach to generate renewable fuels due to their inexpensiveness and environmentally benign process.[8−10]

In 2011, MXenes were a class of novel materials first discovered by Gogotsi and co-workers.[11] MXenes are promising photocatalytic materials that are derived from MAX via acid etching to remove the Al layers, leaving behind the M (transition metals) and X (C or N) with a general formula of $M_{n+1}X_n$. MXenes exist in either 0D quantum dots (QDs) or as 2D layered structures, which provides a higher specific surface area, reaction sites, ameliorated light harvesting, and electron acceptance capability as well as the prolonged lifetime of charge carriers.[12,13] Additionally, they have good mechanical and chemical stability as well as easily tunable

Received: August 7, 2022
Accepted: October 6, 2022
Published: October 20, 2022

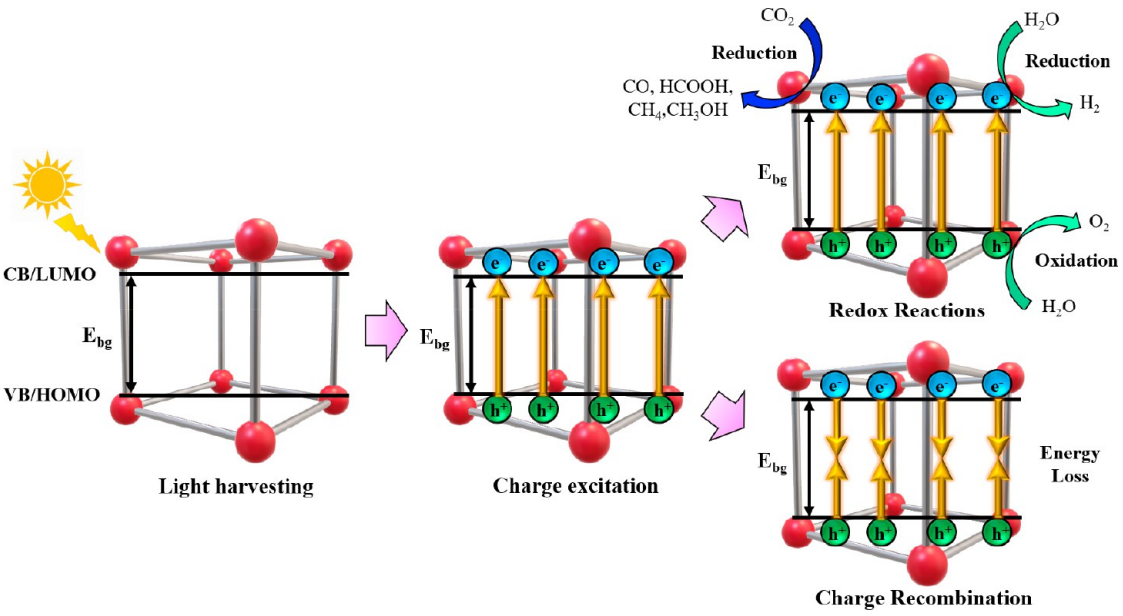

Figure 1. Schematic illustrating the overall mechanism for photocatalysis of CO_2 reduction and hydrogen production. Adapted with permission from ref 30. Copyright 2022 Elsevier.

valence electrons via preparation using lighter and heavier transition metals.[14] Due to its metallic properties, MXenes are able to act as a cocatalyst for photocatalytic reactions due to their ability to form a Schottky junction, which acts as an electron trap and mediator.[15] By pairing the MXenes with other photoresponsive materials, a built-in internal electric field is induced, thus electron separation and migration are promoted.[16] Also, several studies reported that some MXenes exhibit semiconducting properties with band gaps from 0.05 to 2.87 eV.[17] Thus, MXenes are promising cocatalysts and can be coupled with semiconductors to boost reactivity.

Among the semiconductors, metal−organic frameworks (MOF) are a promising class of materials that have different morphologies and dimensionalities, ranging from 1D rods to 2D layered sheets and 3D network structures.[18] Yaghi's group pioneered the discovery and successful preparation of MOFs in 1999.[19] The existence of highest occupied molecular orbitals (HOMOs) and lowest unoccupied molecular orbitals (LUMOs) separated by an energy band gap (E_{bg}) makes them suitable candidates as photocatalysts due to their ability to harvest solar energy. Not only that, MOFs also have various beneficial properties such as extremely large specific surface area,[20] high porosity,[21] and a tunable structure. The light harvesting capability of MOFs is augmented due to the large surface area, which increases the exposed surface area of the material to light irradiation. Moreover, the desirable porosity makes it an excellent CO_2 adsorbent that eases the subsequent conversion to solar fuels.[22]

Researchers all around the world are devoted to discovering highly active catalysts for solar-energy-driven renewable energy evolution. Pristine $Ti_3C_2T_x$ MXene alone cannot be utilized as a photocatalyst for either solar-driven H_2 production or CO_2 reduction due to its inability to generate electron/hole pairs for photoredox reactions. Conversely, they are effective as cocatalysts due to their blackbody, which facilitates light absorption and harvesting.[23] Not only that, $Ti_3C_2T_x$ MXenes are able to function as electron reservoirs, in which they can efficiently trap photogenerated electrons.[24] Hence, $Ti_3C_2T_x$ MXenes must be coupled with other photoresponsive materials to unleash their full potential as a cocatalyst. In the past, $Ti_3C_2T_x$-based composite photocatalysts have been prepared, in which Ti_3C_2-based semiconductor composites were widely employed. For instance, Li et al. paired Ti_3C_2 QDs with a g-C_3N_4 semiconductor as a photocatalyst for H_2 production, where the MXene effectively trapped the photogenerated electrons from the g-C_3N_4 nanosheets.[25] Similarly, a ternary semiconductor-based $TiO_2/C_3N_4/Ti_3C_2$ composite was utilized for solar-driven CO_2 reduction. An S-scheme heterojunction was first obtained between the TiO_2/C_3N_4 interface due to formation of an internal electric field, band bending, and Coulomb force, where the electrons in TiO_2 combined with the holes in the valence band (VB) of C_3N_4. Subsequently, the electrons produced in C_3N_4 were trapped by $Ti_3C_2T_x$ MXenes.[26] However, the composite pairing with semiconductors presents a glaring disadvantage, which is the fast recombination of charge carriers due to large energy band gaps. In efforts to overcome this shortcoming, $Ti_3C_2T_x$-based MOF nanotextures are gaining attention as photocatalysts for solar fuel production. To date, 90,000 different MOF structures have been discovered, each with their own unique properties and energy band gap. This means that the potential combinations of $Ti_3C_2T_x$/MOF composites are limitless, in turn presenting a huge potential and research interest in maximizing solar fuel generation.

Herein, we reviewed the various applications of $Ti_3C_2T_x$ MXene-based MOF composites on the photocatalytic production of solar fuels. First, an in-depth discussion on the principles and mechanism of photocatalysis is conducted. Then the fundamentals of photocatalytic CO_2 reduction and water splitting are discussed by understanding the various possible oxidation and reduction reactions involved. The various preparation method of $Ti_3C_2T_x$ MXenes are thoroughly reviewed, which includes HF etching, acid-containing fluoride ions, water-free etching, alkali etching, electrochemical etching, and molten salt substitution. Then a comprehensive discussion on the preparation of $Ti_3C_2T_x$ MXene-based MOF composites is conducted. Numerous applications of $Ti_3C_2T_x$ MXene-based MOF composites are reviewed and discussed for the

https://doi.org/10.1021/acsomega.2c05030
ACS Omega 2022, 7, 38158−38192

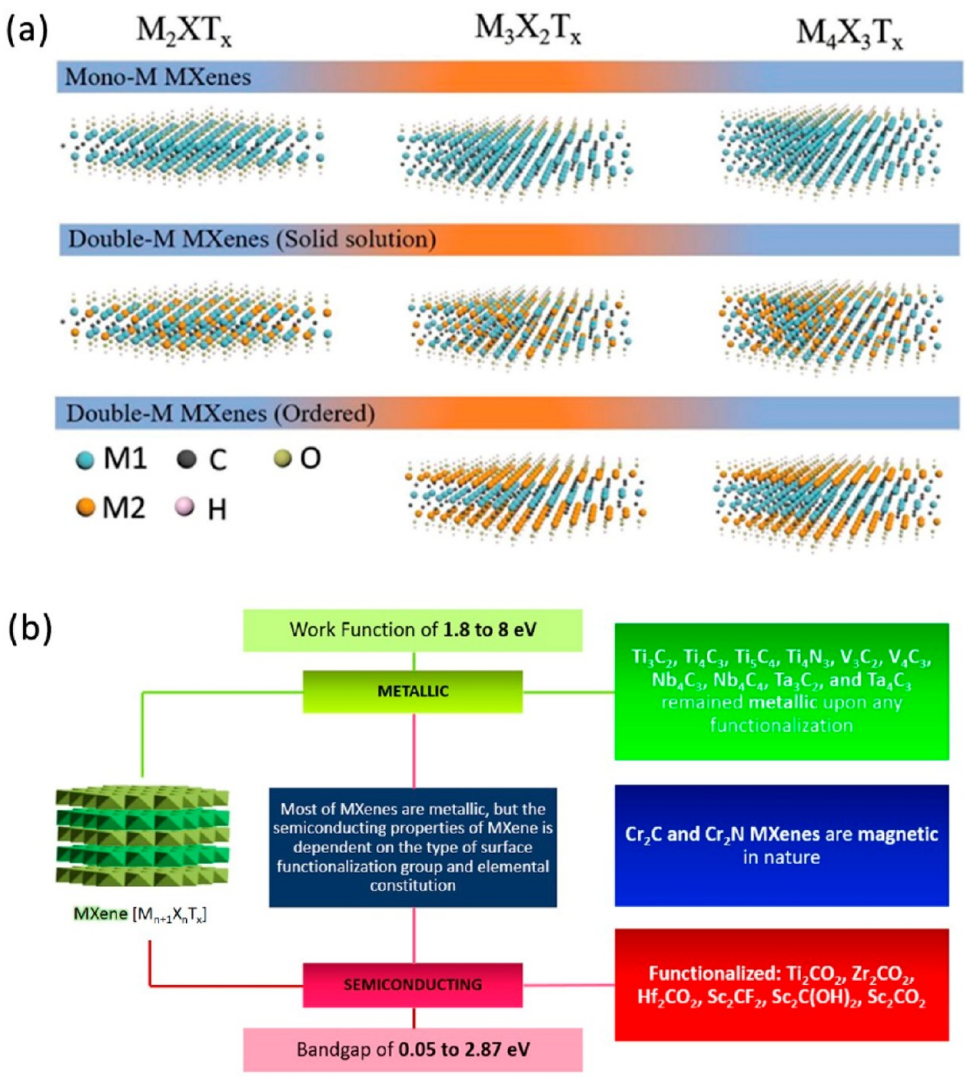

Figure 2. (a) Different compositional formula of $Ti_3C_2T_x$ MXene with different atomic layers. Reprinted with permission from ref 40. Copyright 2019 Wiley. (b) Different electronic properties of $Ti_3C_2T_x$ MXene. Reprinted from ref 15. Copyright 2021 American Chemical Society.

sustainable production of solar fuels. Finally, the challenges and comparative analysis of $Ti_3C_2T_x$ MXenes are conducted over various materials. Despite limited studies conducted on the $Ti_3C_2T_x$–MOF composites, they are definitely promising photocatalysts for solar fuel production and should be further explored for various applications.

2. FUNDAMENTALS AND PRINCIPLES

2.1. Principles of Photocatalysis. Photocatalysis is an up-and-coming sustainable approach to induce catalysis as it only utilizes naturally available solar energy as energy input to the reaction system. The photocatalysis pathway consists of four crucial steps, as shown in Figure 1. They are light harvesting, charge excitation, occurrence of redox reaction, and the recombination of charge carriers.[27] Initially, the photo-responsive materials are exposed to light irradiation. There are three main radiations from solar energy, each with varying energy levels, with UV radiations having the highest energy, followed by visible light and infrared radiation. Hence, UV radiations show the highest efficiency in generating electron/hole pairs, whereas the infrared radiations only function to provide a heating effect.[28] The light harvesting step can be further enhanced through multiple reflections and a light scattering effect over materials with rough surfaces as a result of meso- and macropores.[29] Upon successful light harvesting, electrons are excited with sufficient energy to transverse the E_{bg} from the VB or HOMO to the conduction band (CB) or LUMO. On the other hand, the photogenerated holes are then left behind in the VB or HOMO.[30] Following the charge excitation step where electron/hole pairs are formed, there are two possibilities that may occur, which is the favorable utilization of electron/hole pairs for redox reactions or the unfavorable recombination of charge carriers leading to loss of energy. The CO_2 reduction reaction occurs on the CB/LUMO of the material, where the electrons are utilized to convert CO_2 into solar fuels such as CO, HCOOH, CH_4, and CH_3OH, whereas the oxidation half-reaction occurs over the VB/HOMO.[31] Similarly, photocatalytic water splitting reactions consist of two half-reactions, which is the reduction and oxidation of water to produce H_2 and O_2 gas, respectively. There are two types of recombinations that occur, namely, volume recombination where the charge carriers undergo recombination at the bulk of the material or surface recombination where the electron/hole pairs recombine on the surface of the material.[32] The recombination of charge

https://doi.org/10.1021/acsomega.2c05030
ACS Omega 2022, 7, 38158−38192

carriers will then lead to the loss of energy in the form of heat. Hence, the recombination should be prevented at all costs via different approaches, such as the formation of heterojunctions and surface sensitization, which can trap electrons and provide spatial separation, which prolongs the lifetime of the photogenerated electron/hole pairs.

2.2. Fundamentals of Photocatalytic Solar Fuel Production. Recently, photocatalytic solar fuel production has been gaining traction due to its simplicity, cost-effectiveness, and environmentally benign process. There are two widely known and sustainable technologies to produce renewable fuels, namely, photocatalytic CO_2 reduction and water splitting to produce H_2. For photocatalytic reactions to occur, there are two main processes occurring, which is the reduction and oxidation half-reactions. For a particular reduction half-reaction to occur, the CB/LUMO of the material must be more negative compared to the redox potential. Conversely, the VB/HOMO of the photoresponsive material should be greater than that of the redox potential of the oxidation half-reaction for it to be feasible.[33] Equation 1 shows one electron reduction of CO_2 to the CO_2^- radical.[34] However, the reaction is deemed unfeasible due to it possessing a high redox potential. Not only that, it is impossible for a photocatalyst to supply enough potential to transfer a single electron to a CO_2 molecule.[35] Hence, reactions with low redox potentials are proton-assisted multielectron reactions, making them achievable over a wide range of materials.[36] As shown in eqs 2−5, CO_2 can be reduced to a wide variety of products, namely, CO, HCOOH, CH_3OH, and CH_4, respectively. The product selectivity depends on the amount of the number of electrons supplied to the CO_2 molecule. For instance, photocatalytic CO_2 reduction usually favors the production of CO and HCOOH due to it only requiring two electrons to initiate the reaction. On the other hand, the formation of CH_3OH and CH_4 requires more electrons and protons (6 and 8, respectively) to facilitate the reaction. For the photocatalytic water splitting to produce H_2, it involves two crucial steps. The first step is shown in eq 6, where two holes are utilized to oxidize the water molecules to produce oxygen and two protons. Subsequently, the protons and electrons proceed via eq 7 to produce H_2.[37,38]

$$CO_2 + e^- \rightarrow CO_2^- \quad (-1.90\ \text{eV}) \tag{1}$$

$$CO_2(g) + 2H^+ + 2e^- \rightarrow CO(g) + H_2O \quad (-0.52\ \text{eV}) \tag{2}$$

$$CO_2(g) + 2H^+ + 2e^- \rightarrow HCOOH(aq) \quad (-0.61\ \text{eV}) \tag{3}$$

$$CO_2(g) + 6H^+ + 6e^- \rightarrow CH_3OH(aq) + H_2O \ (-0.38\ \text{eV}) \tag{4}$$

$$CO_2(g) + 8H^+ + 8e^- \rightarrow CH_4(g) + 2H_2O \quad (-0.24\ \text{eV}) \tag{5}$$

$$H_2O(l) + 2h^+ \rightarrow 0.5O_2 + 2H^+ \quad (0.81\ \text{eV}) \tag{6}$$

$$2H^+ + 2e^- \rightarrow H_2 \quad (-0.42\ \text{eV}) \tag{7}$$

2.3. Overview, Fundamentals, and Properties of MXenes. MXenes are a type of two-dimensional (2D) nanomaterial obtained through selective etching of MAX phases. The general formula of MXene is $M_{n+1}X_nT_X$, in which the M stands for the early transitional metal elements such as Sc, Ti, Hf, Mo, Ta, Nb, Cr, and so on. The acronym A represents the Al or Si layer, while X constitutes either C or N elements. The chemical exfoliation of the A element of MAX results in the termination of the M surface with abundant of functional groups, T_x such as −F, −OH, and −O. The first MXene material ever synthesized was in 2011 which is titanium carbide MXene ($Ti_3C_2T_x$) by Naguib and co-workers via chemical etching with hydrofluoric acid (HF).[11] It was known that the mechanical method was not able to exfoliate the $M_{n+1}X_n$ layers due to the strong metallic M−A bonds in MAX phase. Therefore, the selective etching is considered a preferable method to break the M−A bonds owing to the different chemical activities of M−A and M−X bonds in MAX.[39] The *n* in the formula of MXene represents the atomic layer in a unit cell. A different compositional formula of MXene with different atomic layers can be obtained such as M_2XT_x, $M_3X_2T_x$, and $M_4X_3T_x$, as presented in Figure 2a. The typical structure of MXenes could be categorized as mono-M MXenes and double-M MXenes based on their compositional configurations.[40] In mono-M MXenes, the compositional arrangement is distinguished by the position of an early transitional metal covering (M) the C or N (X) elements. On the other hand, double-M MXenes are subcategorized into solid solution and ordered type. In solid solution of double-M MXenes, two early transitional metals, M1 and M2, are randomly distributed into the MXenes, while for ordered type, one of the M metals is positioned between the second transition M metal.

Typically, $Ti_3C_2T_x$ MXenes are metallic materials that exhibit excellent electrical conductivity of 6000−8000 S cm^{-1}, comparable to noble metal and graphene materials. This makes available as significant cocatalysts to promote the photocatalysis process. Additionally, the electrical properties of $Ti_3C_2T_x$ MXenes can also be tailored through different M metal compositions, morphological modulation, and tuning the termination properties.[15] For instance, delaminating the multilayer $Ti_3C_2T_x$ MXene layers into their individual layer is reported to exhibit higher electrical conductivity up to 15000 S cm^{-1}.[41] The findings also suggested that the thickness of the $Ti_3C_2T_x$ MXenes flakes is significantly linked to the electrical conductivity by which the monolayer $Ti_3C_2T_x$ MXenes exhibited higher electrical conductivity compared to that of the bilayers and trilayers.[42]

In the perspective of electronic conductivity, $Ti_3C_2T_x$ MXenes are metallic in nature and thus unable to generate electrons and holes. Therefore, they are typically used as a cocatalyst to assist photocatalytic activity due to the Schottky barrier effects. A higher work function is one of the distinct properties of $Ti_3C_2T_x$ MXenes that give them a significant role as a photocatalytic enhancer and favorable as a noble metal substitution. A work function as high as 6.25 eV could be achieved, which is as high as other renowned metal cocatalysts such as Ag (∼4.5 eV), Au (∼5.38 eV), and Pt (∼6.10 eV).[43−45] In the photocatalysis process, incorporating metal with a higher work function could improve the carrier dynamics and induce a stronger redox reaction.

Nevertheless, the work function of $Ti_3C_2T_x$ MXenes can be varied depending on the tailored surface termination groups. This is because their work function is mainly controlled by the induced dipole moments arising from the transfer of charges between the termination group of $Ti_3C_2T_x$ MXenes and the changes in the total surface dipole moments due to surface relaxation. In this context, the findings suggested that $Ti_3C_2T_x$

https://doi.org/10.1021/acsomega.2c05030
ACS Omega 2022, 7, 38158−38192

Table 1. Various Classification of MOFs and Their Properties

MOF	metal node	linkers	dimension	surface area (m^2/g)	HOMO (eV)	LUMO (eV)	E_{bg} (eV)	refs
ZIF-67	Co	2-methylimidazole	3D	1139.00	1.18	−0.74	1.92	95,96
Co-MOF-74	Co	2,5-dihydroxyterephthalic acid (H_4DOBDC)	1D	1025.00				97
MOF-71	Co	terephthalate acid (H_2BDC)	2D	56.50				98
MOF-5	Zn	terephthalic acid (H_2BDC)	3D	1101.00			3.82	87
ZIF-7	Zn	benzimidazole	3D	167.00				99
ZIF-7-NH_2	Zn	2-aminobenzimidazole	3D	417.00				99
ZIF-8	Zn	dimethylimidazole	3D	1123.00	2.10	−1.20	3.30	20,100
HKUST-1	Cu	1,3,5-tricarboxylic acid (H3BTC)	3D	1143.06	2.01	−0.58	2.59	101
Cu-MOF	Cu	1,3,5-trimesic acid	3D	19.00	1.64	−0.80	2.44	102
$Cu_3(L)_2$(4,4′-bipy)	Cu	4,4′-bipyridine (4,4′-bipy)	3D	83.86			2.82	103
UiO-66	Zr	terephthalic acid (H_2BDC)	3D	835.00	3.19	−0.72	3.91	86
UiO-66-NH_2	Zr	2-aminoterephthalic acid (H_2BDC-NH_2)	3D	917.00	1.82	−1.01	2.83	86
UiO-67	Zr	biphenyl-4,4′-dicarboxylate (H_2BPDC)	3D	2500.00	2.43	−1.20	3.63	63
MIL-101	Fe	1,4-benzenedicarboxylic acid (H_2BDC)	3D	1413.00			2.59	54,104
NH_2-MIL-101	Fe	2-aminoterephthalic acid (NH_2-BDC)	3D	1237.40	0.97	−1.75	2.72	105
PCN-250	Fe	3,3′5,5′-azobenzene tetracarboxylic acid (H_4abtc)	3D	1240.00	1.19	−0.89	2.08	88
MOF-901	Ti	4-aminobenzoid acid	2D	550.0			2.65	106
NH_2-MIL-125	Ti	2-aminoterephthalic acid (H_2BDC-NH_2)	3D	405.40	2.10	−0.40	2.50	53
MIL-125	Ti	terephthalic acid	3D	1510.00	3.43	0.16	3.27	66,107
NTU-9	Ti	2,5-dihydroxyterephthalic acid (H_4DOBDC)	2D	1205.00	0.32	−1.58	1.90	108,109
PCN-415	Ti	terephthalic acid	3D	1050.00			3.31	110

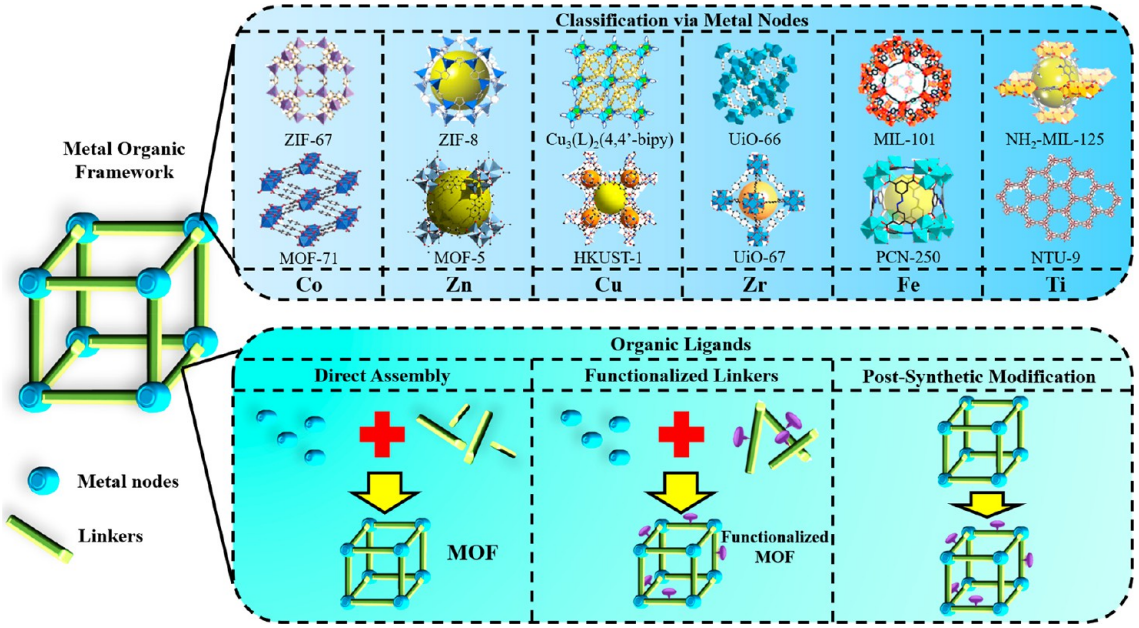

Figure 3. Illustration of the chemistry of MOFs in terms of metal node classification and organic linkers.

MXenes with an −OH terminal group were observed to exhibit a work function of 1.6−2.8 eV. On the other hand, −O-terminated $Ti_3C_2T_x$ MXenes displayed a higher work function between 5.75 and 6.25 eV.[46] Furthermore, the termination of −OH groups caused the decrease of the work function compared to that with −O and −F termination, where the work function was shown to either increase or decrease depending on the M metal constituted.[47] However, theoretical analysis through first-principles calculations indicated that some MXenes can exhibit semiconducting properties depending on the type of M metal constitution, surface terminating group, and the number of the MXene layers, such as that presented in Figure 2b. It was suggested that $Ti_3C_2T_x$ manifests metallic properties regardless of any surface functionalization. The same findings were observed on the MXenes with thicker sheets and a large number of transition metals. Therefore, the probability of MXenes to undergo the shifting of the electronic properties into semiconducting is high in thinner MXenes, such as those with $n = 2$. Therefore, not all MXenes are metallic in nature, and some can exhibit semiconducting properties by configuring their termination groups, morphological structure, and types of metal

https://doi.org/10.1021/acsomega.2c05030
ACS Omega 2022, 7, 38158−38192

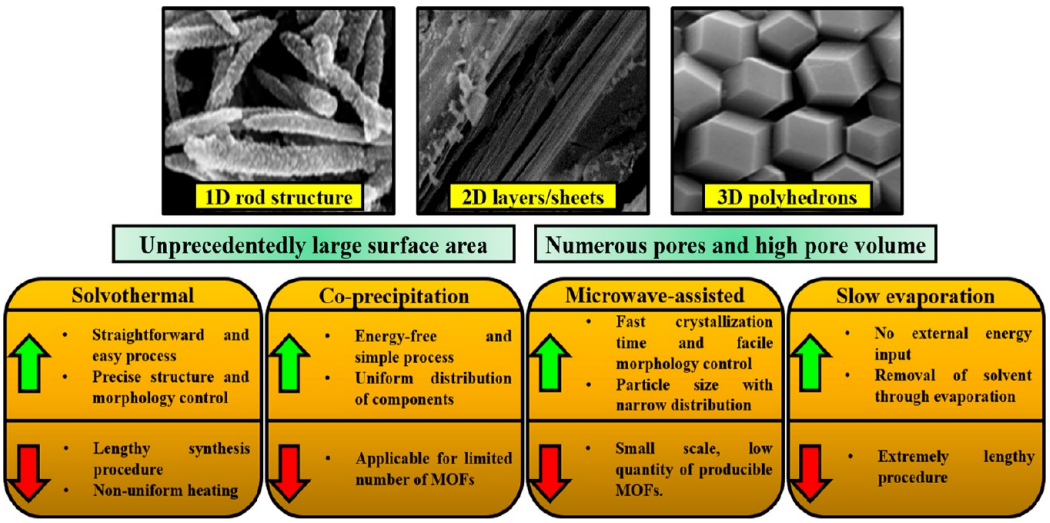

Figure 4. Illustration of the physical properties and preparation method of MOFs.

composition. The feasibility of tailoring the electronic and electrical properties is one of the distinct properties of MXenes that favors them in a wide range of scientific applications.

2.4. Fundamental and Principles of Metal−Organic Frameworks. MOFs are a class of crystalline materials with metal nodes held together by organic linkers, forming highly sophisticated porous structures.[48] Initially, MOFs were mainly used in the field of gas storage, but slowly their role expanded into various applications such as gas/liquid adsorption and separation,[49] electrode development for supercapacitors,[50,51] and batteries[52] as well as heterogeneous catalysis.[53−55] MOFs are able to be used in broad applications mainly due to their unique properties and characteristics, such as an unprecedented specific surface area, high porosity, and easily tunable chemistry.[56] MOFs exists in a variety of morphology and dimensionality, from 1D rod structures to 2D layers and finally 3D network structures. Additionally, MOFs can also act as sacrificial templates to produce a different material such as porous metal oxides and layered double hydroxides. Similar to semiconductor materials, MOFs are also bestowed with impressive optical properties, making them able to induce electron/hole pairs upon irradiation with a light source. Table 1 summarizes the various MOFs discovered over the years with their respective metal nodes, linkers, and physical and optical properties.

2.4.1. Chemistry of Metal−Organic Frameworks. MOFs are composed of two main building blocks, including metal nodes and the bridging organic linkers. More than 60,000 types of MOFs can be discovered due to the endless possibilities of combination between different metal precursors with organic linkers. Figure 3 summarizes the general chemistry of MOFs. One of the more straightforward ways to classify and identify MOFs is through their metal nodes. For instance, Co, Zn, Cu, Zr, Fe, and Ti are some of the typical metal nodes present in monometallic MOFs. Co-based MOFs are highly utilized due to their relatively low cost and simple preparation methods.[57] In the field of catalysis, Co metals were reported to show impressive activity in renewable fuel production.[58] Zn-based MOFs such as ZIF-7 and ZIF-8 are referred to as noble-metal-free systems due to Zn being a cheaper and abundant alternative to noble metals, as well as showing promising performance under light irradiation.[59] Cu is another transition metal that has shown beneficial properties in promoting photocatalytic performance. A study reported that the doping of Cu can enhance the reception of visible light by 35% as well as reduce the energy band gap significantly.[60] Zr-based MOFs possess great structural stability with a high specific surface area due to Zr-carboxylate coordination bonds.[61] UiO-66[62] and UiO-67[63] are two examples of well-known Zr-based MOFs that have been utilized in various photocatalytic reactions. In the case of Fe-MOFs, oxo-iron clusters are present which makes them potential candidates as photocatalysts as they exhibit good visible light harvesting ability.[64] Finally, Ti-based MOFs consist of tetravalent Ti^{4+} cations which can form tough frameworks due to strong metal−ligand bonding. The presence of Ti-oxo clusters contributes to the photocatalytic activity by enhancing the redox reactions.[65]

The second building blocks that are used to prepare MOFs are organic linkers. The linkers are the bridges between metal nodes that originate from organic acids such as terephthalic acid or trimesic acid. Usually, functionality can be introduced to MOFs via the use of functionalized linkers or via postsynthetic modifications. Most notably, the Ti-based MIL-125 and NH_2-MIL-125 have a relatively similar synthesis method with similar metal precursors and solvents used, in which only the organic acids deployed are different. In the case of preparing MIL-125, terephthalic acid is utilized, whereas amine-functionalized terephthalic acid (2-amino terephthalic acid) is used to prepare NH_2-MIL-125.[66] Hence, NH_2-MIL-125 will have amine functional groups on the linkers of the MOF. Another way to induce functionalization is through the postsynthetic modification (PSM) of the linkers.[67] Su's group reported an improvement in water resistance of Mg-MOF-74 via PSM by functionalizing it with tetraethylenepentamine (TEPA). Hence, amine functional groups were introduced to Mg-MOF-74, which inhibits the damaging effects of water entering into the framework.[68]

2.4.2. Physical Property of Metal−Organic Frameworks. MOFs are materials that have been widely researched in various fields and applications due to their desirable and unique physical properties. Here, the physical properties of MOFs such as their surface area, porosity, and various synthesis methods are critically discussed, which is then summarized, as shown in Figure 4. First, MOFs tend to boast

https://doi.org/10.1021/acsomega.2c05030
ACS Omega 2022, 7, 38158−38192

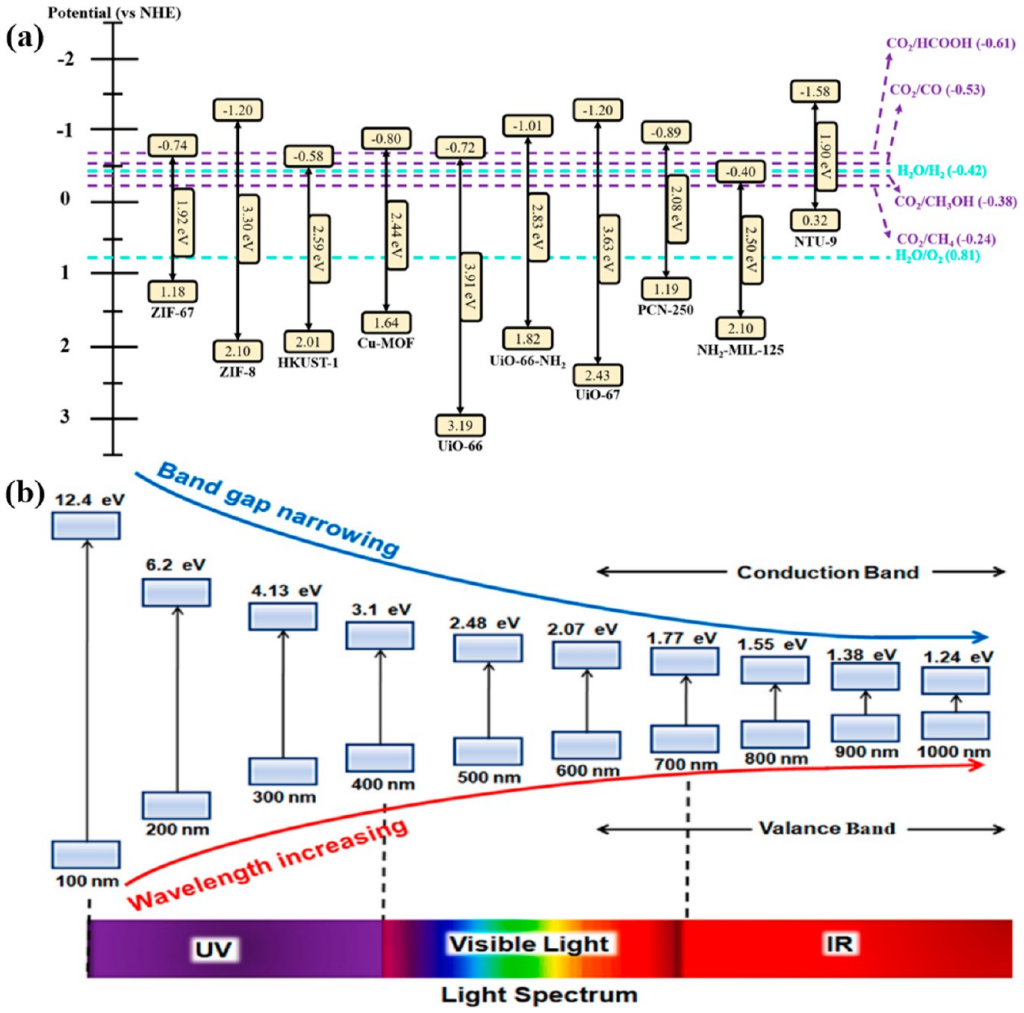

Figure 5. (a) Band structures of various metal−organic frameworks. (b) Relationship between E_{bg} of photoresponsive materials (eV), solar spectrum, and light wavelength. Reprinted with permission from ref 64. Copyright 2021 Elsevier.

incredibly high specific surface area, usually in the range of hundreds if not thousands. Titanium-based MIL-125 has a surface area of 1510 m^2/g,[66] whereas its metal oxide counterpart TiO_2 only has a mere surface area of 35 m^2/g.[69] Moreover, MOFs are also bestowed with numerous pores with large openings. These large pores are beneficial for enabling them to function as effective materials for gas adsorption and capture. A chromium-based MIL-101 features a high pore volume of 1.63 cm^3/g, in turn promoting a huge N_2 uptake capacity of 1003 cm^3/g.[70] Interestingly, the porosity of MOFs not only is limited to gas adsorption but also enables them to capture large heavy metal molecules, as well. Nimbalkar et al. noticed that UiO-66 with a free carboxylic group is riddled with micropores of 0.4−0.7 nm, in turn providing a high lead and methylene blue adsorption capacity of 100 and 169 mg/g, respectively.[71] Hence, a large surface area and pore volume is a highly sought-after property as it opens doors to various applications such as catalysis and adsorption.

Even though most of the MOFs exist as three-dimensional (3D) polyhedrons, there are also some MOFs exhibiting 1D rods and 2D sheet structures. Recently, a novel 1D chiral imine Zr-MOF (DUT-136) was synthesized via the use of Schiff base of (*R*,*R*)-1,2-diphenylethylenediamine and 4-formylbenzoic acid linkers.[72] Similarly, a number of 2D MOFs have been discovered by researchers, such as NUS-1[73] and MIL-169.[74] In the past, various preparation methods for MOFs have been discovered. The most common approach to prepare MOFs is through the solvothermal method. Here, the metal precursors and linkers were first dissolved in solvent, such as methanol and *N*,*N*-dimethylformamide (DMF). Then the mixture was placed in a Teflon-lined stainless-steel autoclave where heat was introduced to the system to initiate the chemical reaction. Finally, the obtained slurry was washed and dried to obtain the MOF crystals.[75] The solvothermal synthesis step usually utilizes a reaction temperature of not more than 200 °C, with a reaction time ranging from 12 to 72 h. A titanium-based NH_2-MIL-125 was prepared via a conventional solvothermal method with reaction conditions of 150 °C and 72 h.[76] Correspondingly, an Fe-MOF was prepared by first dissolving $FeCl_3 \cdot 6H_2O$ and H_2BDC precursors in DMF solvent, followed by reaction for 24 h at 110 °C.[77] Despite the easy process of the solvothermal synthesis method, it is limited by various factors such as a long synthesis time and inhomogeneous heating of reactants.[78]

MOFs can also be prepared via a straightforward co-precipitation method where the reactants are mixed until precipitates are formed without involving external energy sources.[79] Co-precipitation provides a uniform distribution of components. ZIF-67 is a prime example of a MOF prepared via the co-precipitation method. The synthesis step is relatively

https://doi.org/10.1021/acsomega.2c05030
ACS Omega 2022, 7, 38158−38192

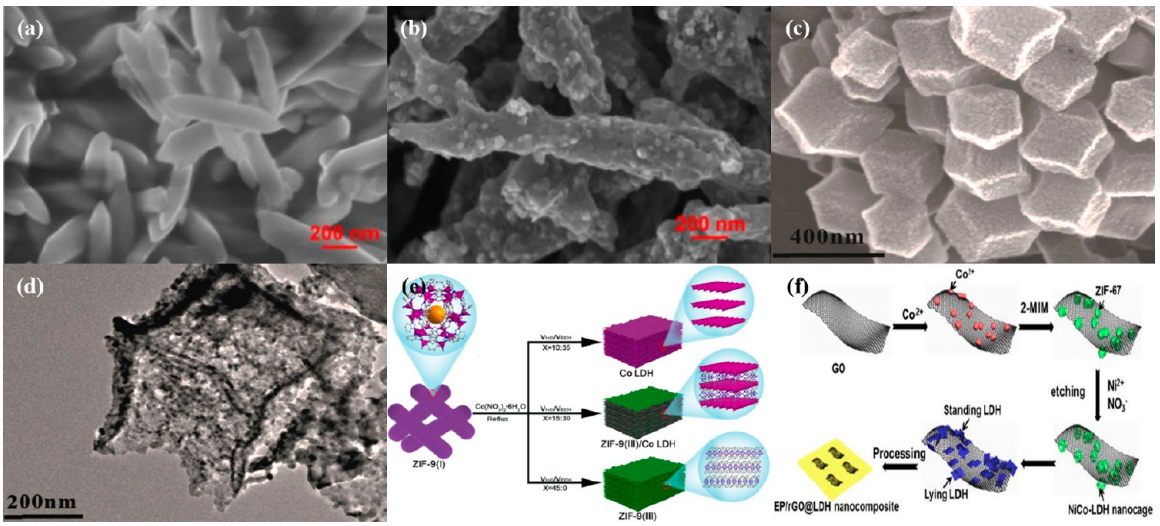

Figure 6. SEM images of (a) Fe-MOF and (b) Fe_2O_3 derived from Fe-MOF. Reprinted from ref 90. Copyright 2020 American Chemical Society. (c) SEM image of ZIF-67 and (d) TEM image of Co_3O_4 hollow polyhedrons. Reprinted with permission from ref 91. Copyright 2018 Elsevier. (e) Scheme of solvent ratio influence on formation of ZIF-9, ZIF-9/Co LDH, and Co LDH. Reprinted with permission from ref 92. Copyright 2021 Elsevier. (f) Preparation scheme of Ni−Co LDH on reduced graphene oxide. Reprinted with permission from ref 93. Copyright 2017 Elsevier.

straightforward: Co precursors were mixed with linkers (2-methylimidazole) in methanol and stirred for 6 h. Then the resulting solution was washed and dried to obtain 3D purple dodecahedral crystals.[80] However, to date, there is only a limited number of MOFs prepared using this method. MOFs are also prepared using an energy-free approach, which is the slow evaporation method. In this method, the solvent is gradually evaporated at room conditions, leaving behind the dried MOF powders. Even though this process does not consume any energy, the synthesis requires a long period of time. Ghosh and co-workers reported a preparation period of 1 week for the synthesis of an Fe-MOF ($[C_{18}H_{22}FeN_2O_6]NO_3$) via the slow evaporation method.[81] In another study, 2 weeks were consumed to prepare purple Co-MOF crystals via the slow evaporation approach.[82] Finally, microwave-assisted synthesis was also employed to achieve rapid synthesis of MOFs. This technique utilizes microwaves to provide a heating effect to initiate the chemical reaction, in turn producing nanosized crystals.[83] The microwave-assisted approach is almost similar to the conventional solvothermal method but provides additional benefits such as fast crystallization time and facile morphology control and produces MOFs with narrow particle size distribution.[64] Most notably, Reza et al. discovered that using a microwave-assisted method to prepare UiO-67 required a much shorter preparation time (2.5 h) compared to that with the conventional solvothermal method (24 h). This is because the microwave heating couples directly with the solvent molecules, causing a rapid rise in temperature at the reaction media, which induces localized superheating. This provides a much more efficient heat transfer compared to conventional heating, resulting in a much shorter reaction time.[84]

2.4.3. Optical Property of Metal−Organic Frameworks. Solar energy is a renewable source of energy that can be easily accessed. To fully utilize this abundant source of energy, researchers have been devoted to discovering materials that can effectively harvest and adsorb solar energy. Solar energy mainly comprises three main irradiations, namely, infrared, visible light, and ultraviolet (UV) radiations. Here, UV radiation has the highest energy content (shortest wavelength), followed by visible light and infrared radiation. Only high energy UV and visible light can generate electron/hole pairs over photoresponsive materials. However, despite the highest energy content of UV radiation, it only accounts for less than 4% of the solar spectrum, whereas visible light and infrared radiation constitutes 43 and 53% of solar energy, respectively.[85] Hence, to effectively utilize solar energy for photocatalysis, suitable materials must be explored to efficiently harvest visible light radiations.

In this context, MOFs are highly sought-after materials due to their desirable optical properties, which makes them photoresponsive materials. To address the energy crisis, MOFs are employed as photocatalysts to harvest solar energy to generate renewable fuels. First, MOFs have a narrow energy band gap (E_{bg}) which allows electron to migrate over from the VB/HOMO to the CB/LUMO. The migration of charge carriers is only possible when photons with energy equal to or greater than E_{bg} strikes the surface of the MOF.[64] Second, there has been a lot of MOFs discovered over the years, each with their own unique E_{bg}, as shown in Figure 5a. Some MOFs tend to have a wider band gap, such as UiO-66[86] and MOF-5[87] with E_{bg} of 3.91 and 3.82 eV, respectively. However, there are also MOFs with narrow band gaps, such as PCN-250[88] (2.08 eV) and NTU-9[102] (1.90 eV). A narrow E_{bg} means that photons with lower energy are required to induce charge carrier formation. This means that visible light irradiation is sufficient to facilitate the photocatalytic reaction. Inversely, a wide E_{bg} requires more energy to generate electron/hole pairs, implying that UV irradiation will be more effective compared to visible light to drive photocatalysis. The relationship between the E_{bg}, the solar spectrum, and light wavelengths is illustrated in Figure 5b.

2.4.4. Metal−Organic Frameworks as Sacrificial Templates. MOFs in their original form are proper candidates as photocatalysts but can also serve as sacrificial templates to produce other materials. One of the more common MOF derivatives is metal oxides, which are obtainable by simple thermal annealing of MOFs. By calcinating the MOF at elevated temperature, the organic linkers will be removed, leaving behind the metal nodes which are then oxidized,

https://doi.org/10.1021/acsomega.2c05030
ACS Omega 2022, 7, 38158−38192

producing metal oxides which inherit the morphology, porosity, and surface area of the parent MOF.[89] An Fe-MOF was synthesized via a solvothermal method with $FeCl_3{\cdot}6H_2O$ as the precursor and 1,4-benzenedicarboxylic acid linkers. The as-prepared MOF showed a well-defined nanospindle structure with a smooth surface, as illustrated in Figure 6a. Upon annealing the Fe-MOF in a N_2 atmosphere, Fe_2O_3 was obtained while retaining the spindle structure of the parent MOF. From Figure 6b, it was noticed that the surface of the Fe-MOF-derived Fe_2O_3 was rougher with nanoparticles on the surface.[90] Similarly, a Co-based MOF ZIF-67 was successfully converted into Co_3O_4 hollow polyhedrons via calcination treatment at 300 °C for 3 h. From the SEM image in Figure 6c, ZIF-67 particles have well-defined polyhedral shapes with a width of around 200 nm. After thermal treatment, the Co_3O_4 retained a similar polyhedral morphology with a specific surface area of 44.28 m^2/g but had a hollow structure which is clearly observed in the TEM image in Figure 6d.[91] Recently, there have been numerous reports on MOFs as templates to produce layered double hydroxides (LDHs). One study conducted by Chen et al. successfully converted 3D ZIF-9 into 2D Co LDH by varying the water/ethanol solvent volume ratio. According to the scheme in Figure 6e, when a 45:0 water/ethanol ratio was used, pure ZIF-9 with a 3D structure was obtained. However, as the ethanol amount increased from 15:30 to 10:35, ZIF-9 changed to ZIF-9/Co LDH and finally to pure 2D Co LDH.[92] A bimetallic Ni−Co LDH-grown reduced graphene oxide (rGO) was also prepared via the etching of ZIF-67 by H^+ upon the hydrolysis of nickel nitrate. As depicted in Figure 6f, ZIF-67 was first grown on GO. After successfully growing the ZIF-67 particles, the addition of nickel nitrate caused the framework of ZIF-67 to collapse into LDH platelets, resulting in the platelets inheriting a 3D structure of the parent MOF, forming standing and lying LDH on the GO.[93] Another study reported an almost similar procedure to prepare Ni−Co LDH nanosheets, in which Co-MOF nanosheets were gradually decomposed and transformed into LDH via a hydrolyzed etching step.[94] Thus, MOF templating is a useful way to produce other materials such as metal oxides and LDHs as the derivatives tend to retain the beneficial properties of the parent MOF, in turn promoting an enhanced photocatalytic activity.

2.5. Fabrication of a MXene-Based Schottky Junction.

The performance efficiency of single semiconductor materials such as MOFs in photocatalytic solar fuel conversion can be enhanced through engineering modifications such as hybridization with other semiconductor materials, forming heterojunction composites. Other modifications included engineering the morphology of the semiconductor into different dimensions, defect engineering, and creation of vacancies.[27] However, one of the techniques that has been proven effective in creating higher-performance semiconductor materials is by the addition of metallic material. In this regard, the performance efficiency can be enhanced through an improvement in the carriers' dynamics. This indicates that $Ti_3C_2T_x$ MXene possesses a higher metallic electrical conductivity, which provides them with the ability to form a potential barrier at the metal−semiconductor interfaces, known as the Schottky junction.[111] $Ti_3C_2T_x$ MXenes are, in general, unable to generate electrons and holes as they are naturally a metallic material. Therefore, they are mostly employed as a cocatalyst and paired with other semiconductor materials such as MOFs to promote the photoactivity through the synergy of a metal−semiconductor junction. The role of adding $Ti_3C_2T_x$ MXene material is to improve the separation efficiency and promote the transfer of electrons in single semiconductor materials.

Fundamentally, the charge transfer mechanism in $Ti_3C_2T_x$ MXene-based composites was achieved through the difference in the work function between $Ti_3C_2T_x$ MXene and the semiconductor materials.[112] The built-in internal electric field at the metal−semiconductor junction called Schottky barrier was formed through the band alignment when both the semiconductor and $Ti_3C_2T_x$ MXene are in contact with each other. The $Ti_3C_2T_x$ MXenes normally serve as electron acceptors due to their large metal work function. Typically, the electrons will migrate from higher Fermi level to lower Fermi level materials, which is the case for MOF-$Ti_3C_2T_x$ MXene composites, where the electrons will migrate from a higher Fermi level of the MOF to a lower Fermi level for $Ti_3C_2T_x$ MXene.[113] Note that the metal work function value (ϕ) is defined as the energy required to transfer an electron from the Fermi level to the vacuum level, where the vacuum level is the reference level at which the electrons possess an energy level outside of the metal with zero kinetic energy. It is worth mentioning that the larger the difference of the work function between the two hybrid materials, the stronger the Schottky barrier that offers excellent separation of the photocarriers. Therefore, metal with a higher work function value such as noble metals and $Ti_3C_2T_x$ MXene are highly sought after to optimize the solar to fuel conversion.[114] Figure 7 illustrates the electron transfer mechanism in Schottky

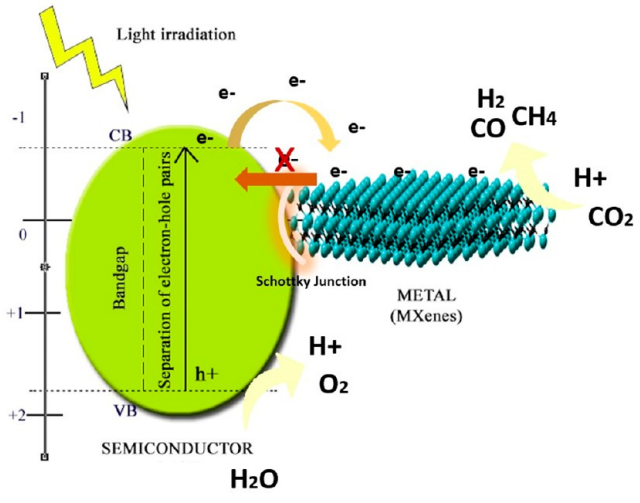

Figure 7. Construction of a Schottky junction and electron transfer mechanism.

junction composite materials. It can be observed that the electrons migrated to the surfaces of the $Ti_3C_2T_x$ MXene are trapped and unable to return back to the semiconductor MOF; therefore, they reserve more electrons to undergo the redox reaction. The creation of a Schottky junction between MOF-$Ti_3C_2T_x$ MXene interfaces prevents the reverse injection of electrons, hastens the electrons transfer to the $Ti_3C_2T_x$ MXene surfaces, and inhibits the recombination of photogenerated charges.[115]

3. DIFFERENT SYNTHESIS TECHNIQUES OF MXene

In general, several different techniques are available to synthesize $Ti_3C_2T_x$ MXene. One of the common and most

https://doi.org/10.1021/acsomega.2c05030
ACS Omega 2022, 7, 38158−38192

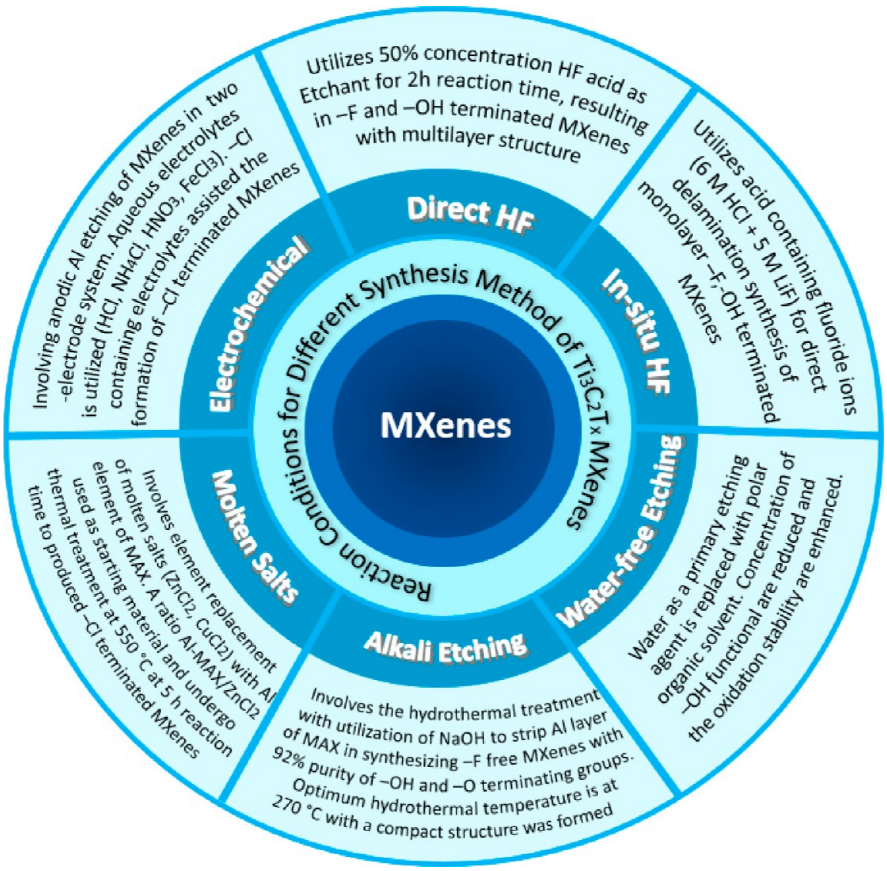

Figure 8. Different synthesis techniques of $Ti_3C_2T_x$ MXenes. Reprinted from ref 117. Copyright 2022 American Chemical Society.

applied techniques for synthesizing $Ti_3C_2T_x$ MXene is HF etching, which utilizes hydrofluoric acid as a primary etchant. The utilization of an etchant is significant, especially in breaking the Ti−Al bond in Ti_3AlC_2 MAX, as the mechanical method cannot exfoliate the Al layer. Since the pioneering study of $Ti_3C_2T_x$ MXene synthesis through HF etching, several other techniques have been developed to combat the utilization of concentrated HF acid, which is non-ecological, especially in wide-scale industrial production. Therefore, safer routes such as acid-containing fluoride etchant, alkali etching, electrochemical etching, halogen etching, water-free etching, and molten salt substitution techniques are among the alternatives to synthesize $Ti_3C_2T_x$ MXene. Among them, the etching process through the utilization of acid-containing fluoride etchant, known as the in situ HF technique, has been broadly employed after the HF etching technique, unlike other newly developed techniques that have not been deeply researched.[116] Figure 8 summarizes the various preparation methods together with their reaction conditions for the synthesis of $Ti_3C_2T_x$ MXenes, and Table 2 provides the reaction parameters for the different $Ti_3C_2T_x$ synthesis methods.

3.1. HF Etching. The HF etching technique is considered to be a pioneering technique and is an extensively used method to synthesize $Ti_3C_2T_x$ MXene. HF was initially chosen as the primary etching agent due to its ability to break the large particle of MAX into smaller grains and its distinct properties to be one of the few selected etchants that can etch the titanium oxide layer typically present as a protective layer of $Ti_3C_2T_x$ MAX.[118] It was suggested that $Ti_3C_2T_x$ MXene could be formed by treating the Ti_3AlC_2 MAX with 50% of HF acid under continuous stirring at room temperature.[11,119] From the morphological perspectives, as presented in Figure 9a, the SEM image reveals an accordion-like structure, suggesting that the 2D structures of $Ti_3C_2T_x$ MXene are formed after 2 h etching with HF. Studies also suggested that different morphologies of $Ti_3C_2T_x$ MXene such as rolls, nanotubes, and multilayers were obtained after sonication. Moreover, the X-ray diffraction (XRD) pattern in Figure 9b shows that other parameters such as etching time could affect the removal of the Al layer of MAX. In this regard, the (104) peak at 2θ = 39, subjected to the MAX phase, was observed to slowly diminish with increasing etching time and was shown to completely disappear after 15 h of etching. This further revealed that increasing the etching time could assist the removal of the Al layer and the formation of $Ti_3C_2T_x$ MXene. Further details on the mechanism of the Ti−Al bond breaking and the formation of $Ti_3C_2T_x$ MXene is presented in eqs 8−10.[120]

$$M_{n+1}AlX_n + 3HF \rightarrow M_{n+1}X_n + AlF_3 + 1.5H_2 \quad (8)$$

$$M_{n+1}X_n + 2H_2O \rightarrow M_{n+1}X_n(OH)_2 + H_2 \quad (9)$$

$$M_{n+1}X_n + 2HF \rightarrow M_{n+1}X_nF_2 + H_2 \quad (10)$$

Generally, $Ti_3C_2T_x$ MXene is formed by removing the Al layer sandwiched between the individual layer of $Ti_3C_2T_x$. As presented in eq 8, Ti_3AlC_2 MAX will react with three molecules of HF to form white small solid particles of AlF_3 with the generation of H_2 gas. The loss of the metallic bonding leads to the formation of layered $Ti_3C_2T_x$ MXene, where the surface of Ti is terminated with functional groups such as −F and −OH such as that shown in eqs 9 and 10. It has been

https://doi.org/10.1021/acsomega.2c05030
ACS Omega 2022, 7, 38158−38192

Table 2. Summary of Preparation Methods and Parameters of Ti_3C_2 MXenes

synthesis method	catalyst	etching agents	termination group	synthesis parameters	comments	refs
HF etching	TiO_2/Ti_3C_2	HF	O, OH, F	20 mL of 48% HF, 15 h etching time	multilayer MXene produced with lower photocatalytic efficiency compared to monolayer counterpart	138
	2D/2D HCN/MXene	HF		39% HF, 24 h etching time	high purity of MXene was produced with well-defined multilayer structure	139
				39% HF, 48 h etching time	the growth of anatase TiO_2 on exfoliated multilayers MXene	
				39% HF, 96 h etching time	the growth of anatase and rutile TiO_2 was observed on MXene layer; more exfoliated layer and increase in the growth of TiO_2 NP with increasing etching time	
	TiO_2/Ti_3C_2	HF	O, OH, F	49% HF, 24 h etching time (35 °C); ethyl alcohol as a washing agent; hydrothermally treated at 450 °C	the formation of TiO_2/Ti_3C_2 safflower-like morphology with ∼1 μm safflower size and shorter nanorods formation	140
				49% HF, 24 h etching time (35 °C); ethyl alcohol as a washing agent; hydrothermally treated at 550 °C	average safflower size ∼2 μm upon heat increase heat treatment; well-formed safflower morphology	
				49% HF, 24 h etching time (35 °C); ethyl alcohol as a washing agent; hydrothermally treated at 650 °C	average safflower size ∼2 μm with lower spatial density of TiO_2/Ti_3C_2 nanorods compared to at 550 °C heat treatment; the safflower morphology slightly deformed at higher temperature	
	BQ/TiC/UCN	HF		40% HF, 72 h etching time, 20 mL DMSO, 24 h intercalation time	ultrathin MXene sheet is produced, effectively function as the electron mediator	141
	Ti_3C_2-QD/Ni-MOF	HF		20 mL HF, 24 h etching time, DMF intercalating agent	MXene QD constructed with enhance charge transfer and higher separation capabilities of the photocarriers	142
	2D/2D g-C_3N_4/$Ti_3C_2T_{A/R}$ (CN/TCT) MXene	HF		39% HF, 24 h etching time	less distribution of TiO_2 NPs on the surface of MXene	121
				39% HF, 96 h etching time	higher amount of TiO_2 growth/conversion with more of rutile phase compared to anatase	
				49% HF, 24 h etching time	higher distribution of TiO_2 on the MXene surface when employing more concentrated etchants	
				49% HF, 96 h etching time	both TiO_2 (rutile) and TiO_2 (anatase) having higher concentration due to more oxidation	
acid-containing fluoride ions	TiO_2/Ti_3C_2	LiF + HCl	O, OH, F	LiF with 6 M HCl, 24 h etching time	MXene flakes exhibit excellent hydrophilicity and dispersity with flakes size range of 10−100 nm	138
	ZnCdS/TiO2/Na-MXene	LiF + HCl		LiF with 9 M of HCl, 24 h etching time (35 °C)	the preintercalation of Na^+ and attachment of ZnCdS nanoparticles on the MXene flakes improve the oxidation stability and slowing the oxidation to TiO_2	143
	2D-Bi_2MoO_6@2D MXene	LiF + HCl	O, OH	LiF with 9 M of 20 mL HCl, 24 h etching time (35 °C)	2D MXene serves as effective platform for impeding the agglomeration and support the growth of Bi_2MoO_6 constructing a hierarchical composite structure	144
				3.08 M LiF/HCl, 6 h etching time; 1, 3, 6, 24, and 36 h	delaminated MXene with more conversion to $Ti_3C_2T_x$ than 1 h etched	
	$Ti_3AlC_2/Ti_3C_2T_x$	LiF + HCl		3.08 M LiF/HCl, 24 h etching time	delaminated MXene are formed with residual of Ti_3AlC_2 was observed	145
				3.08 M LiF/HCl, 36 h etching time	delaminated MXene with residual of Ti_3AlC_2 was observed; partial delamination occurs even at 36 h etched time	
	$Ti_3C_2T_x$	LiF + HCl	O, OH, F	LiF with 9 M HCl, 24 h etching time (30 °C)	c-lattice parameter of 25.75 Å	146
				LiF with 9 M HCl, 24 h etching time (35 °C), ethanol as washing agent	the highest c-lattice parameter of 30.99 Å obtained with ethanol as washing agent with improved delamination ratio	
alkaline etching	$Ti_3C_2T_x$	KOH	O, OH	5 M KOH, 120 °C hydrothermal treatment	less developed of accordion-like structure of MXene; more exposed of Ti-OH sites with with alkali etching	147
	$Ti_3C_2T_x$	NaOH	O, OH	27.5 M NaOH treatment at 270 °C	higher purity (92%) of multilayer MXene produced with removal of −F termination group	129
				27.5 M NaOH treatment at 250 °C	$Ti_3C_2T_x$ yield decrease with reaction temperature	
				5−10 M NaOH treatment at 270 °C	formation of Na/K−Ti−O compounds (NTOs) due to lower concentration of NaOH, increasing the water content and facilitate oxidation	
				NaOH treatment at 100−220 °C	no formation of MXene as reation cannot happen at lower temperature regardless of any concentration	
electrochemical etching	$Ti_3C_2T_x$	NH_4Cl, TMAOH	O, OH	1 M NH_4Cl, 0.2 M TMAOH	higher yield of single or bilayer (>90%) with larger average dimension	126
	Ti_2C	HCl	−Cl, −O, −OH	1 M HCl, 0.6 V, 1 day etching	less conversion of MXene sheets.	128

https://doi.org/10.1021/acsomega.2c05030
ACS Omega 2022, 7, 38158−38192

Table 2. continued

synthesis method	catalyst	etching agents	termination group	synthesis parameters	comments	refs
				2 M HCl, 0.6 V, 5 days etching	the formation of carbon-derived-carbide (CDC) as the results of overetching	
	$Ti_3C_2T_x$	$CuCl_2$	−Cl, −O	Ti_3SiC_2 in $CuCl_2$ molten salt (750 °C)	delamination of the layer proceed with the aid of $SiCl_4$ gas molecules produced through etching process	136
molten salt substitution	$Ti_3C_2T_x$	$ZnCl_2$	−Cl, −O	Ti_3ZnC_2 + $ZnCl_2$ (annealed time: 0.5 h, 1 h, 1.5 h, 3.0 h)	the increasing of the ratio of molten salt, $ZnCl_2$ in the starting precursor, a gradual conversion to $Ti_3C_2Cl_2$ can be observed	134
	$Ti_3C_2T_x$	NaCl, KCl, $CuCl_2$	−I, −Br, −Cl	NaCl, KCl, $CuCl_2$ (mixed ratio of 1:2:2:3), 10 h annealed time in Ar (700 °C)	well-configured Lewis acidic etching route could tailored the surface chemistry of MXene	148

noted that the termination groups present are dependent on the type of etchants utilized. Therefore, the utilization of HF as a primary etching agent successfully etched away the Al layer of MAX. This technique has been favored due to the cost-effective and straightforward procedures. However, our research group found that the etching time could affect the creation of TiO_2 on the $Ti_3C_2T_x$ MXene surfaces.[121] In this context, the etching of $Ti_3C_2T_x$ MXene was carried out by utilizing 39 and 49% HF concentration, and both were etched at 24 and 96 h. It was suggested that increasing etching time with HF assisted the formation of TiO_2 nanoparticles (NPs) on the surfaces of $Ti_3C_2T_x$ MXene, as represented in Figure 9c. In this regard, the increasing number of active TiO_2 semiconductor formation suggests a robust photocatalytic activity due to metal−semiconductor synergy. Even though the HF etching technique is highly utilized, the synthesis parameters, such as the concentration of HF and the etching time, are significant to ensure the purity of the produced $Ti_3C_2T_x$ MXene. Moreover, controlling the synthesis parameters could essentially affect the photocatalytic activity of the $Ti_3C_2T_x$ MXene-based materials.

3.2. Acid-Containing Fluoride Ions. Another synthesis technique that garnered scientific attention for the synthesis of $Ti_3C_2T_x$ MXene is the acid-containing fluoride ion method. In order to minimize the use of concentrated HF acid, researchers have sought a new environmentally safe technique to synthesize $Ti_3C_2T_x$ MXene. In this context, acid-containing fluoride ion etchants have been utilized to etch Al layers of Ti_3AlC_2 MAX, which at the same time delaminates their multilayer structure into the individual compartment.[122] In this regard, the synthesis and delamination of $Ti_3C_2T_x$ MXene can be achieved in a single step, unlike those by HF etching which requires intercalating agents to delaminate the multilayered structure of $Ti_3C_2T_x$ MXene. The pioneering study reported that the single-step preparation method could be achieved by reacting $Ti_3C_2T_x$ MXene with 6 M HCl with LiF at 45 °C for 45 h. Further analysis by powder XRD observed the removal of the Al layer from the Ti_3AlC_2 MAX, where the disappearance of Ti_3AlC_2 can be seen from Figure 9d. In this method, different types of acid and fluoride ions can be utilized, such as using sulfuric acid (H_2SO_4) containing NaF, KF, NH_3F, CsF, and tetrabutylammonium fluoride.[123] However, each combination might affect the properties of the synthesized $Ti_3C_2T_x$ MXene. For instance, a study found that utilizing HCl might improve the electrochemical capacity of $Ti_3C_2T_x$ MXene compared to those by HF.[124] Additionally, each fluoride salt utilized might require different synthesis parameters such as the reaction temperatures and etching time. It has been suggested that utilizing fluoride salts such as NaF and KF might require 48 h etching time at 40 °C to ensure a complete etching process. However, acid-containing NH_4F shows complete delamination after 24 h at 30 °C. A similar morphology can be observed in all synthesized $Ti_3C_2T_x$ MXenes regardless of any types of fluoride ions. In this regard, the accordion-like structure is present, suggesting that different acid-containing fluoride ions successfully form the $Ti_3C_2T_x$ MXene.

3.3. Electrochemical Etching. One of the newly developed techniques in synthesizing $Ti_3C_2T_x$ MXene is the electrochemical etching by which the fluoride-based etchant can be eliminated. In this synthesized process, the electrode and electrolytes are required for the reaction to occur. The Al layer will be selectively etched with the assistance of

https://doi.org/10.1021/acsomega.2c05030
ACS Omega 2022, 7, 38158−38192

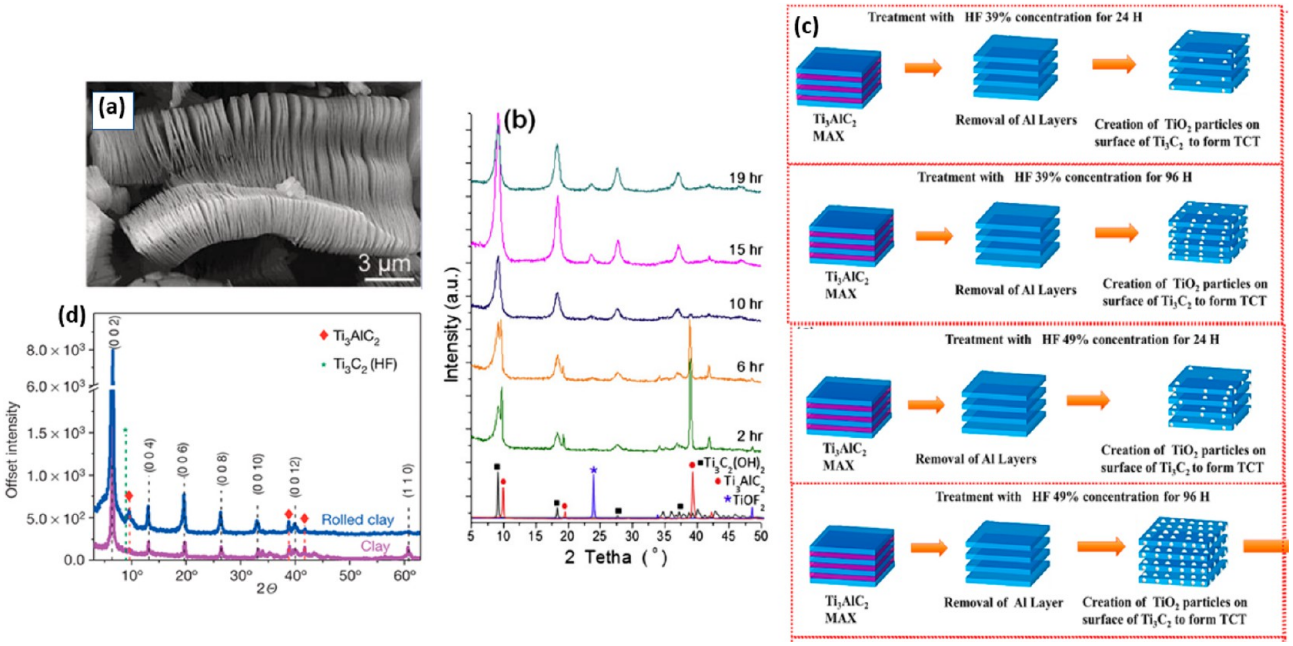

Figure 9. (a) SEM image of the 2D structure of $Ti_3C_2T_x$ MXene after 2 h etching with HF. Reprinted from ref 119. Copyright 2012 American Chemical Society. (b) XRD analysis on $Ti_3C_2T_x$ MXene at different etching times. Reprinted with permission from ref 125. Copyright 2013 Elsevier. (c) Formation of TiO_2 on the $Ti_3C_2T_x$ MXene sheets at different etching times. Reprinted with permission from ref 121. Copyright 2021 Elsevier. (d) XRD analysis on the formation of $Ti_3C_2T_x$ MXene through reaction with LiF with HCl solution. Reprinted with permission from ref 122. Copyright 2014 Springer.

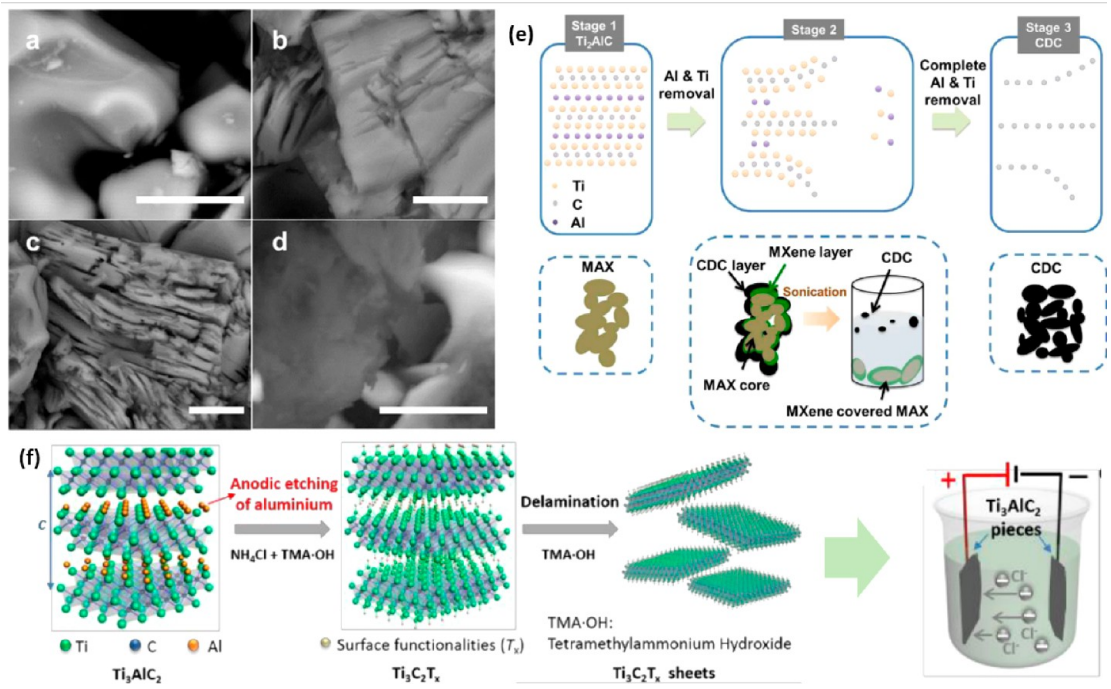

Figure 10. (a) SEM images MAX, (b) Ti_2CT_x MXene etched with 1 M of HCl at 0.6 V for 1 day, (c) 2 M of HCl at 0.6 V for 5 days, (d) 2 M of HCl at 0.6 V for 14 days. (e) Synthesis illustration of the Al removal from MAX phase and formation of three-layered Ti_2CT_x MXene structure. Reprinted with permission from ref 128. Copyright 2017 Royal Society of Chemistry. (f) Synthesis process of electrochemical etching of Ti_2CT_x MXene in two-electrode system. Reprinted with permission from ref 126. Copyright 2018 Wiley.

electrolytes through anodic etching.[126] In general, the Ti_3AlC_2 MAX will serve as a working electrode where the etching reaction will take place. Particularly, chemical and electrochemical etching is part of the surface reaction involving electron transfer, suggesting the possibility of forming $Ti_3C_2T_x$ MXene by electrochemically etching the MAX phase. A study found that the Ti_2AlC MAX can be electrochemically etched to form Ti_2CT_x MXene by utilizing an aqueous HCl (2 M) electrolyte. The absence of fluoride ions significantly yields fluoride-free terminated Ti_2CT_x MXene with the presence of −Cl, −O, and −OH terminal groups. In this approach, a three-layered structure of Ti_2CT_x MXene is formed, consisting of

https://doi.org/10.1021/acsomega.2c05030
ACS Omega 2022, 7, 38158−38192

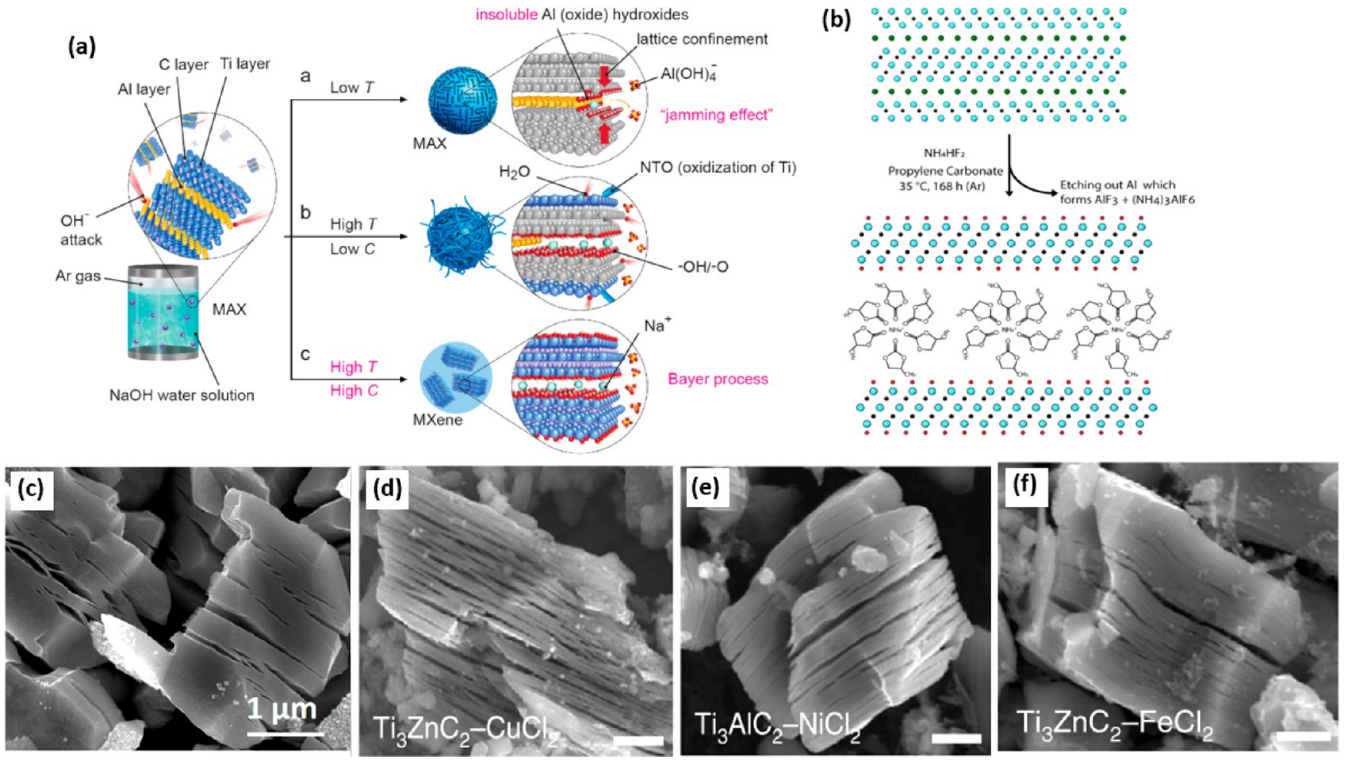

Figure 11. (a) Synthesis process of $Ti_3C_2T_x$ MXene through alkali etching. Reproduced with permission from ref 129. Copyright 2018 Wiley. (b) Schematic representation of water-free etching of MXene by utilizing propylene carbonate. Reproduced with permission from ref 137. Copyright 2020 Elsevier. (c) SEM image of $Ti_3C_2T_x$ MXene prepared through molten salt substitution. Reproduced from ref 134. Copyright 2019 American Chemical Society. (d–f) SEM image of $Ti_3C_2T_x$ MXene by utilizing different types of MAX with chloride molten salts. Reproduced with permission from ref 136. Copyright 2020 Springer.

carbon-derived carbide (CDC), Ti_2CT_x MXene, and unetched MAX. Parameter study such as voltage, etching time, and electrolyte concentration was observed to affect the morphology and properties of Ti_2CT_x MXene, such as that shown in Figure 10a–d. In particular, increasing the concentration of the HCl and etching time shows pronounced delamination surfaces. However, overetching of Ti_2CT_x MXene might lead to the formation of CDC. Even though the three-layered structures consisting of CDC, MXene, and MAX are formed, bath sonication could separate the layered structure to obtain Ti_2CT_x MXene. The synthesis process of Ti_2CT_x MXene through this electrochemical etching is demonstrated in Figure 10e.

Another study revealed that $Ti_3C_2T_x$ MXene was successfully formed by utilizing binary aqueous electrolytes in a two-electrode system, such as that present in Figure 6f.[126] In this method, the electrolyte consisting of 1 M NH_4Cl and 0.2 M tetramethylammonium hydroxide (TMAOH) at pH >9 was employed for a 5 h reaction time to etch the Al layer and undergo intercalation to extract the carbide flakes. The presence of a Cl ion in the electrolyte expedites the anodic Al etching and breaks the Ti–Al bond. Intercalation by the ammonium hydroxide (NH_4OH) promotes the etching underlying the surfaces. This approach successfully yields 90% of single and double $Ti_3C_2T_x$ MXene layers with flakes larger than those in the conventional HF technique. On the other hand, the fluoride-free $Ti_3C_2T_x$ MXene offers better capacitance (220 mF cm^{-2}) than those conventionally prepared. Even though this synthesis method is shown to offer $Ti_3C_2T_x$ MXene with Cl termination and successfully eliminate the –F functional, the formation of CDC required much attention. As mentioned, overetching the MAX phase in dilute HF, HCl, and NaCl electrolytes might lead to the removal of both Al and Ti layers.[127] Moreover, the newly developed technique requires in-depth scientific study to ensure a successful formation of $Ti_3C_2T_x$ MXene with excellent catalytic properties.

3.4. Alkali Etching. Aside from acid utilization as the etching agent, the study has found that alkali can also be employed to eliminate the Al layer of Ti_3AlC_2 MAX.[129] A study on alkali etching revealed that the hydrothermal-assisted technique utilizing NaOH as the etching agent successfully etched the Al layer of Ti_3AlC_2 MAX to form $Ti_3C_2T_x$ MXene. Alkali etching is one of the techniques to synthesize a fluorine-free $Ti_3C_2T_x$ MXene as it does not utilize any fluoride-containing chemicals. Additionally, this newly developed preparation method was also revealed to yield high-purity (~92%) $Ti_3C_2T_x$ MXene with a multilayered structure. The strong binding ability of the NaOH with the Al element assists the etching process, thus making it possible. It has been noted that the synthesis parameters such as the reaction temperature and etching concentration are significant to ensure successful elimination of the Al layer. This is because, as demonstrated in Figure 11a, the low temperature might prevent the Al extraction process by the Al (oxide) hydroxides. Moreover, the inability to form $Al_4(OH)^-$ due to lattice confinement from the Ti layer, known as the "jamming effect", blocks formation of $Ti_3C_2T_x$ MXene. On the other hand, utilizing a higher concentration of NaOH at a higher temperature leads to the oxidation of $Ti_3C_2T_x$ MXene and the formation of NTOs such as $Na_2Ti_3O_7$ and $Na_2Ti_5O_{11}$. Higher water content promotes the oxidation of Ti to form NTOs. Therefore, a suitable

https://doi.org/10.1021/acsomega.2c05030
ACS Omega 2022, 7, 38158–38192

reaction temperature and alkali concentration are required to ensure a complete formation of $Ti_3C_2T_x$ MXene. The hydrothermal reaction at 270 °C with 27.5 M NaOH concentration successfully yielded $Ti_3C_2T_x$ MXene with high purity compared to HF-etched MXene. In this hydrothermal-assisted NaOH etching method, controlling the temperature is essential to ensure a complete formation of $Ti_3C_2T_x$ MXene, while the optimum concentration of $Ti_3C_2T_x$ MXene controlled the purity of the produced $Ti_3C_2T_x$ MXene. Even though the alkali-assisted, hydrothermal synthesis method has been shown to successfully generate $Ti_3C_2T_x$ MXene, preventing the $Ti_3C_2T_x$ MXene from overetching to form NTOs is one of the challenges and requires extra attention. In addition, this method needs in-depth research to confirm the successful formation of fluoride-free $Ti_3C_2T_x$ MXene. Through this technique, −O and −OH terminal groups can be formed, and their role in stimulating photocatalytic activity and fuel conversion can be further extended.

3.5. Water-Free Etching. Water-free etching is another alternative in producing $Ti_3C_2T_x$ MXene with outstanding oxidation stability.[130] In this synthesis process, the employment of water as a primary solvent is replaced by the polar organic solvent to ensure no presence of water. The exceptional potential of $Ti_3C_2T_x$ MXenes in a wide array of applications indicates that they are one of the most favored materials. However, their hydrophilicity and tendency to oxidize limit their potential in applications requiring a longer storage period. Therefore, water-free etching was found to improve oxidation stability and broadened their role in any water-sensitive applications. In this preparation method, ammonium dihydrogen fluoride was utilized as the etching agent due to its capability to dissociate into NH_4F and HF when dissolved in the polar solvents. Three reaction steps are required: etching, washing, and delamination. Specifically, as presented in Figure 11b, the etching process occurred at which Ti_3AlC_2 MAX underwent a reaction with NH_4HF_2, where the Al layer was etched out in the form of AlF_3 and $(NH_4)_3Al_6$. Reaction with propylene carbonate (PC) promotes delamination into single-layer $Ti_3C_2T_x$ MXene. It has also been suggested that higher interlayer spacing of $Ti_3C_2T_x$ MXene is obtained compared to water-etched $Ti_3C_2T_x$ MXene.[131] Controlling the termination groups are favorable as it has been revealed that, through this technique, approximately 70% of −F and −30% of −O/−OH containing MXene was obtained.[132] In short, this method utilizes polar organic solvent, PC to replace water which was found to reduce the presence of the −OH terminating group. The control of the terminating group significantly enhances the oxidation stability, which raises $Ti_3C_2T_x$ MXene potential in the water-sensitive applications as the finding suggested that more exposure of the Ti−OH species of $Ti_3C_2T_x$ MXene expedites the oxidation process.[133]

3.6. Molten Salt Substitution. Another alternative in producing −Cl-terminated $Ti_3C_2T_x$ MXene is through molten salt substitution.[134] This method utilizes molten salts such as $ZnCl_2$ and $CuCl_2$ to undergo a substitution reaction with Ti_3AlC_2 MAX for the removal of the Al layer. This reaction process significantly produces nanolaminated $Ti_3C_2T_x$ MXene with −Cl termination, which was found to be more stable than −F-terminated $Ti_3C_2T_x$ MXene.[135] The reaction mechanism is presented in eqs 11−13, which generally involves the replacement of the A element of MAX with the metal salts.

$$Ti_3AlC_2 + 1.5ZnCl_2 \rightarrow Ti_3ZnC_2 + 0.5Zn + AlCl_3 \quad (11)$$

$$Ti_3AlC_2 + 1.5ZnCl_2 \rightarrow Ti_3C_2 + 1.5Zn + AlCl_3 \quad (12)$$

$$Ti_3C_2 + Zn \rightarrow Ti_3ZnC_2 \quad (13)$$

In eqs 11−13, the Zn^{2+} from the molten salts undergoes elemental replacement with the Al^{3+} from the Ti_3AlC_2 MAX. Stronger Lewis acidity by $ZnCl_2$ promotes the substitution of Zn^{2+} with Al^{3+}, forming Ti_3ZnC_2 MAX. Additionally, Zn^{2+} acts as a Lewis acid in the molten salt as it is a stronger Cl^- and electron acceptor. Specifically, molten salt of $ZnCl_2$ was ionized into Zn^{2+} and $ZnCl_4^{2-}$ in its molten state, while Al from Ti_3AlC_2 MAX undergoes redox conversion into Al^{3+}. The formation of $AlCl_3$ occurred through the bonding of ionic Al^{3+} with Cl^-, where it will be evaporated. Rapid evaporation of $AlCl_3$ facilitates the outward diffusion of the Al atom to undergo a substitution reaction. The elemental replacement further takes place when the reduced Zn atoms intercalate into the Al layer in the MAX phase, forming Ti_3ZnC_2, which is further exfoliated into Ti_3C_2−Cl_2 MXene. The SEM image in Figure 11c reveals the morphology of the Cl-terminated MXene, where it shows a more compact structure with a less distinct accordion sheet compared to other conventional preparation techniques. Another study by Li et al. revealed that the synthesis of $Ti_3C_2T_x$ MXene from different types of MAX phases could be achieved by employing different types of chloride molten salts such as $CuCl_2$, $FeCl_2$, $NiCl_2$, and AgCl.[136] Different morphology of MXenes etched by different chloride molten salts can be observed in Figure 11d−f, by which most of them show a prominent accordion-like structure of MXene.

4. DESIGN PRINCIPLES AND CONSIDERATIONS FOR $Ti_3C_2T_x$ MXene-BASED MOF COMPOSITE

4.1. Morphological Design and Engineering of $Ti_3C_2T_x$ MXenes and MOFs. In the context of morphological development, $Ti_3C_2T_x$ MXenes intrinsically manifest a unique accordion-like multilayer structure. However, their morphology can be modified into different dimensional structures, such as 0D quantum dots, 2D delaminated flakes, and 3D hierarchical/multidimensional structures. Delaminating $Ti_3C_2T_x$ MXenes into single flakes was shown to supply more exposed catalytic active sites and was observed to be highly efficient in driving the redox reaction compared to their multilayer morphology.[149] Typically, delaminating of $Ti_3C_2T_x$ MXene can be mainly performed through direct delamination or a two-step delaminating process. It has to depend on the preparation method of the $Ti_3C_2T_x$ MXene itself. Direct delamination can be achieved via an acid-containing fluoride ion etching technique.[150] In this regard, no intercalating agents are required to separate the layer as the fluoride ions can serve as intercalants to aid in the delamination process. On the other hand, the HF etching technique is regarded as a two-step process, requiring intercalating agents to assist the layer separation. Commonly used intercalating agents include dimethyl sulfoxide (DMSO), dimethylformamide (DMF), tetrabutylammonium hydroxide (TBAOH), and tetramethylammonium hydroxide (TMAOH).[151−153] Interestingly, a comparison study by Su et al. shows that monolayer $Ti_3C_2T_x$ MXene is more reactive toward the photoredox reaction due to its thinner sheet structure.[138] This is because the size and structure of $Ti_3C_2T_x$ MXenes distinctly affect their photocatalytic property and are correlated with their Fermi level

https://doi.org/10.1021/acsomega.2c05030
ACS Omega 2022, 7, 38158−38192

Figure 12. Morphological development of $Ti_3C_2T_x$ MXene into monolayer, quantum dots, and hierarchical/multidimensional structure.

energy. Hydrogen yield with 2.5 times enhancement was disclosed by employing monolayer $Ti_3C_2T_x$ MXene compared to their multilayer counterpart. Even though the precise location of active sites in $Ti_3C_2T_x$ MXenes is yet to be confirmed, through structural analysis, it was inferred to be positioned at the edge of the monolayer flakes. This corroborates with the experimental study where $Ti_3C_2T_x$ MXenes with smaller flake sizes were observed to have an exceptional catalytic activity compared to that of a denser multilayer structure. More exposure of the catalytic active sites due to size effects and exposed flake edges supports the conjecture. Correspondingly, delaminated $Ti_3C_2T_x$ MXenes through intercalation with TMAOH were revealed to have an apparent effect on the photocatalytic activity with 1.49 times activity improvement over that of the standard HF-etched multilayered $Ti_3C_2T_x$ MXene.[154] Moreover, the 2D geometry of monolayer $Ti_3C_2T_x$ MXene offers excellent support for other semiconductor photocatalysts, especially for nanoparticle materials from agglomeration, providing uniform dispersion. Therefore, the solar absorption performance can be augmented owing to a larger light receiving area.[155]

Additionally, the tunability of their morphology indicates that they are a highly selective cocatalyst for photocatalytic enhancement. For instance, quantum dot $Ti_3C_2T_x$ MXene can be constructed through layer cutting by DMSO intercalant and thermal treatment with PEI.[25,156] Another study reported the preparation of $Ti_3C_2T_x$ MXene QD through an ammonia-assisted hydrothermal reaction.[157] Moreover, hydrothermal intercalation with DMF was also found to convert the nanosheets into QD structures.[142] A benefit in converting into smaller nanosize QDs is to offer better solvent solubility and to expose more active edge sites. As mentioned, dimensional size has a great impact on the photoreaction activity, which highlights the significance of well-controlled morphology. The smaller dimensional size of the $Ti_3C_2T_x$ MXene QD is shown to provide an effective coating for stabilizing the oxidation of other semiconductor materials. For instance, the $Ti_3C_2T_x$ MXene QD was found to cover the porous surface of Cu_2O NWs by coating them and hindering the easy oxidation of the NWs.[25] In this regard, the photoreaction stability was observed to maintain up to six long cycles and retain as high as 86% methanol yield. The relevance of morphologically tuning the $Ti_3C_2T_x$ MXene into a QD structure can prevail with their outstanding photoreaction activity for hydrogen generation, successfully obtaining their 2D nanosheet structure. A study found that the $Ti_3C_2T_x$ MXene QD successfully produced solar hydrogen generation with as high as 10 times enhancement than that of $Ti_3C_2T_x$ MXene nanosheets and 3 times higher than that incorporated with Pt, disclosing the novelty of the $Ti_3C_2T_x$ MXene QD as a noble metal replacement.[25]

Aside from morphologically constructing $Ti_3C_2T_x$ MXene into single flakes and quantum dots, hierarchical and multidimensional $Ti_3C_2T_x$ MXene constructed through the combination of different dimensional domains was observed to benefit them through a supportive platform. Typically, multidimensional $Ti_3C_2T_x$ MXene can be constructed by hybridizing them with other dimensional photocatalysts. For instance, the $Ti_3C_2T_x$ MXene safflower shape was successfully generated by hydrothermal oxidation followed by ion exchange to form $TiO_2/Ti_3C_2T_x$ MXene with a 3D porous framework.[140] Thermally oxidized $Ti_3C_2T_x$ MXene could support the formation of TiO_2 nanoparticles and, through the ionic exchange process, form the safflower-like-shaped $TiO_2-Ti_3C_2T_x$. The merit of having a 3D structure framework could hinder the agglomeration of the nanoparticles and sheet aggregation, which could reduce the absorption efficiency. Thinner and smaller sizes of $Ti_3C_2T_x$ MXene are highly beneficial for the carrier's transmission where shorter distances are required to carry out the redox reaction, but the implication of agglomerated sheets is one of the serious drawbacks.[158] The creation of a multidimensional structure of a $Ti_3C_2T_x$ MXene-based composite with a 1D/2D structure highly benefits the carrier dynamics as different dimensional domains have an individual contribution for photocatalytic enhancement. For instance, 1D/2D $CdS/Ti_3C_2T_x$ MXene constructed through in situ assembly and solvothermal treatment was found to give an eminent improvement in the

https://doi.org/10.1021/acsomega.2c05030
ACS Omega 2022, 7, 38158−38192

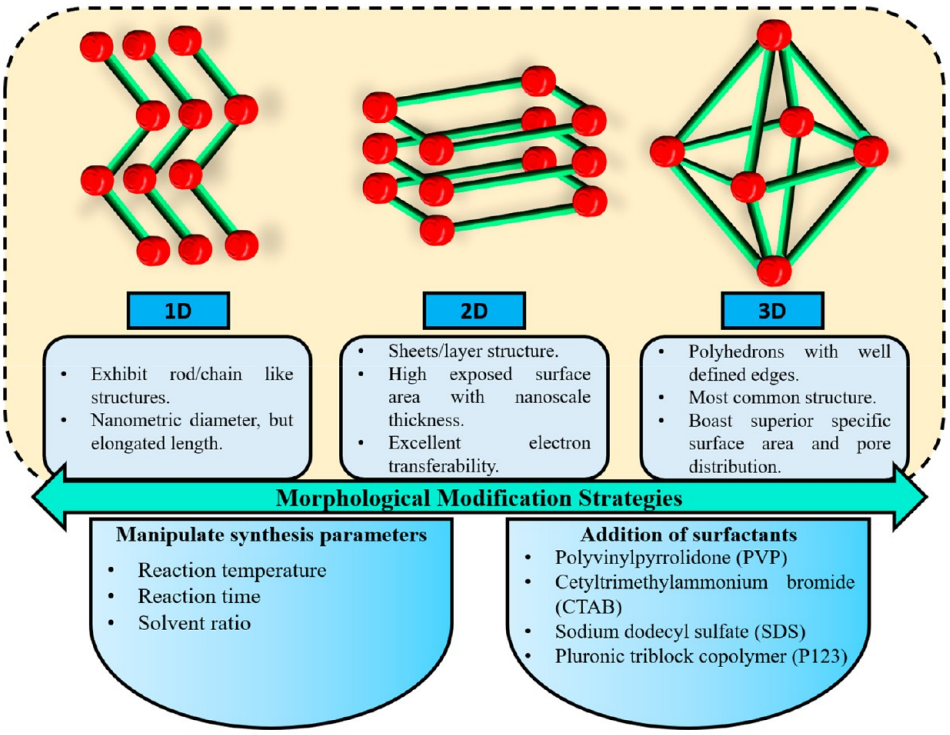

Figure 13. Scheme illustrating the general morphology and morphological engineering of MOFs.

photocatalytic activity compared to that of their intrinsic counterpart.[149] The effective platform of 2D $Ti_3C_2T_x$ MXene sheets for CdS nanorod growth provides intimate contact and aids in the separation of charges. For instance, the longitudinal oriented charge transmission with high length-to-diameter ratio semiconductors could improve the separation efficiency as a longer time is needed for the charges to travel back and recombine. On the other hand, hierarchical nanoflower-like core−shell morphology is constructed by in situ hydrothermal LDH on $Ti_3C_2T_x$ MXene.[159] The growth of smaller LDH nanoflakes creates a $Ti_3C_2T_x$ MXene with abundant active sites for photocatalytic CO_2 reduction. The well-dispersed LDH nanoflakes covering the $Ti_3C_2T_x$ MXene surfaces in the core−shell-like shape improve the light absorption and hinder the serious agglomeration typically observed in LDH nanoflakes. Therefore, designing $Ti_3C_2T_x$ MXene into different morphological structures is one of the promising engineering considerations for producing a very efficient photocatalyst for solar fuel conversion. Figure 12 summarizes the development of $Ti_3C_2T_x$ MXene into different morphological structures.

As mentioned previously, MOFs tend to naturally occur in 1D rods, 2D sheets, or 3D polyhedrons, in which the latter tend to be the more common morphology. 1D MOFs are usually identified by their nanometric diameter together with an extended length, adopting chains or rod structures. On the other hand, 2D MOFs exist as sheets or layers that have a nanoscale thickness. 2D MOFs have a few beneficial properties as an efficient photocatalyst, such as high exposed surface area to light irradiation and reactants, as well as excellent electron transferability.[160,161] Finally, 3D MOFs are held together by strong chemical bonds, which come together to form a highly complicated network structure. These polyhedrons boast an extremely high surface area, with uniform pore size distributed all over the surface of the MOF.[30] Nevertheless, the morphology and dimensions of MOFs can be further regulated via two main approaches which is (1) modification of synthesis parameters and (2) introduction of additives. First, various synthesis parameters were reported to modify the morphology of MOFs, such as temperature, reaction time, and solvent ratio. Yuan et al. noticed that the structure of Ni-MOF alters according to the solvothermal synthesis temperature. At room temperature and 60 °C, the Ni-MOF exhibits an urchin-like structure with a diameter of approximately 200 nm. As the temperature increased to 100 °C, one-dimensional nanowires with 10 nm diameter were obtained. The change in morphology was mainly due to the dynamic viscosity of 2-methylimidazole linkers, which limits the mass transfer through the temperature change.[162] In another study, the effects of reaction temperature and time were studied with a Co-MOF. The original 2D nanoplates of Co-MOF were transformed into 1D layered microrods as both the reaction temperature (120 to 160 °C) and time (5 to 30 min) increased.[163] The solvent ratio can also effectively alter the structure of the MOF due to the role of solvent as a directing agent as well as ligands, where they can be incorporated onto the lattice of the MOF. It was previously reported that by manipulating the DMF/ethanol solvent ratio from 3 to 1, the 3D structure of the MOF was converted into 2D nanosheets.[164]

Second, the use of additives such as modulators and surfactants is effective at tuning the morphology of MOFs. For example, a 3D hollow porous concave octahedral bimetallic Fe−Zn MOF was prepared via a conventional solvothermal method using $FeCl_3{\cdot}6H_2O$, $Zn(NO_3)_2{\cdot}6H_2O$, and terephthalic acid as linkers, with DMF and C_2H_5OH alcohol as solvent. Upon introduction of polyvinylpyrrolidone (PVP), the morphology of the MOF showed a drastic change, from 3D octahedrons to 1D hollow porous nanorods.[165] Additionally, Sarawade et al. investigated the effect of various surfactants on the morphology on a Co-MOF with linkers of 2,6-naphthalenedicarboxylic acid (H_2ndc) and *trans*-1,2-bis(4-

https://doi.org/10.1021/acsomega.2c05030
ACS Omega 2022, 7, 38158−38192

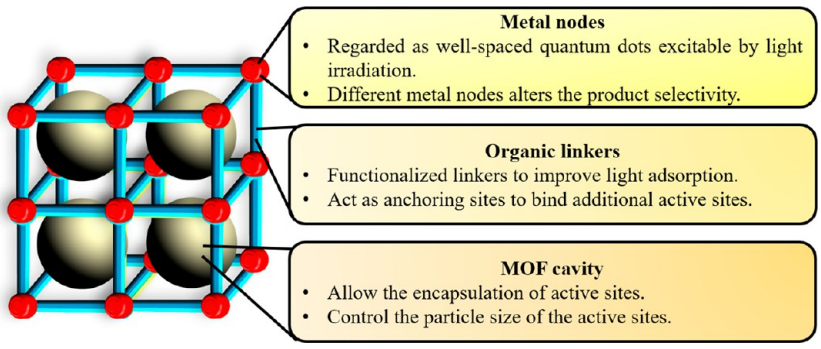

Figure 14. Overview of the active sites present over metal−organic frameworks.

pyridyl)ethylene (bipyen). Without the use of surfactant, the Co-MOF exhibited a spindle-like microrod structure. However, upon the use of cetyltrimethylammonium bromide, sodium dodecyl sulfate (SDS), and Pluronic triblock copolymer (P123) surfactants, the original morphology was converted into 2D nanoplates, nanosheets, and 1D nanorods, respectively.[163] The morphology engineering of MOFs was then summarized, as shown in Figure 13. MOFs tend to exist mainly in 3D structures, with some MOFs naturally existing in 1D rods or 2D sheets. However, the morphology and dimensions of MOFs can be further engineered either by varying the synthesis parameters or by using additives.

4.2. Active Sites over $Ti_3C_2T_x$ MXene-Based MOF Composite. Active sites are the locations or specific sites where a certain reaction has the highest activity. It is of utmost importance to identify the active sites over photocatalysts to gain a deeper understanding of how to quantify and optimize the active sites with respect to a specific chemical reaction. This is because the types of active sites present on the surface of the catalyst can influence the overall selectivity of the products. The role of active sites is especially evident in thermal and photothermal catalysis. For example, the utilization of Ni[166] and Co[80] metals tends to yield a higher production of CH_4 from the CO_2 hydrogenation reaction. However, the use of Fe promotes the Fischer−Tropsch reaction, in turn exhibiting a higher C_{2+} hydrocarbon evolution.[167,168] From these examples, we can get a general idea on the active sites of MOFs. MOFs are made up of a variety of metal nodes, such as Co, Zr, and Ti and can be regarded as isolated quantum dots that can be excited upon light irradiation.[169] Second, the organic linkers can also function as active sites or be functionalized to anchor active sites. Most notably, UiO-66 linkers modified with Cu(II) porphyrins not only enhanced the overall photocatalytic activity but also boosted the light adsorption of the photocatalyst.[170] Similarly, MOF-525, which consists of porphyrin linkers anchored Co metal, successfully incorporated the Co active sites onto the framework of the MOF. The introduction of CO active sites to the framework prolonged the lifetime of charge carriers and improved the CH_4 production from photocatalytic CO_2 reduction.[171] Lastly, the huge cavity of MOFs is a suitable host for encapsulating photoactive metal nanoparticles. Zhao's group successfully encapsulated Ni nanoparticles within the pores of UiO-66, which limited the growth of Ni via agglomeration.[172] Interestingly, the encapsulation is not limited to only metals. Li et al. reportedly boosted the photocatalytic CO_2 reduction by embedding carbon dots inside NH_2−UiO-66 particles. These carbon dots function as electron receptors and photosensitizers, which promote charge separation and transfer.[173] The discussion on the active sites of MOFs are summarized in Figure 14, where they exist either at the metal nodes, organic linkers, or within the cavity of MOFs.

Up to the current development, the exact active sites of $Ti_3C_2T_x$ MXene are still under exploration. Some studies inferring the position of the active sites might be located at the edges of the $Ti_3C_2T_x$ MXene sheet. This has been experimentally hypothesized by which delaminating MXene into thinner flakes exposed more of the active sites and induced higher reaction activity compared to that with the multilayer structure.[138] Therefore, engineering the morphology $Ti_3C_2T_x$ MXene was observed to affect the photoreaction activity which is highly linked to the degree of exposure of the catalytic active sites. Nevertheless, despite the vagueness in specifying the active site of MXene, an analysis study revealed that the termination group has a prominent role in tailoring the stability and catalytic properties of $Ti_3C_2T_x$ MXene. The type of the termination group can be qualitatively controlled through parameter regulation. Designing $Ti_3C_2T_x$ MXene with suitable termination groups is significant to fit the application requirement and control its environmental stability. For instance, the formation of −F termination has been linked with poor ambient stability in a colloidal dispersion, which led to the formation of −F free terminated Ti_3C_2 MXene by Shi et al.[174] On the other hand, $Ti_3C_2T_x$ MXene can easily be oxidized under ambient environments, and the exposure of the Ti atom with oxygen could lead to the formation of TiO_2. Worth mentioning is that the functional group is the active oxidative site which could affect the oxidation stability of $Ti_3C_2T_x$ MXene. For instance, computational analysis on each type of termination group revealed that the termination group is linked with the defect formation energy. In this regard, the −OH termination group relating to lower oxidation stability is due to lower energy formation of the vacancy. However, ═O termination is oxidatively stable due to higher energy formation of the vacancy. Moreover, it was confirmed by the study conducted indicating that the Ti−OH group is highly reactive owing to the lower work function.[175] The abundance of reactive sites in Ti−OH further facilitates the oxidation of $Ti_3C_2T_x$ MXene. The removal of −OH through hydrogen annealing was found to improve the oxidation stability of $Ti_3C_2T_x$ MXene.[133] In additional, preparing $Ti_3C_2T_x$ MXene with −Cl termination was observed to possess higher oxidation stability compared to that of −F- and ═O-terminated $Ti_3C_2T_x$ MXene.[176] Therefore, perfect control of the surface termination is significant, especially for ensuring a highly stable

https://doi.org/10.1021/acsomega.2c05030
ACS Omega 2022, 7, 38158−38192

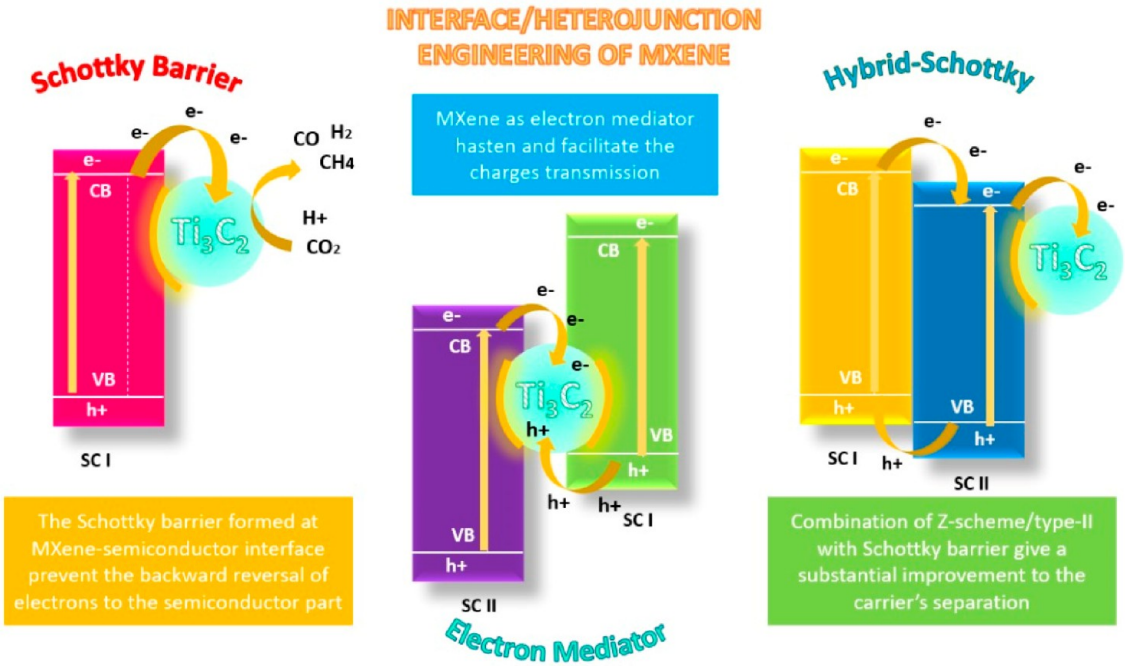

Figure 15. Overall representation of the electron transfer mechanism in MXene as a cocatalyst.

$Ti_3C_2T_x$ MXene in an ambient environment. This is because it was noticed that $Ti_3C_2T_x$ MXene could easily be oxidized during the thermal treatment even with no support of oxidizing agents due to the presence of surface terminating groups.[177]

4.3. Modification Strategies through Interfacial/Heterojunction Engineering. *4.3.1. $Ti_3C_2T_x$ MXene.* Another design consideration to increase the potential of $Ti_3C_2T_x$ MXene is through interfacial/heterojunction engineering. The metallic nature and excellent electrical conductivity in $Ti_3C_2T_x$ MXene make it the most influential cocatalyst to assist the solar fuel conversion.[178−181] $Ti_3C_2T_x$ MXene could serve as an electron trapper through the creation of an electrostatic potential barrier at the $Ti_3C_2T_x$ MXene/semiconductor junction. This phenomenon is termed the Schottky barrier, where electrons that transfer from the semiconductor to $Ti_3C_2T_x$ MXene are trapped and unable to transfer back to the semiconductor counterpart and recombine with holes. The Schottky barrier can be constructed through the contact formation between $Ti_3C_2T_x$ MXene with other semiconductor photocatalysts. $Ti_3C_2T_x$ MXene with a large work function could highly benefit from the carrier separation. This is because the higher the difference between the metal work function and the semiconductor, the stronger the potential barrier created at the metal−semiconductor junction, making the electrons from the $Ti_3C_2T_x$ MXene unable to travel back. The Schottky barrier induced by $Ti_3C_2T_x$ MXene is a distinction that aids photocatalytic enhancement.

In addition to the creation of the Schottky barrier, $Ti_3C_2T_x$ MXene could also serve as a mediator to assist electron transmission and is prominent in the construction of the Z-scheme heterojunction system.[182] For the first time, $Ti_3C_2T_x$ MXene was employed as a mediator in the three-phase Z-scheme system catalyst of CdS@Ti_3C_2@TiO_2 by Liu et al.[183] The electron sinking effects by $Ti_3C_2T_x$ MXene with a well-matched band configuration give a substantial improvement in the photocatalytic activity through the creation of a Z-scheme electron transfer system. In this system process, $Ti_3C_2T_x$ MXene serves as an electron-trapping center and as the mediator. The role of $Ti_3C_2T_x$ MXene as the electron mediator facilitates the electrons from the CB of TiO_2 to transfer to the VB of CdS, hastening the electron migration. Another study disclosed the significance of $Ti_3C_2T_x$ MXene in mediating the electron transfer between g-C_3N_4 and $MoSe_2$, constructing a Z-scheme heterojunction system.[184] Separation of photocarriers was enhanced, and the electrons effectively transferred from one semiconductor to another semiconductor to undergo a redox reaction. The vital role of $Ti_3C_2T_x$ MXene as a trapping center and a mediator provides greater reductive/oxidative ability as more electrons are available and less recombination occurs. Nevertheless, the employment of $Ti_3C_2T_x$ MXene as an electron mediator in the Z-scheme system is still not widely explored compared to other cocatalysts such as reduced graphene oxide (rGO), which might be due to their thicker sheet reducing the contact formation with multiple semiconductor photocatalysts.[183]

In general, thermally oxidized $Ti_3C_2T_x$ MXene could generate a $Ti_3C_2T_x$ MXene−TiO_2 hybrid.[185] Moreover, our group also investigated the construction of anatase/rutile TiO_2 formation by regulating the etching time with HF.[121] Therefore, employing a $Ti_3C_2T_x$ MXene−TiO_2 hybrid with other semiconductor photocatalysts such as g-C_3N_4, CdS, and MoS_2 could induce a hybrid Schottky−Z-scheme/Schottky−type II heterojunction system. In this context, the electrons will migrate following the Z-scheme/type II configuration to the TiO_2-induced MXene and will then migrate to the reductive $Ti_3C_2T_x$ MXene to undergo a reduction reaction.[121,139,186,187] The Schottky barrier will be formed at the TiO_2−$Ti_3C_2T_x$ junction and thus suppress the backward reversal of electrons back to TiO_2. Therefore, the combination of Schottky−Z-scheme/Schottky−type II heterojunction is highly propitious for boosting the photocatalytic performance of $Ti_3C_2T_x$ MXene in the solar fuel conversion. Figure 15 presents the electron transfer mechanism of MXene as an electron

https://doi.org/10.1021/acsomega.2c05030
ACS Omega 2022, 7, 38158−38192

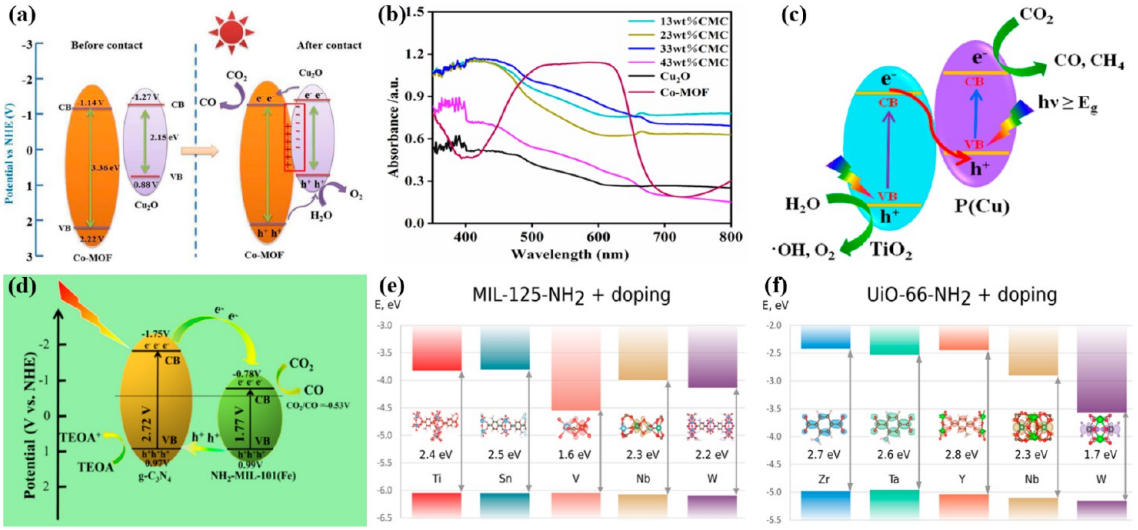

Figure 16. (a) Type II heterojunction system between Co-MOF and Cu_2O. (b) UV−vis diffuse reflectance spectra of Co-MOF and Cu_2O composites (x-CMC). Reprinted with permission from ref 189. Copyright 2022 Elsevier. (c) Z-scheme heterojunction system on PCN-224(Cu)/TiO_2 photocatalysts. Reprinted from ref 190. Copyright 2019 American Chemical Society. (d) Type II heterojunction scheme over NH_2-MIL-125/g-C_3N_4. Reprinted from ref 105. Copyright 2020 American Chemical Society. Influence of different metal dopant on the E_{bg} of (e) MIL-125-NH_2 and (f) UiO-66-NH_2. Reprinted from ref 194. Copyright 2019 American Chemical Society.

mediator, in a Schottky barrier and a hybrid Schottky heterojunction system.

4.3.2. MOFs. Since MOFs are photoresponsive materials that can generate electron/hole pairs when irradiated with solar energy, their photocatalytic activity can be enhanced via two main approaches, which is the prolongation of the lifetime of charge carriers and narrowing of band gap energy (E_{bg}). The lifetime of charge carriers can be prolonged by adopting various strategies to provide spatial separation of the electron/hole pairs. Additionally, the light harvesting ability of MOFs in the visible light region can be enhanced by modulating the E_{bg} of MOFs. Here, several approaches to promote the photocatalytic activity of MOFs will be discussed, such as the formation of heterojunctions, surface sensitization, MOF functionalization, doping of MOFs, and utilization of photosensitizers.

Heterojunctions are formed upon contact of two photoresponsive materials, in which different heterojunction systems have been discovered such as type I, type II, type III, Z-scheme, and step-scheme heterojunctions. The formation of heterojunctions not only promotes the adsorption of visible light but also provides spatial separation of charge carriers.[188] Figure 16a shows a type II heterojunction between Co-MOF and Cu_2O (x-CMC). Here, electrons migrate from the CB of Cu_2O to the LUMO of Co-MOF, whereas the holes from HOMO of Co-MOF transfers to the VB of Cu_2O, achieving good spatial separation of charge carriers. Additionally, the formation of heterojunctions drastically improved the visible light adsorption of pristine Cu_2O, as shown in the UV−vis diffuse reflectance spectra in Figure 16b.[189] In another study, a Z-scheme heterojunction system (Figure 16c) was achieved over PCN-224(Cu)/TiO_2 photocatalysts which improved the overall photocatalytic reaction.[190] Surface sensitization is achieved when the Schottky junction is formed upon introduction of metals. Xiao's group successfully encapsulated Cu nanoparticles within the pores of UiO-66 through an advanced double-solvent approach. Due to the intimate contact between the metals and MOF, a Schottky junction was generated, in which solar energy utilization and separation of charge carriers were ameliorated.[191] By combining MOFs with MXenes, Schottky junction together with heterojunctions can be generated as reported by Wu et al. A Ti_3C_2-modulated MIL-125-NH_2 nanohybrid exhibited both type II heterojunctions and Schottky junctions. This is because $Ti_3C_2T_x$ MXenes tend to oxidize into the TiO_2 semiconductor, allowing the heterojunction between TiO_2 and MIL-125-NH_2, while the metallic $Ti_3C_2T_x$ MXenes induce a Schottky junction. Hence, the photogenerated electron is efficiently separated via migration to $Ti_3C_2T_x$, while the holes are left behind in the HOMO of the MOF.[192] Functionalization is another promising strategy to enhance visible light adsorption as it can reduce the energy band gap of MOF. For instance, pristine UiO-66 has an E_{bg} of 3.91 eV, which decreased to 2.83 eV upon functionalization with an amine group.[86] Dao's group reported an efficient type II heterojunction system over NH_2-MIL-125/g-C_3N_4 for photocatalytic CO_2 reduction, as shown in Figure 16d. The $-NH_2$ functional group not only enhanced CO_2 adsorption but also promoted light adsorption in the visible light range.[105]

Doping is a type of point defect where impurities or foreign atoms are introduced, which disrupts the original lattice structure of the material.[193] A study conducted by Syzgantseva et al. reported that the doping of metals into the lattice of MOFs is able to modulate the energy band gap of MOFs. Here, two MOFs, namely, MIL-125-NH_2 and UiO-66-NH_2, were doped with different types of metals, and their E_{bg} were observed. From Figure 16e, the doping of MIL-125-NH_2 with Sn increased the E_{bg}, but doping with Nb, W, and V narrowed the E_{bg} to 2.3, 2.2, and 1.6 eV, respectively. Similarly, UiO-66-NH_2 (Figure 16f) doped with Y element caused a slight increase in E_{bg}, whereas Ta, Nb, and W dopants further reduced the E_{bg} to 2.6, 2.3, and 1.7 eV, respectively.[194] A narrower band gap is able to promote a broader light adsorption spectrum. Finally, utilizing photosensitizers can promote light harvesting especially in the visible region due to them possessing a strong optical absorption over a wide range

https://doi.org/10.1021/acsomega.2c05030
ACS Omega 2022, 7, 38158−38192

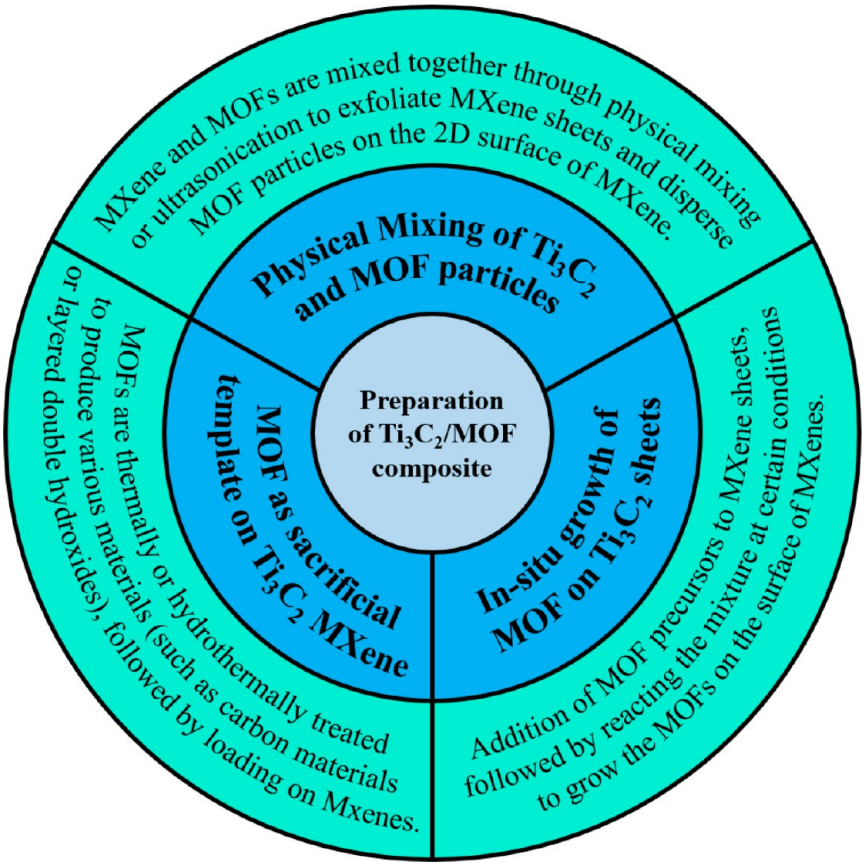

Figure 17. Overview of approaches to prepare Ti_3C_2 MXene-based MOF composites.

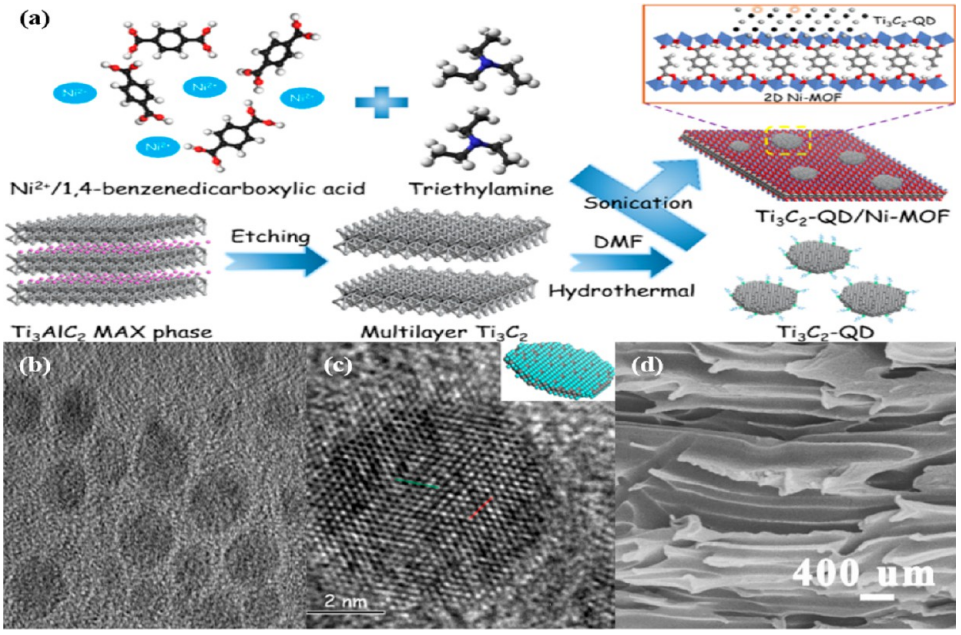

Figure 18. (a) Illustration of Ti_3C_2-QD/Ni-MOF synthesis via ultrasonication approach. (b,c) HRTEM images of Ti_3C_2-QD/Ni-MOF. Reprinted from ref 142. Copyright 2020 American Chemical Society. (d) FE-SEM image of layered Ti_3C_2/NiCo-MOF. Reprinted with permission from ref 200. Copyright 2020 MDPI.

of wavelengths.[195] When photosensitizers are used together with MOFs, MOFs benefit by obtaining energy from the incident light that is absorbed by the photosensitizer.[196] Mu's group coated CdS nanorods with Co(BDC) MOF and applied a $[Co(bpy)_3]^{2+}$ photosensitizer. The MOF layer successfully bridges the heterogeneous photosensitizer and molecular cocatalyst, which enhanced the CO_2 reduction reaction and prevented photocorrosion of the photosensitizer.[197] In another study, the $Ru(bpy)_2]Cl_2$ photosensitizer and $Re(CO)_3Cl$ molecular catalyst were grafted into the framework of MOF-

https://doi.org/10.1021/acsomega.2c05030
ACS Omega 2022, 7, 38158−38192

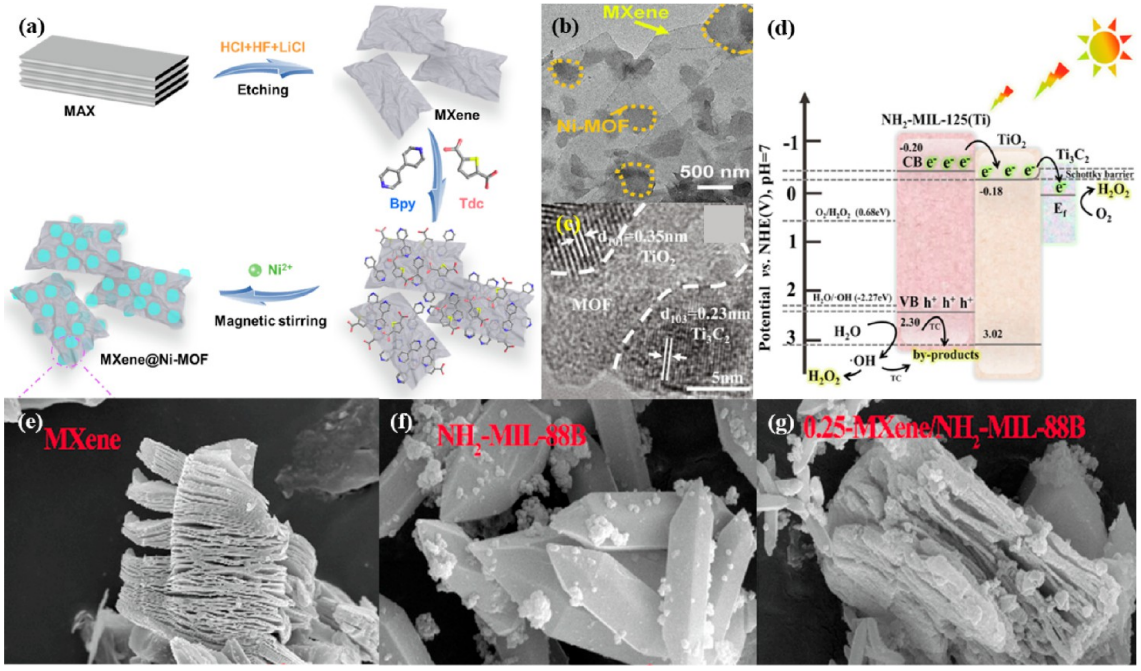

Figure 19. (a) Scheme of in situ growth for Ti_3C_2 MXene@Ni-MOF composite. (b) HRTEM image of MXene@Ni-MOF. Reprinted with permission from ref 201. Copyright 2022 Elsevier. (c) HRTEM image and (d) energy level diagram for NH_2-MIL-125/TiO_2/Ti_3C_2 composite. Reprinted with permission from ref 192. Copyright 2020 Elsevier. SEM images of (e) Ti_3C_2 MXene, (f) NH_2-MIL-88B, and (g) MXene/NH_2-MIL-88B composites. Adapted with permission from ref 202. Copyright 2021 Elsevier.

808. It was noted that the covalent grafting of the photosensitizer not only enhanced the light harvesting ability of the photocatalyst but also improved the lifetime of electron/hole pairs and shortened the transport distance of charge carriers.[198] Therefore, it is clear that the photocatalytic activity of MOFs in terms of spatial separation of charge carriers and light adsorption ability can be further regulated with various modification strategies.

5. SYNTHESIS OF MXene-BASED MOF COMPOSITES AND THEIR CHARACTERIZATION

In the past, there have been various ways to prepare Ti_3C_2 MXene-based MOF composites for various applications. The composite can be prepared by two main ways, which is either through physical mixing of both MOF and MXene together or by growing the MOF particles on the surface of MXenes. Also, MOFs can be used as sacrificial templates to prepare various materials such as carbon materials and layered double hydroxides, which is then dispersed on the surface of the MXenes. Herein, a thorough discussion on the various synthesis approaches and their characterization are explored, where the overview of the approaches is summarized as shown in Figure 17.

One of the more common approaches to prepare the Ti_3C_2 MXene-based MOF composite is by physically mixing both Ti_3C_2 and MOF together. By mixing them, the MOFs and Ti_3C_2 MXenes will be randomly bound and be in contact with each other. Ultrasonication is a promising way to successfully synthesize MXene/MOF composites. This is because, under ultrasonication, the Ti_3C_2 sheets can be exfoliated into multilayers.[199] For instance, Qin et al. prepared a Ti_3C_2 MXene-based MOF composite (Ti_3C_2-QD/Ni-MOF) through a facile ultrasonic method, as illustrated in Figure 18a. Ti_3C_2 quantum dots were prepared in two steps, which is the etching of the MAX phase to Ti_3C_2 multilayers, followed by hydrothermal treatment to obtain the Ti_3C_2 QDs. Then the prepared Ni-MOF was mixed with Ti_3C_2 QDs under continuous ultrasonication for 4 h. High-resolution transmission electron microscopy (HRTEM) images in Figure 18b,c show the successful preparation of the composite, in which a uniform dispersion of quantum dots on the 2D Ni-MOF was observed. Also, point defects are observed over the surface of Ti_3C_2, supplying coordination-unsaturated sites for catalytic reactions.[142] Similarly, Liu and co-workers adopted the sonication method to prepare the MXene/MOF composite. First, NiCo-MOF nanosheets were prepared via a precipitation method. Upon obtaining the MOF powders, they were dispersed into a Ti_3C_2 aqueous solution under sonication. Due to the two-dimensional structure of both MOF and MXene, the ultrasonication promotes the interlacing of both materials, as studied over the field emission scanning electron microscopy (FE-SEM) image in Figure 18d. The interconnected porous networks which are developed between the MXene/MOF composite restricts the self-restacking of the NiCo MOF and Ti_3C_2 sheets.[200]

Another way to prepare the composite is through in situ growth of the MOF on the surface of MXenes. By growing the MOF particles on the MXenes, a more intimate contact between the two materials can be achieved. Zheng et al. anchored a 3D pillared Ni-MOF on the surface of 2D layered Ti_3C_2 MXenes, as illustrated in Figure 19a. The 4,4′-bipyridine (Bpy) and thiophene-2,5-dicarboxylate (Tdc) linkers were first introduced to the Ti_3C_2 sheets, followed by subsequent addition of $NiCl_2{\cdot}6H_2O$ into the solution. The addition of the linkers to the MXene bound the organic ligands to the interlayer functional groups of MXene. Then the addition of Ni^{II} coordinated the organic ligands over the Ti_3C_2 surface to produce a Ti_3C_2@Ni-MOF composite. The HRTEM images in Figure 19b display the successful growth of Ni-MOF on the

https://doi.org/10.1021/acsomega.2c05030
ACS Omega 2022, 7, 38158−38192

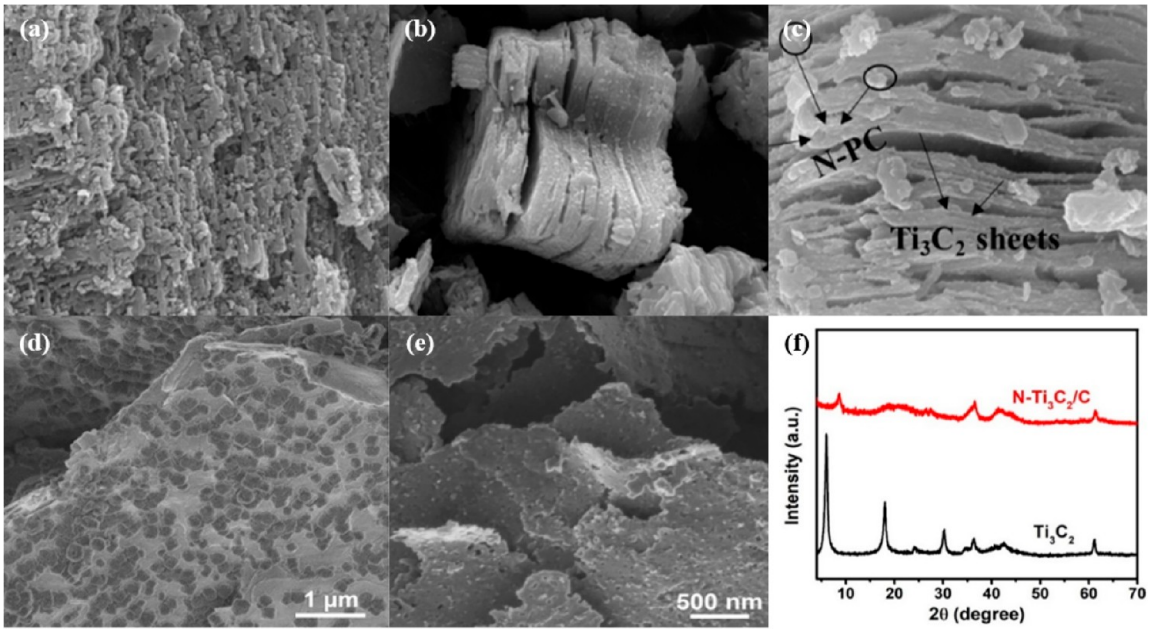

Figure 20. SEM images of (a) N-PC, (b) Ti_3C_2 MXene, and (c) Ti_3C_2/N-PC. Reprinted with permission from ref 204. Copyright 2020 Elsevier. (d) Ti_3C_2/ZIF-67 and (e) N−Ti_3C_2/C, and (f) XRD plot of N−Ti_3C_2/C and Ti_3C_2. Reprinted with permission from ref 205. Copyright 2019 Elsevier.

surface of the 2D Ti_3C_2 sheets. The growth of Ni-MOF on MXene can prevent the oxidation of MXene due to the ample interlayer functional groups which diminish the exposure of surface atoms on MXenes.[201] In another study, dual heterojunction NH_2-MIL-125 modulated with a Ti_3C_2 hybrid was prepared using an in situ construction approach. Here, Ti_3C_2 nanosheets were added dropwise into the precursor aqueous solution for NH_2-MIL-125, followed by subsequent hydrothermal synthesis at 150 °C for 1 day. Interestingly, as shown in the TEM images in Figure 19c, TiO_2 is formed in the process, which is due to the hydrolysis of unreacted tetrabutyltitanate. Thus, Figure 19d shows that a type II heterojunction was formed between NH_2-MIL-125 and TiO_2, whereas a Schottky junction is formed where Ti_3C_2 acts as cocatalyst to trap photogenerated electrons.[192] Long's group also grew NH_2-MIL-88B particles on the surface of Ti_3C_2 MXenes. Figure 19e,f depicts the accordion layered structure of Ti_3C_2 MXene and hexagonal prism structure of NH_2-MIL-88B, respectively. Upon successful in situ growth of MOF on MXene, it can be observed that an optimal dispersion of NH_2-MIL-88B is achieved over the Ti_3C_2 surface, where the MXene provides growth platforms for the MOF particles, as shown in Figure 19g.[202]

Finally, MXene-based MOF composites can also be prepared by using MOFs as sacrificial templates to prepare various materials. For example, MOFs can be used to derive various carbon materials that are usually used for electrochemical applications such as batteries, supercapacitors, and electrochemical detection.[203] Nitrogen-doped porous carbon (N-PC) was prepared by carbonizing a Zn-based MOF-5-NH_2 in an Ar atmosphere at 900 °C over 2 h. Then N-PC (Figure 20a) was introduced to the Ti_3C_2 MXene (Figure 20b) via mixing and ultrasound treatment, obtaining the final MOF-derived composite denoted as Ti_3C_2/N-PC. From Figure 20c, it is noticed that the interlamellar spacing of the Ti_3C_2 MXene was enlarged, due to the successful insertion of N-PC between the gaps of the sheets.[204] Likewise, Jiang and co-workers reported the in situ decoration of MOF-derived carbon on N-doped Ti_3C_2 nanosheets for applications in Li−S batteries. Ti_3C_2 solution and PVP solution were first mixed together for 10 min, followed by the addition of $Co(NO_3)_2{\cdot}6H_2O$ and 2-methylimidazole for the growth of ZIF-67 on the surface of the MXene. Figure 20d illustrates the SEM image of Ti_3C_2/ZIF-67, indicating the effective growth of MOF on the MXene surface. Upon carbonizing the composite at 800 °C for 2 h, the 2D nanosheet morphology of N−Ti_3C_2/C inherited from the parent Ti_3C_2/ZIF-67 composite can be seen in Figure 20e. Also, in situ growth of ZIF-67-derived porous carbon mitigated the restacking of Ti_3C_2 sheets, as observed in the weaker XRD peak intensity of N−Ti_3C_2/C compared to that of Ti_3C_2 (Figure 20f).[205] Not only that, MOFs can also act as precursors to derived LDHs.[206] Hu's work reported the growth of ZIF-67 on Ti_3C_2/nickel foam (Ti_3C_2/NF), followed by an etching−doping process, where $Fe(SO_4)_2{\cdot}7H_2O$ and urea were added. The etching−doping process then yielded a MOF-derived LDH/MXene composite denoted as CoFe MLDH/NF. The LDH was obtained due to the etching of the Co ions due to the addition of urea, in which Fe salt was gradually co-precipitated with Co ions and some anions, producing CoFe LDH.[207]

6. $Ti_3C_2T_x$ MXene-BASED MOF COMPOSITES FOR SOLAR FUEL PRODUCTION

In the past, there have been numerous studies conducted on $Ti_3C_2T_x$ MXene-based composites and MOF-based composites for the photocatalytic production of solar fuels.[208] For instance, MOFs are materials that have HOMO and LUMO separated by an energy band gap, indicating their capability to generate charge carriers upon light irradiation. Even though pristine MOFs are reported to show photocatalytic activity for solar fuel production,[209,210] their efficiency is very low due to the fast recombination of charge carriers. On the other hand, due to the metallic properties of $Ti_3C_2T_x$ MXene, they can act as a cocatalyst to form a Schottky junction with other

https://doi.org/10.1021/acsomega.2c05030
ACS Omega 2022, 7, 38158−38192

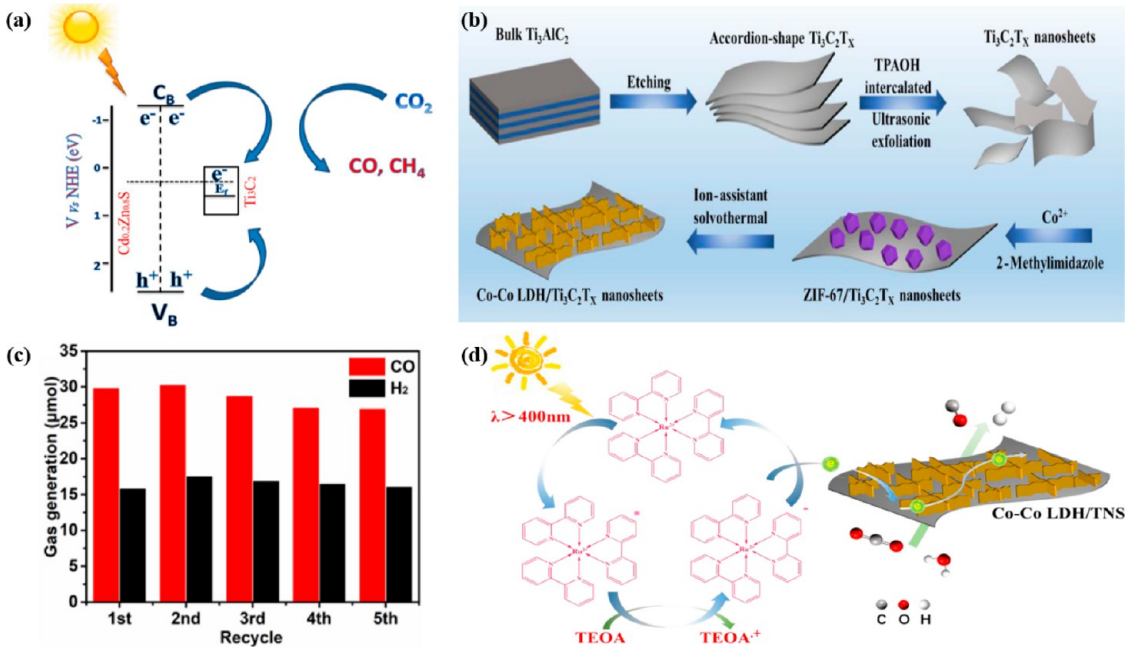

Figure 21. (a) Scheme of Schottky junction between CdZnS@Ti_3C_2 nanocomposite for CO_2 reduction. Reprinted with permission from ref 211. Copyright 2021 Elsevier. (b) Schematic diagram of the preparation of MOF-derived Co−Co LDH/$Ti_3C_2T_x$ nanosheets. (c) Photocatalytic stability over Co−Co LDH/$Ti_3C_2T_x$ for CO_2 reduction reaction. (d) Mechanism of the CO_2 reduction over the nanocomposite with $[Ru(bpy)_3]Cl_2$ photosensitizer and TEOA sacrificial agent. Reprinted with permission from ref 206. Copyright 2020 Elsevier.

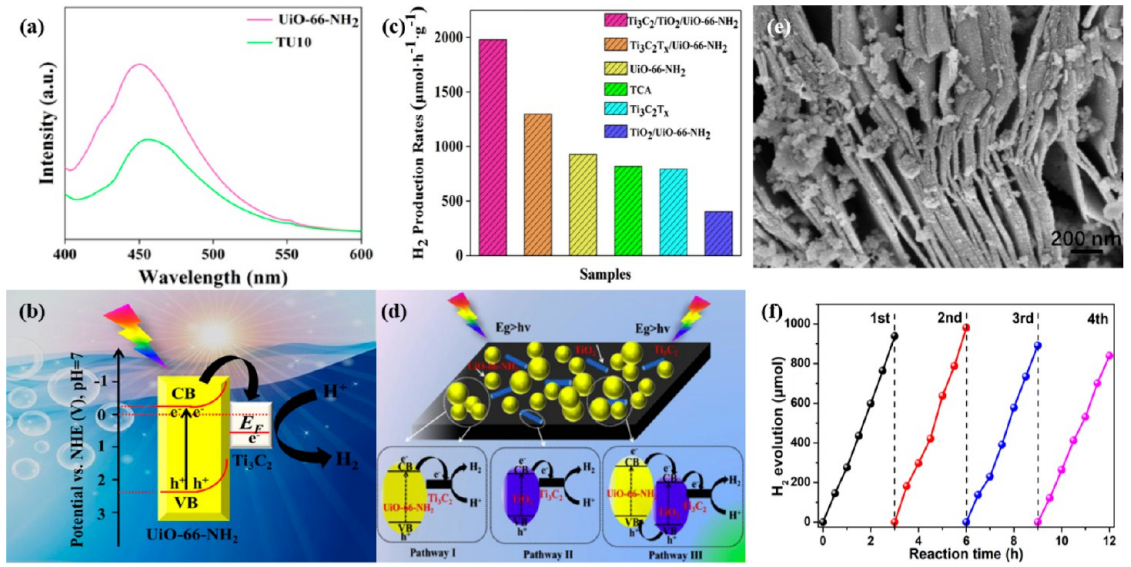

Figure 22. (a) Photoluminescence plot of pristine UiO-66-NH_2 and TU10. (b) Mechanism of the Schottky junction between UiO-66-NH_2 and $Ti_3C_2T_x$ MXenes. Reprinted with permission from ref 215. Copyright 2019 Elsevier. (c) Photocatalytic H_2 production over different catalysts, (d) Proposed mechanism of the hydrogen evolution reaction over Ti_3C_2/TiO_2/UiO-66-NH_2. Reprinted with permission from ref 216. Copyright 2019 Elsevier. (e) SEM image of Ti_3C_2@MIL-NH_2. (f) Stability test of photocatalytic H_2 formation over Ti_3C_2@MIL-NH_2. Reprinted with permission from ref 217. Copyright 2021 Elsevier.

photoactive materials to effectively trap photogenerated electrons. It was observed that the Schottky junction between the CdZnS/Ti_3C_2 nanocomposite (Figure 21a) successfully ameliorated the photocatalytic reduction of CO_2 to form CH_4 and CO due to a highly efficient charge carrier separation.[211] $Ti_3C_2T_x$ MXene-based MOF composites present a number of advantageous synergies. First, MOFs which possess high surface area and porosity are able to host MXenes and prevent the restacking and agglomeration of MXene layers. The composites are also able to show improved stability due to the synergistic effects between the surface terminal groups of MXenes and functionalities of MOFs.[212] Not only that, a built-in electric field between the MXene and MOF known as the Schottky junction is induced, where efficient separation, rapid mobility, and transportation of charge carriers are promoted.[213] $Ti_3C_2T_x$ MXene-based MOF composites can function as attractive photocatalysts for CO_2 reduction and H_2 production via water splitting. However, there are only a handful of studies conducted on the composite for solar fuel production.

https://doi.org/10.1021/acsomega.2c05030
ACS Omega 2022, 7, 38158−38192

Table 3. Summary of Ti_3C_2 MXene-Based MOF Photocatalyst for Production of Solar Fuels

catalysts	operating conditions	results	ref
MOF-derived Co−Co LDH/$Ti_3C_2T_x$	•0.5 mg of catalyst •$[Ru(bpy)_3]Cl_2·6H_2O$ photosensitizer •MeCN/H_2O/TEOA = 3/2/1 mL •5 W LED lamp •light intensity = 32.3 mW cm^{-2}	•CO = 6.248 μmol h^{-1} •CO = 1.25 × 10^4 μmol h^{-1} g^{-1} •AQE = 0.92%	206
Ti_3C_2/UiO-66-NH_2	•20 mg of catalyst •0.1 M Na_2S and 0.1 M Na_2SO_3 (50 mL) •350 W Xe lamp •atmospheric temperature and pressure •light intensity = 10 mW cm^{-2}	•formation of Schottky junction •H_2 = 204 μmol h^{-1} g^{-1}	215
Ti_3C_2/TiO_2/UiO-66-NH_2	•20 mg of catalyst •0.1 M Na_2S and 0.1 M Na_2SO_3 (50 mL) •300 W Xe lamp •T = 5 °C •light intensity = 10 mW cm^{-2}	•formation of Schottky junction and heterojunctions •H_2 = 1980 μmol h^{-1} g^{-1}	216
in situ grown Ti_3C_2@MIL-NH_2	•70 mg of catalyst •20 mL of CH_3OH and 0.3 mL of TEOA •300 W Xe arc lamp •light intensity = 552 mW cm^{-2}	•H_2 = 4383.1 μmol h^{-1} g^{-1}	217
TiO_2−Ti_3C_2−CoS_x	•20 mg of catalyst •40 mL of distilled water and 10 mL of methanol •300 W Xe arc lamp •UV−visible irradiation	•CoS_x derived from ZIF-67 •H_2 = 0.95 mmol h^{-1} g^{-1}	218
UiO-66-NH_2(Zr/Ti)/ carboxyl-functionalized MXene (UZR/CFMX)	•10 mg of catalyst •10 vol % triethanolamine and 400 μL of H_2PtCl_6 •300 W Xe lamp	•decorated carboxyl group on Ti_3C_2 MXene •H_2 = 2187 μmol g^{-1} h^{-1}	219

Chen and co-workers prepared a $Ti_3C_2T_x$ composite with MOF-derived Co−Co LDH nanosheets, as shown in Figure 21b, for visible light CO_2 reduction in the presence of a $[Ru(bpy)_3]Cl_2$ photosensitizer. The bulk Ti_3AlC_2 MAX was subjected to etching to remove the Al layers, followed by ultrasonic exfoliation to obtain $Ti_3C_2T_x$ nanosheets (TNS). Then in situ growth of ZIF-67 was conducted on the $Ti_3C_2T_x$ nanosheets. Upon successful loading of ZIF-67, the nanocomposite was subjected to solvothermal treatment, in which Co−Co LDH/TNS nanosheets were obtained. Pristine $Ti_3C_2T_x$ nanosheets did not show any photocatalytic CO_2 reduction activity. However, upon optimal loading of 15 mg of TNS on the MOF-derived Co−Co LDH, maximum CO generation rate of 1.25 × 10^4 μmol h^{-1} g^{-1} was achieved. The nanocomposite also exhibited an excellent stability, maintaining good photocatalytic performance for up to five cycles, as illustrated in Figure 21c. Figure 21d depicts the photocatalytic mechanism of the Co−Co LDH/TNS nanocomposite in the presence of a photosensitizer. Upon visible light irradiation, the photosensitizer is excited but is subsequently quenched by the TEOA electron donor to form a $[Ru(bpy)_3]Cl_2^-$ reduced state. The electrons are then transmitted to the nanocomposite, where the electrons are rapidly migrated to the Co active sites for the reduction of CO_2 to CO.[206]

$Ti_3C_2T_x$ MXene-based composites are also widely used as catalysts for photocatalytic water splitting to produce H_2. $Ti_3C_2T_x$ MXenes are two-dimensional sheets that boast a large surface area/volume ratio as well as strong hydrophilicity, which improves the interaction between the photocatalyst and water molecules.[214] Tian et al. modified $Ti_3C_2T_x$ nanosheets by introducing a water-stable and porous Zr-based UiO-66-NH_2 for efficient photocatalytic hydrogen evolution reaction. It was observed that the pristine UiO-66-NH_2 MOF displayed limited H_2 production at only 25.6 μmol h^{-1} g^{-1}. Upon introduction of Ti_3C_2 nanosheets, the photocatalytic activity of the composite (denoted as TU10) increased 8-fold, achieving H_2 formation of 204 μmol h^{-1} g^{-1}. This is obviously due to the formation of a Schottky junction between $Ti_3C_2T_x$ and UiO-66-NH_2. As shown in the photoluminescence plot in Figure 22a, the $Ti_3C_2T_x$-modified UiO-66-NH_2 sample showed an intensity lower than that of unmodified UiO-66-NH_2, elucidating a lower recombination rate over the composite. Figure 22b illustrates the energy level diagram of TU10, in which the electrons are first excited from the VB to CB of the UiO-66-NH_2, followed by migration of electrons from CB of the MOF to Ti_3C_2. The efficient migration and spatial separation of electrons was mainly attributed to the O-terminated Ti_3C_2 having a low Gibbs free energy and highly positive Fermi level, which makes it trap electrons from the MOF for H_2 production.[215]

Similarly, Ti_3C_2 MXenes were first annealed in a N_2 atmosphere to obtain TiO_2 layers, followed by coating UiO-66-NH_2 on the surface of $Ti_3C_2T_x$ layers, obtaining a Ti_3C_2/TiO_2/UiO-66-NH_2 composite. From the activity test shown in Figure 22c, the annealing of $Ti_3C_2T_x$ to produce TiO_2 increased the photocatalytic production by 1.5 times compared to that of its Ti_3C_2/UiO-66-NH_2 counterpart. This is because the formation of TiO_2 induced a negative shift in the Mott−Schottky plots, elucidating an enhanced electron/hole pair separation as well as stronger reducibility. Not only that, the intimate contact as well as the favorable Fermi level and band gaps of Ti_3C_2, UiO-66-NH_2, and TiO_2 constructed various pathways for accelerating the transfer of electron/hole pairs. As illustrated in Figure 22d, the first and second pathway is via the

https://doi.org/10.1021/acsomega.2c05030
ACS Omega 2022, 7, 38158−38192

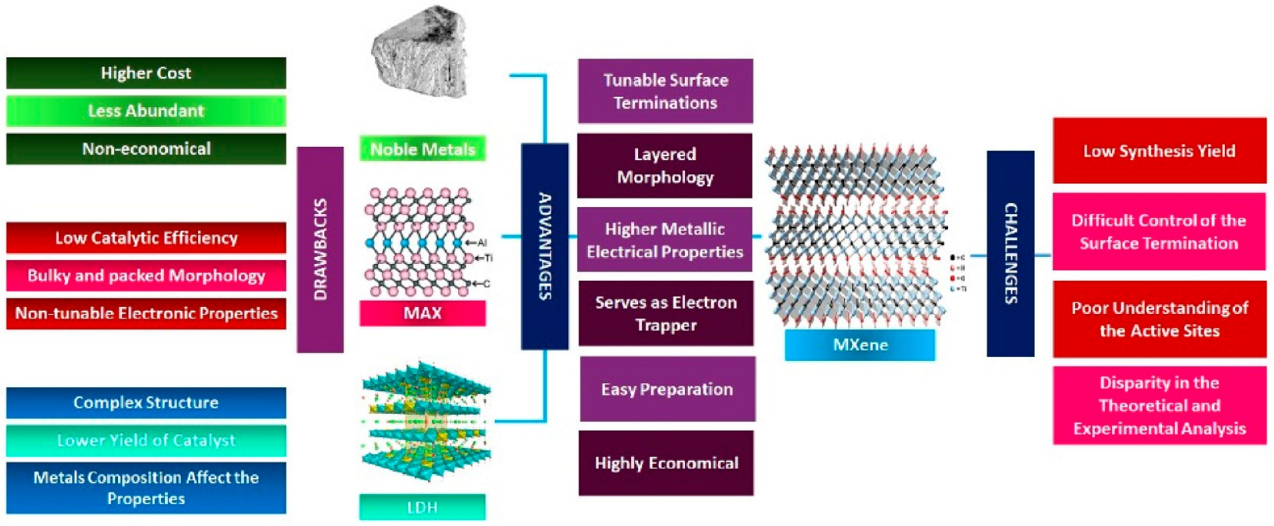

Figure 23. Drawbacks of other cocatalysts and advantages of MXenes.

Schottky junction between Ti_3C_2 nanosheets with UiO-66-NH_2 and TiO_2, respectively. The third pathway is the type II heterojunction system between UiO-66-NH_2 and TiO_2, followed by the transfer of electrons from the CB of TiO_2 to Ti_3C_2 MXene.[216] Fascinatingly, Li and co-workers successfully coordinated the Ti atom in Ti_3C_2 MXenes with MIL-NH_2 via in situ growth, producing a Ti_3C_2@MIL-NH_2 composite. Compared to conventional physical mixing of Ti_3C_2 with MIL-NH_2, the in situ grown Ti_3C_2@MIL-NH_2 boasted a 5-fold H_2 production rate compared to that of the former. This is due to the intimate contact between the Ti_3C_2 and MIL-NH_2, as shown in the SEM image in Figure 22e. Also, the self-aggregation of the MIL-NH_2 is inhibited due to the even immobilization of MIL-NH_2 on the surface of the MXene. Figure 22f displays that Ti_3C_2@MIL-NH_2 also exhibited excellent stability, where the H_2 production rate showed insignificant decrease even after four cycles. The excellent photoactivity and stability are attributed to the rapid photoinduced electrons from the MOF to Ti_3C_2 via the Ti−N path. This in turn enriches the Ti_3C_2 with electrons, where H^+ is effectively adsorbed and reduced to H_2.[217] Nevertheless, despite limited studies conducted, 2D Ti_3C_2 sheets coupled with MOF composites show great promise as a photocatalyst for efficient solar fuel production and should be studied intensively in future works. Table 3 presents the summary of Ti_3C_2 MXene-based MOF photocatalysts for the production of solar fuels.

7. CHALLENGES AND COMPARATIVE ANALYSIS OF $Ti_3C_2T_x$ MXene

Here, the challenges and comparative analysis of Ti_3C_2 MXenes with other materials are discussed and summarized, as shown in Figure 23. Higher work function in $Ti_3C_2T_x$ MXene and their role as an electron trapper gave them potential to maximize the solar fuel production. However, some challenges that require attention for employing $Ti_3C_2T_x$ MXene as photoactivity enhancer include the control of their termination functional groups. The tunable termination groups, T_x, have a significant influence in the electronic and optical properties. Studies suggested that MXene materials could either exhibit semiconducting or metallic properties depending on the type of termination groups present.[47] Different termination properties might affect their photocatalytic efficiency due to differences in the work function value. The difference in the work function based on terminating groups was theoretically explicated due to changes in the total surface dipole moments and the transfer of charge between active sites of $Ti_3C_2T_x$ MXene with the termination groups.[46] Theoretical studies divulged that the −O-terminated $Ti_3C_2T_x$ MXene exhibits a work function of 5.75−6.25 eV, whereas −OH-terminated $Ti_3C_2T_x$ MXene was found to possess a work function of 1.6−2.8 eV.[220] In photocatalysis processes, such as that in hydrogen production, studies suggested that a large difference in the metal work function between the main catalyst and the metal cocatalyst could optimally stimulate the solar to hydrogen conversion.[114] However, experimental evaluation revealed that a perfect single termination group is not possible to achieve, causing a great disparity with the theoretical analysis. Moreover, it is difficult to control the distribution of the termination groups in the MXene materials.[11] Therefore, the synthesis of mixed terminating $Ti_3C_2T_x$ MXene might offer different results and catalytic efficiency. Other challenges can be observed in the thicker layer of $Ti_3C_2T_x$ MXene, which is found to be difficult to employ as an electron mediator, resulting in weak contact formation between two photocatalysts.[183] In the context for commercializing $Ti_3C_2T_x$ MXene in high-scale production, it was noticed that the yield is still low, and up to the current development, many preparation methods are still unable to develop high-yield $Ti_3C_2T_x$ MXene which can par up to high scalability industrial production.

Nevertheless, in the regards of their beneficial attribution, most of the studies suggested that employing $Ti_3C_2T_x$ MXene as a cocatalyst offers an indisputable and positive result in ameliorating the performances of the semiconductors.[121,139,199,221] Higher metal electrical conductivity and unique properties prevailed them as one of the potentially influence materials to substitute non-economic and low efficiency cocatalysts. Moreover, a tailorable work function to fit specific application requirements is one of the distinct properties of $Ti_3C_2T_x$ MXene compared to other metallic materials such as noble metals. Not to mention, their economical synthesis cost and easily accessible precursor is one of the positive attributes which leads the way for

https://doi.org/10.1021/acsomega.2c05030
ACS Omega 2022, 7, 38158−38192

commercialization. On the other hand, $Ti_3C_2T_x$ MXene material is new and is still under exploration where the their physical, catalytic, and chemical properties is still undergoing thorough research for more improvement which may facilitate more promising discoveries. Their unique morphology and possible conversion to different morphological dimension is one of the compelling characteristics of $Ti_3C_2T_x$ MXene. This is due to the ability of their multilayer structure to delaminate into monolayer flakes, convert to quantum dots, and form a hierarchical structure, extending their performance in the field of photocatalysis.

Other materials that have similar properties of $Ti_3C_2T_x$ MXene include noble metals such as Ag, Au, and Pt. The compelling characteristics of noble metal in the energy conversion field such as surface plasmon resonance effects and their potential to create the Schottky barrier enable them to be one of the leading metal cocatalysts. However, the main drawback in employing noble metals despite their positive influence on the photocatalytic activity is due to the exorbitant prices.[222] Comparatively, $Ti_3C_2T_x$ MXene is regarded as the best substitution for noble metals with similar functionality and affordable material cost, which is commercially viable. Therefore, a high-scale production of semiconductor materials is more economic by employing $Ti_3C_2T_x$ MXene compared to noble metals. Moreover, the work function of $Ti_3C_2T_x$ MXene is highly comparable to those of noble metals ranging from 3.9 to 6.25 eV.[223] In parallel, functional properties similar to those of noble metal including the creation of a potential energy barrier between the metal−semiconductor enhance the carrier dynamics and efficiently mediate the electrons transfer.

In terms of the morphological structure, $Ti_3C_2T_x$ MXenes are known to be morphologically layered with a 2D structure, which is often referred to as an accordion-like shape. The accordion-like structure of $Ti_3C_2T_x$ MXene offers a large surface area compared to that of the Ti_3AlC_2 MAX precursor, which is bulky, compact, and has dense layers.[224] Loose layers with a bigger space interval of $Ti_3C_2T_x$ MXene provide efficient site attachment for other semiconductors compared to MAX material, which exhibits more packed layers. Stronger interfacial contact between the semiconductor and $Ti_3C_2T_x$ MXene supports the charge transmission and expedites the redox reaction. Moreover, $Ti_3C_2T_x$ MXene offers a stable platform for a uniform distribution of the particulate semiconductors and inhibits the agglomeration. In addition, the well-defined layers of $Ti_3C_2T_x$ MXene with a space interval support the redox reaction taking place at the inner and outer layers.[139] Even though numerous studies suggested that Ti_3AlC_2 MAX could promote the solar to fuel conversion, their catalytic efficiency is still not comparable to that of $Ti_3C_2T_x$ MXene.[225] As previously mentioned, the removal of an Al layer through chemical etching could terminate the surfaces of Ti with functional groups such as −OH, −F, and −O. These functional groups known as surface terminations provide excellent contact with water molecules and exhibit stronger hydrophilicity. Compared to Ti_3AlC_2 MAX, the presence of functional group such as −OH stimulate the hydrogen generation through the reduction into hydrogen through water capture.

In different material studies, similar layered structures often utilized as a cocatalyst known as layered double hydroxide exhibit the flexibility and diversity in their compositional matrix. Similar to MXene materials, LDH existed in a multilayered structure form, and their electronic properties are easily tuned according to the types of metal cations and anions present in their matrix structures.[27] LDH consisted of layers that stacked onto each other, where they exhibit negatively and positively charged layer. Generally, the positively charged layer of LDH consisted of metal cations while the negatively charged layers, known as interlamellar spaces, are composed of the intercalated anions. Therefore, the unique structure of LDHs attracts research attention to further explore their potential in photocatalytic fuel conversion field. However, the LDH structure, the metal coordination, and their nature need to be meticulously studied. In addition, their complicated structure and design criterion are some of the great challenges in employing LDH as a cocatalyst. Some criteria that require extra attention in designing LDH material include the nature of metal cations incorporated into the host layer of LDH, the compositional control of each metal cations, and their valence states and the anion intercalation. The mentioned design parameters could affect the fabrication of the LDH materials and their photocatalytic efficiency.[226] For instance, mismatched metal cation pairing will lower the photocatalytic performances, and some might be inactive. Even though their energy gap can be tuned to meet specific application requirements, their complicated synthesis process and design criteria limit their role as compelling semiconductors. Therefore, the best alternative is to employ $Ti_3C_2T_x$ MXene, which is economically affordable, is easily fabricated, and exhibits tunable electronic properties, unique structural properties, and excellent photocatalytic efficiency.

8. CONCLUSION

In conclusion, $Ti_3C_2T_x$ MXenes are a class of materials that has seen widespread use in the field of photocatalysis. MXenes tend to exist in 0D quantum dots but usually adopt 2D layered morphologies that are able to provide a high surface area/volume ratio. However, pristine MXenes are unable to initiate any photocatalytic activity for solar fuel production as they do not have energy band gaps. The absence of a band gap means that there will not be any formation of electron/hole pairs despite light irradiation. Nevertheless, $Ti_3C_2T_x$ is an excellent cocatalyst for photocatalytic fuel production due to its metallic properties, which allows it to function as an efficient electron sink and trap. $Ti_3C_2T_x$ MXenes are usually hybridized with other materials containing energy band gaps such as semiconductors. This is due to the photogenerated electrons from the CB of the semiconductor to the $Ti_3C_2T_x$ MXene, which has a more positive Fermi level. The efficient transfer of electrons will then ameliorate and prolong the lifetime of charge carriers, enhancing the photocatalytic formation of solar fuels.

The employment of $Ti_3C_2T_x$ MXene in the solar fuel conversion field offers a sustainable approach for producing a clean and renewable energy source. Excellent metallic electrical conductivity of $Ti_3C_2T_x$ MXene endows them with the ability to construct an electrostatic potential barrier which aids in the improvement of carrier dynamics and elevates their potential as highly sought-after cocatalysts. Mainly, HF etching is the pioneering technique for synthesizing $Ti_3C_2T_x$ MXene with a −F termination group. However, their prominent role as a photocatalytic driver led to the development of various synthesis techniques, which facilitate tailoring their surface terminating groups. It is worth mentioning the blossoming of the synthesis techniques favoring the morphological development of $Ti_3C_2T_x$ MXene into different structural growth.

https://doi.org/10.1021/acsomega.2c05030
ACS Omega 2022, 7, 38158−38192

Tailorable functional groups with modifiable structure boosted their photoredox activity and improved the overall photocatalytic efficiency.

Metal−organic frameworks are another class of materials that possess a wide range of unique properties that make them promising candidates as photocatalysts. First, they have an extremely high surface area, usually in the range of a few thousand square meters per gram. Pores with large volume and uniform size are riddled all over the surface of the MOF, allowing them to effectively adsorb small gas molecules as well as large dye molecules. Interestingly, despite the usual 3D polyhedrons of MOFs, they can also naturally exist in 1D rods or 2D sheets, as well. These multidimensional MOFs can be obtained via different synthesis steps, namely, the solvothermal synthesis, the co-precipitation method, the slow evaporation method, and the microwave-assisted approach. Under solar energy irradiation, MOFs are able to generate photoinduced charge carriers. This is because they have a narrow energy band gap, where electrons can be excited from the HOMO to LUMO when photons with sufficient energy strike the surface of the MOF. Finally, MOFs can function as a sacrificial template to form other derivatives. Metal oxides are derived when MOFs are subjected to thermal treatment, whereas LDHs can be obtained when the MOFs undergo the hydrolyzed etching step.

In an effort to further improve the photocatalytic activity of both $Ti_3C_2T_x$ MXenes and MOFs, various design principles and considerations were taken into account. In this context, the design considerations were discussed in three main criteria, namely, the morphological engineering of $Ti_3C_2T_x$ and MOFs, the active sites over $Ti_3C_2T_x$-based MOF nanocomposites, and the interfacial/heterojunction engineering. In recent years, huge strides have been made in modifying the conventional 2D accordion-like multilayer of $Ti_3C_2T_x$, such as the formation of 0D quantum dots, 2D delaminated flakes, and 3D multidimensional structures. These can be achieved via various approaches such as delamination with or without intercalating agents and combining with various domains of different dimensions. Similarly, the morphology and dimensions of MOFs can be tuned between 1D rods, 2D sheets, or 3D polyhedrons by adjusting the synthesis parameters such as reaction time, temperature, and solvent ratio. Also, the use of surfactants such as polyvinylpyrrolidone and cetyltrimethylammonium bromide can effectively modulate the structure of MOFs. The active sites of MOFs were also discussed, where active sites can be found naturally on the MOF or by further introduction of the MOF by anchoring them on the organic ligands or cavity of the MOF.

The metallic nature of $Ti_3C_2T_x$ MXenes make them highly promising cocatalysts due to their ability to trap electrons via the formation of a Schottky barrier with other photoresponsive materials. Interestingly, a $Ti_3C_2T_x$ MXene−TiO_2 hybrid could be generated as a result of oxidation, opening the door to hybrid Schottky−Z-scheme/Schottky−type II heterojunction systems. Also, there are reports that $Ti_3C_2T_x$ can also serve as an electron mediator for Z-scheme heterojunction systems. Similar to semiconductors, MOFs are able to generate electron/hole pairs upon light irradiation, making them serviceable photocatalysts. However, their efficiency can be further improved via a series of strategies, such as formation of heterojunctions with other photoresponsive materials, surface sensitization with materials with metallic properties, functionalization of MOFs, doping, and use of photosensitizers. By deploying these strategies, the photocatalytic activity of MOFs can be enhanced as the light harvesting especially in the visible spectrum is ameliorated, and a narrower E_{bg} is achieved, and spatial charge carrier separation is realized. By preparing $Ti_3C_2T_x$ MXene-based MOF photocatalysts, the photocatalytic activity can be effectively enhanced due to various synergistic effects such as boosted stability and formation of a built-in electric field known as the Schottky junction. Despite promising findings from Ti_3C_2-based MOF composites for solar fuel production, there is still very limited studies conducted. Hence, it is recommended to further explore Ti_3C_2 with various MOFs for photocatalytic CO_2 reduction and water splitting reactions.

9. FUTURE PERSPECTIVE

In short, $Ti_3C_2T_x$ and MOFs have made huge progress over the years. For instance, various new synthesis approaches were discovered, in turn producing a wide range of structures for both $Ti_3C_2T_x$ MXene and MOFs. Similarly, both materials have seen an increasing role as photocatalysts in the production of renewable solar fuels. Hence, $Ti_3C_2T_x$ MXene-based MOF nanotextures are highly promising photocatalysts for the production of green and renewable solar fuels. This is due to the synergistic effect between the two materials, in which MOFs are able to generate electron/hole pairs, whereas MXenes can effectively trap the electrons. This in turn will prolong the lifetime of charge carriers and ameliorate the production of solar-driven fuels. However, up to now, there is only a handful of research done on Ti_3C_2 MXene-based MOF composite on the applications of CO_2 reduction and solar-driven H_2 production. Thus, the future prospects are as follows:

1. Different type of MXenes as well as morphologies should be utilized for the photocatalytic production of solar fuels. For example, different MXenes such as Nb_2C, V_2C, and Mo_2C should be explored as cocatalysts for renewable fuel production. Other than 2D accordion layered structures of MXenes, facile synthesis approaches for 0D MXene quantum dots and exfoliated monolayer MXenes should also be researched intensively.
2. The exact active sites of $Ti_3C_2T_x$ MXene are yet to be confirmed. It is suggested for more studies to be conducted to identify, quantify, and gain a deeper understanding on the active sites over MXenes. Also, the study on the active sites can provide more insights into ways to further boost the role of $Ti_3C_2T_x$ MXene as a cocatalyst for solar fuel production.
3. Over the years, MXenes are mainly prepared using HF etching, which is detrimental to the environment due to the use of harsh chemicals. Also, formation of QDs of monolayered MXenes utilizes various intercalating agents like DMSO TMAOH, which may pose environmental threats. Therefore, more research must be conducted on the green synthesis of MXenes to reduce the negative impact on the environment.
4. A solvothermal synthesis method is most commonly used to prepare a wide range of MOFs. However, they are severely limited by their long reaction time, inhomogeneous heating, and huge heat loss. Thus, it is recommended that more studies be conducted on other synthesis methods such as the microwave-assisted

https://doi.org/10.1021/acsomega.2c05030
ACS Omega 2022, 7, 38158−38192

method to not only speed up the preparation period but also improve the efficiency and homogeneity of heating.

5. More combinations of MOFs must be explored by either experimenting with different metal nodes, metal clusters, or linkers to obtain MOFs with enhanced photocatalytic activity for solar fuel production. Also, energy band gap engineering should also be conducted to further improve the light harvesting and utilization of MOFs especially in the visible light spectrum.
6. Lastly, more research is needed on $Ti_3C_2T_x$ MXene-based MOF nanotextures to produce renewable solar fuels. Despite its promising properties and characteristics, there are still limited studies on MXene/MOF for CO_2 reduction and production of H_2 solar fuels. Different types of MOFs can be paired together with $Ti_3C_2T_x$ MXene to further unveil and gain a better understanding on the interaction and mechanism of the overall photocatalytic process.

AUTHOR INFORMATION

Corresponding Author

Muhammad Tahir − *Chemical and Petroleum Engineering Department, UAE University, Al Ain, United Arab Emirates;* orcid.org/0000-0002-2937-5645;
Email: muhammad.tahir@uaeu.ac.ae, bttahir@yahoo.com

Authors

Wei Keen Fan − *School of Chemical and Energy Engineering, Universiti Teknologi Malaysia, 81310 Johor Bahru, Johor, Malaysia*

Areen Sherryna − *School of Chemical and Energy Engineering, Universiti Teknologi Malaysia, 81310 Johor Bahru, Johor, Malaysia*

Complete contact information is available at: https://pubs.acs.org/10.1021/acsomega.2c05030

Notes

The authors declare no competing financial interest.

ACKNOWLEDGMENTS

The financial supports for this work were provided by Ministry of Higher Education (MOHE) under Fundamental Research Grant Scheme (FRGS, R.J130000.7351.4L952).

REFERENCES

(1) Lingampalli, S. R.; Ayyub, M. M.; Rao, C. N. R. Recent Progress in the Photocatalytic Reduction of Carbon Dioxide. *ACS Omega* **2017**, *2* (6), 2740−2748.

(2) Fan, W. K.; Tahir, M. Structured clay minerals-based nanomaterials for sustainable photo/thermal carbon dioxide conversion to cleaner fuels: A critical review. *Sci. Total Environ.* **2022**, *845*, 157206.

(3) Ranjekar, A. M.; Yadav, G. D. Steam Reforming of Methanol for Hydrogen Production: A Critical Analysis of Catalysis, Processes, and Scope. *Ind. Eng. Chem. Res.* **2021**, *60* (1), 89−113.

(4) Fan, W. K.; Tahir, M. Investigating the product distribution behaviour of CO_2 methanation through thermodynamic optimized experimental approach using micro/nano structured titania catalyst. *Energy Convers. Manage.* **2022**, *254*, 115240.

(5) Hurtado, L.; Mohan, A.; Ulmer, U.; Natividad, R.; Tountas, A. A.; Sun, W.; Wang, L.; Kim, B.; Sain, M. M.; Ozin, G. A. Solar CO_2 hydrogenation by photocatalytic foams. *Chem. Eng. J.* **2022**, *435*, 134864.

(6) Qureshi, W. A.; Hong, X.; He, X.; Liu, Q.; Xu, D.; Maouche, C.; Sun, Z.; Yang, J. Dual plasmonic Au and TiN cocatalysts to boost photocatalytic hydrogen evolution. *Chemosphere* **2022**, *291*, 132987.

(7) Tahir, M.; Fan, W. K.; Hasan, M. Investigating influential effect of methanol-phenol-steam mixture on hydrogen production through thermodynamic analysis with experimental evaluation. *Int. J. Energy Res.* **2022**, *46*, 964−979.

(8) Li, G.; Yang, C.; He, Q.; Liu, J. Ag-based photocatalytic heterostructures: Construction and photocatalytic energy conversion application. *J. Environ. Chem. Eng.* **2022**, *10*, 107374.

(9) Tasleem, S.; Tahir, M. Investigating the performance of liquid and gas phase photoreactors for dynamic H_2 production over bimetallic TiO_2 and Ni_2P dispersed MAX Ti_3AlC_2 monolithic nanocomposite under UV and visible light. *J. Environ. Chem. Eng.* **2021**, *9* (4), 105351.

(10) Zhang, C.; Zhang, W.; Qian, J.; Cheng, H.; Ren, S.; Zhang, C.; Ma, J.; Guo, Z. Simple Preparation of Hierarchically Porous Ce/TiO_2/Graphitic Carbon Microspheres for the Reduction of CO_2 with H_2O under Simulated Solar Irradiation. *ACS Omega* **2019**, *4* (16), 16833−16839.

(11) Naguib, M.; Kurtoglu, M.; Presser, V.; Lu, J.; Niu, J.; Heon, M.; Hultman, L.; Gogotsi, Y.; Barsoum, M. W. Two-dimensional nanocrystals produced by exfoliation of Ti_3AlC_2. *Adv. Mater.* **2011**, *23* (37), 4248−53.

(12) Yang, W.; Ma, G.; Fu, Y.; Peng, K.; Yang, H.; Zhan, X.; Yang, W.; Wang, L.; Hou, H. Rationally designed Ti_3C_2 MXene@TiO_2/$CuInS_2$ Schottky/S-scheme integrated heterojunction for enhanced photocatalytic hydrogen evolution. *Chem. Eng. J.* **2022**, *429*, 132381.

(13) Biswal, L.; Mohanty, R.; Nayak, S.; Parida, K. Review on MXene/TiO_2 nanohybrids for photocatalytic hydrogen production and pollutant degradations. *J. Environ. Chem. Eng.* **2022**, *10* (2), 107211.

(14) Tahir, M.; Ali Khan, A.; Tasleem, S.; Mansoor, R.; Fan, W. K. Titanium Carbide (Ti_3C_2) MXene as a Promising Co-catalyst for Photocatalytic CO_2 Conversion to Energy-Efficient Fuels: A Review. *Energy Fuels* **2021**, *35* (13), 10374−10404.

(15) Sherryna, A.; Tahir, M. Role of Ti_3C_2 MXene as Prominent Schottky Barriers in Driving Hydrogen Production through Photo-induced Water Splitting: A Comprehensive Review. *ACS Appl. Energy Mater.* **2021**, *4* (11), 11982−12006.

(16) Tariq, A.; Ali, S. I.; Akinwande, D.; Rizwan, S. Efficient Visible-Light Photocatalysis of 2D-MXene Nanohybrids with Gd(3+)- and Sn(4+)-Codoped Bismuth Ferrite. *ACS Omega* **2018**, *3* (10), 13828−13836.

(17) Nguyen, T. P.; Tuan Nguyen, D. M.; Tran, D. L.; Le, H. K.; Vo, D.-V. N.; Lam, S. S.; Varma, R. S.; Shokouhimehr, M.; Nguyen, C. C.; Le, Q. V. MXenes: Applications in electrocatalytic, photocatalytic hydrogen evolution reaction and CO_2 reduction. *Mol. Catal.* **2020**, *486*, 110850.

(18) Xia, B.; Yang, Y.; Zhang, Y.; Xia, Y.; Jaroniec, M.; Yu, J.; Ran, J.; Qiao, S.-Z. Metal−organic framework with atomically dispersed Ni−N_4 sites for greatly-raised visible-light photocatalytic H_2 production. *Chem. Eng. J.* **2022**, *431*, 133944.

(19) Li, H.; Eddaoudi, M.; O'Keeffe, M.; Yaghi, O. M. Design and synthesis of an exceptionally stable and highly porous metal-organic framework. *Nature* **1999**, *402* (6759), 276−279.

(20) Yang, X.; Wen, Z.; Wu, Z.; Luo, X. Synthesis of ZnO/ZIF-8 hybrid photocatalysts derived from ZIF-8 with enhanced photocatalytic activity. *Inorg. Chem. Front.* **2018**, *5* (3), 687−693.

(21) Chen, D.; Xing, H.; Wang, C.; Su, Z. Highly efficient visible-light-driven CO_2 reduction to formate by a new anthracene-based zirconium MOF via dual catalytic routes. *J. Mater. Chem. A* **2016**, *4* (7), 2657−2662.

(22) Fan, W. K.; Tahir, M. Current Trends and Approaches to Boost the Performance of Metal Organic Frameworks for Carbon Dioxide Methanation through Photo/Thermal Hydrogenation: A Review. *Ind. Eng. Chem. Res.* **2021**, *60* (36), 13149−13179.

(23) Huang, K.; Li, C.; Li, H.; Ren, G.; Wang, L.; Wang, W.; Meng, X. Photocatalytic Applications of Two-Dimensional Ti_3C_2 MXenes: A Review. *ACS Appl. Nano Mater.* **2020**, *3* (10), 9581−9603.
(24) Tang, R.; Xiong, S.; Gong, D.; Deng, Y.; Wang, Y.; Su, L.; Ding, C.; Yang, L.; Liao, C. Ti_3C_2 2D MXene: Recent Progress and Perspectives in Photocatalysis. *ACS Appl. Mater. Interfaces* **2020**, *12* (51), 56663−56680.
(25) Li, Y.; Ding, L.; Guo, Y.; Liang, Z.; Cui, H.; Tian, J. Boosting the Photocatalytic Ability of g-C_3N_4 for Hydrogen Production by Ti_3C_2 MXene Quantum Dots. *ACS Appl. Mater. Interfaces* **2019**, *11* (44), 41440−41447.
(26) He, F.; Zhu, B.; Cheng, B.; Yu, J.; Ho, W.; Macyk, W. 2D/2D/0D $TiO_2/C_3N_4/Ti_3C_2$ MXene composite S-scheme photocatalyst with enhanced CO_2 reduction activity. *Appl. Catal., B* **2020**, *272*, 119006.
(27) Sherryna, A.; Tahir, M.; Nabgan, W. Recent advancements of layered double hydroxide heterojunction composites with engineering approach towards photocatalytic hydrogen production: A review. *Int. J. Hydrogen Energy* **2022**, *47* (2), 862−901.
(28) Fan, W. K.; Tahir, M. Recent developments in photothermal reactors with understanding on the role of light/heat for CO_2 hydrogenation to fuels: A review. *Chem. Eng. J.* **2022**, *427*, 131617.
(29) Li, X.; Yu, J.; Jaroniec, M. Hierarchical photocatalysts. *Chem. Soc. Rev.* **2016**, *45* (9), 2603−2636.
(30) Fan, W. K.; Tahir, M. Recent advances on cobalt metal organic frameworks (MOFs) for photocatalytic CO_2 reduction to renewable energy and fuels: A review on current progress and future directions. *Energy Convers. Manage.* **2022**, *253*, 115180.
(31) Tahir, M.; Fan, W. K.; Tahir, B. MOF-Based Catalysts for Production of Value-Added Fine Chemicals from Carbon Dioxide. *Metal−Organic Frameworks for Carbon Capture and Energy*; American Chemical Society, 2021; pp 155−171.
(32) Khan, A. A.; Tahir, M. Recent advancements in engineering approach towards design of photo-reactors for selective photocatalytic CO_2 reduction to renewable fuels. *J. CO2 Util.* **2019**, *29*, 205−239.
(33) Zhang, W.; Mohamed, A. R.; Ong, W. J. Z-Scheme Photocatalytic Systems for Carbon Dioxide Reduction: Where Are We Now? *Angew. Chem., Int. Ed.* **2020**, *59* (51), 22894−22915.
(34) Costentin, C.; Robert, M.; Savéant, J.-M. Catalysis of the electrochemical reduction of carbon dioxide. *Chem. Soc. Rev.* **2013**, *42* (6), 2423−2436.
(35) Habisreutinger, S. N.; Schmidt-Mende, L.; Stolarczyk, J. K. Photocatalytic reduction of CO_2 on TiO_2 and other semiconductors. *Angew. Chem., Int. Ed.* **2013**, *52* (29), 7372−7408.
(36) Barton Cole, E.; Lakkaraju, P. S.; Rampulla, D. M.; Morris, A. J.; Abelev, E.; Bocarsly, A. B. Using a one-electron shuttle for the multielectron reduction of CO_2 to methanol: kinetic, mechanistic, and structural insights. *J. Am. Chem. Soc.* **2010**, *132* (33), 11539−11551.
(37) Sherryna, A.; Tahir, M. Role of surface morphology and terminating groups in titanium carbide MXenes ($Ti_3C_2T_x$) cocatalysts with engineering aspects for modulating solar hydrogen production: A critical review. *Chem. Eng. J.* **2022**, *433*, 134573.
(38) Huang, S.; Long, Y.; Ruan, S.; Zeng, Y. J. Enhanced Photocatalytic CO_2 Reduction in Defect-Engineered Z-Scheme WO_{3-x}/g-C_3N_4 Heterostructures. *ACS Omega* **2019**, *4* (13), 15593−15599.
(39) Handoko, A. D.; Steinmann, S. N.; Seh, Z. W. Theory-guided materials design: two-dimensional MXenes in electro- and photocatalysis. *Nanoscale Horizons* **2019**, *4* (4), 809−827.
(40) Li, Z.; Wu, Y. 2D Early Transition Metal Carbides (MXenes) for Catalysis. *Small* **2019**, *15* (29), 1804736.
(41) Zhang, J.; Kong, N.; Uzun, S.; Levitt, A.; Seyedin, S.; Lynch, P. A.; Qin, S.; Han, M.; Yang, W.; Liu, J.; Wang, X.; Gogotsi, Y.; Razal, J. M. Scalable Manufacturing of Free-Standing, Strong $Ti_3C_2T_x$ MXene Films with Outstanding Conductivity. *Adv. Mater.* **2020**, *32* (23), 2001093.
(42) Lipatov, A.; Goad, A.; Loes, M. J.; Vorobeva, N. S.; Abourahma, J.; Gogotsi, Y.; Sinitskii, A. High electrical conductivity and breakdown current density of individual monolayer Ti_3C_2T MXene flakes. *Matter* **2021**, *4* (4), 1413−1427.
(43) Uda, M.; Nakamura, A.; Yamamoto, T.; Fujimoto, Y. Work function of polycrystalline Ag, Au and Al. *J. Electron Spectrosc. Relat. Phenom.* **1998**, *88*−*91*, 643−648.
(44) Agresti, A.; Pazniak, A.; Pescetelli, S.; Di Vito, A.; Rossi, D.; Pecchia, A.; Auf der Maur, M.; Liedl, A.; Larciprete, R.; Kuznetsov, D. V.; Saranin, D.; Di Carlo, A. Titanium-carbide MXenes for work function and interface engineering in perovskite solar cells. *Nat. Mater.* **2019**, *18* (11), 1228−1234.
(45) Derry, G. N.; Ji-Zhong, Z. Work function of Pt(111). *Phys. Rev. B Condens Matter* **1989**, *39* (3), 1940−1941.
(46) Chertopalov, S.; Mochalin, V. N. Environment-Sensitive Photoresponse of Spontaneously Partially Oxidized Ti_3C_2 MXene Thin Films. *ACS Nano* **2018**, *12* (6), 6109−6116.
(47) Khazaei, M.; Ranjbar, A.; Arai, M.; Sasaki, T.; Yunoki, S. Electronic properties and applications of MXenes: a theoretical review. *Journal of Materials Chemistry C* **2017**, *5* (10), 2488−2503.
(48) Dutta, A.; Pan, Y.; Liu, J.-Q.; Kumar, A. Multicomponent isoreticular metal-organic frameworks: Principles, current status and challenges. *Coord. Chem. Rev.* **2021**, *445*, 214074.
(49) Yoo, D. K.; Bhadra, B. N.; Jhung, S. H. Adsorptive removal of hazardous organics from water and fuel with functionalized metal-organic frameworks: Contribution of functional groups. *J. Hazard. Mater.* **2021**, *403*, 123655.
(50) Zhou, X.; Dai, H.; Huang, X.; Ren, Y.; Wang, Q.; Wang, W.; Huang, W.; Dong, X. Porous trimetallic fluoride Ni−Co−M (M = Mn, Fe, Cu, Zn) nanoprisms as electrodes for asymmetric supercapacitors. *Materials Today Energy* **2020**, *17*, 100429.
(51) Kang, C.; Ma, L.; Chen, Y.; Fu, L.; Hu, Q.; Zhou, C.; Liu, Q. Metal-organic framework derived hollow rod-like NiCoMn ternary metal sulfide for high-performance asymmetric supercapacitors. *Chem. Eng. J.* **2022**, *427*, 131003.
(52) Hao, R.; Chen, J.; Wang, Z.; Huang, Y.; Liu, P.; Yan, J.; Liu, K.; Liu, C.; Lu, Z. Trimetallic Zeolitic imidazolite framework-derived Co nanoparticles@CoFe-nitrogen-doped porous carbon as bifunctional electrocatalysts for Zn-air battery. *J. Colloid Interface Sci.* **2021**, *586*, 621−629.
(53) Ikreedeegh, R. R.; Tahir, M. Indirect Z-scheme heterojunction of NH_2-MIL-125(Ti) MOF/g-C_3N_4 nanocomposite with RGO solid electron mediator for efficient photocatalytic CO_2 reduction to CO and CH_4. *J. Environ. Chem. Eng.* **2021**, *9* (4), 105600.
(54) Guo, Y.; Feng, C.; Qiao, S.; Wang, S.; Chen, T.; Zhang, L.; Zhao, Y.; Wang, J. Magnetic Fe_3O_4-encapsulated VAN@ MIL-101 (Fe) with mixed-valence sites and mesoporous structures as efficient bifunctional water splitting photocatalysts. *Nanoscale* **2020**, *12* (23), 12551−12560.
(55) Zeng, L.; Wang, Y.; Li, Z.; Song, Y.; Zhang, J.; Wang, J.; He, X.; Wang, C.; Lin, W. Highly Dispersed Ni Catalyst on Metal-Organic Framework-Derived Porous Hydrous Zirconia for CO_2 Methanation. *ACS Appl. Mater. Interfaces* **2020**, *12* (15), 17436−17442.
(56) Li, X.; Yang, X.; Xue, H.; Pang, H.; Xu, Q. Metal−organic frameworks as a platform for clean energy applications. *EnergyChem.* **2020**, *2* (2), 100027.
(57) Sreedhar, I.; Varun, Y.; Singh, S. A.; Venugopal, A.; Reddy, B. M. Developmental trends in CO2 methanation using various catalysts. *Catal. Sci. Technol.* **2019**, *9* (17), 4478−4504.
(58) Yan, S.; Ouyang, S.; Xu, H.; Zhao, M.; Zhang, X.; Ye, J. Co-ZIF-9/TiO2 nanostructure for superior CO2 photoreduction activity. *J. Mater. Chem. A* **2016**, *4* (39), 15126−15133.
(59) Dou, Y.; Zhou, J.; Zhou, A.; Li, J.-R.; Nie, Z. Visible-light responsive MOF encapsulation of noble-metal-sensitized semiconductors for high-performance photoelectrochemical water splitting. *J. Mater. Chem. A* **2017**, *5* (36), 19491−19498.
(60) Mahmoud, M. S.; Ahmed, E.; Farghali, A. A.; Zaki, A. H.; Abdelghani, E. A. M.; Barakat, N. A. M. Influence of Mn, Cu, and Cd−doping for titanium oxide nanotubes on the photocatalytic activity toward water splitting under visible light irradiation. *Colloids Surf., A* **2018**, *554*, 100−109.

https://doi.org/10.1021/acsomega.2c05030
ACS Omega 2022, 7, 38158−38192

(61) Deria, P.; Yu, J.; Balaraman, R. P.; Mashni, J.; White, S. N. Topology-dependent emissive properties of zirconium-based porphyrin MOFs. *Chem. Commun. (Camb)* **2016**, *52* (88), 13031−13034.
(62) Shi, L.; Wang, T.; Zhang, H.; Chang, K.; Ye, J. Electrostatic Self-Assembly of Nanosized Carbon Nitride Nanosheet onto a Zirconium Metal-Organic Framework for Enhanced Photocatalytic CO2 Reduction. *Adv. Funct. Mater.* **2015**, *25* (33), 5360−5367.
(63) Katz, M. J.; Brown, Z. J.; Colon, Y. J.; Siu, P. W.; Scheidt, K. A.; Snurr, R. Q.; Hupp, J. T.; Farha, O. K. A facile synthesis of UiO-66, UiO-67 and their derivatives. *Chem. Commun.* **2013**, *49* (82), 9449−9451.
(64) Ikreedeegh, R. R.; Tahir, M. A critical review in recent developments of metal-organic-frameworks (MOFs) with band engineering alteration for photocatalytic CO_2 reduction to solar fuels. *J. CO2 Util.* **2021**, *43*, 101381.
(65) Chen, X.; Peng, X.; Jiang, L.; Yuan, X.; Yu, H.; Wang, H.; Zhang, J.; Xia, Q. Recent advances in titanium metal−organic frameworks and their derived materials: Features, fabrication, and photocatalytic applications. *Chem. Eng. J.* **2020**, *395*, 125080.
(66) Kim, S.-N.; Kim, J.; Kim, H.-Y.; Cho, H.-Y.; Ahn, W.-S. Adsorption/catalytic properties of MIL-125 and NH_2-MIL-125. *Catal. Today* **2013**, *204*, 85−93.
(67) Bavykina, A.; Kolobov, N.; Khan, I. S.; Bau, J. A.; Ramirez, A.; Gascon, J. Metal-Organic Frameworks in Heterogeneous Catalysis: Recent Progress, New Trends, and Future Perspectives. *Chem. Rev.* **2020**, *120* (16), 8468−8535.
(68) Su, X.; Bromberg, L.; Martis, V.; Simeon, F.; Huq, A.; Hatton, T. A. Postsynthetic Functionalization of Mg-MOF-74 with Tetraethylenepentamine: Structural Characterization and Enhanced CO2 Adsorption. *ACS Appl. Mater. Interfaces* **2017**, *9* (12), 11299−11306.
(69) Baamran, K. S.; Tahir, M.; Mohamed, M.; Hussain Khoja, A. Effect of support size for stimulating hydrogen production in phenol steam reforming using Ni-embedded TiO_2 nanocatalyst. *J. Environ. Chem. Eng.* **2020**, *8* (1), 103604.
(70) Xie, Y.; Fang, Z.; Li, L.; Yang, H.; Liu, T. F. Creating Chemisorption Sites for Enhanced CO2 Photoreduction Activity through Alkylamine Modification of MIL-101-Cr. *ACS Appl. Mater. Interfaces* **2019**, *11* (30), 27017−27023.
(71) Nimbalkar, M. N.; Bhat, B. R. Simultaneous adsorption of methylene blue and heavy metals from water using Zr-MOF having free carboxylic group. *J. Environ. Chem. Eng.* **2021**, *9* (5), 106216.
(72) Nguyen, K. D.; Ehrling, S.; Senkovska, I.; Bon, V.; Kaskel, S. New 1D chiral Zr-MOFs based on in situ imine linker formation as catalysts for asymmetric C C coupling reactions. *J. Catal.* **2020**, *386*, 106−116.
(73) Zhang, M.; Feng, G.; Song, Z.; Zhou, Y. P.; Chao, H. Y.; Yuan, D.; Tan, T. T.; Guo, Z.; Hu, Z.; Tang, B. Z.; Liu, B.; Zhao, D. Two-dimensional metal-organic framework with wide channels and responsive turn-on fluorescence for the chemical sensing of volatile organic compounds. *J. Am. Chem. Soc.* **2014**, *136* (20), 7241−4.
(74) Assi, H.; Pardo Pérez, L. C.; Mouchaham, G.; Ragon, F.; Nasalevich, M.; Guillou, N.; Martineau, C.; Chevreau, H.; Kapteijn, F.; Gascon, J.; et al. Investigating the case of titanium (IV) carboxyphenolate photoactive coordination polymers. *Inorg. Chem.* **2016**, *55* (15), 7192−7199.
(75) Kashyap, A.; Singh, N. K.; Soni, M.; Soni, A. Deposition of thin films by chemical solution-assisted techniques. *Chemical Solution Synthesis for Materials Design and Thin Film Device Applications*; Elsevier, 2021; pp 79−117.
(76) Sun, D.; Ye, L.; Li, Z. Visible-light-assisted aerobic photocatalytic oxidation of amines to imines over NH_2-MIL-125(Ti). *Appl. Catal., B* **2015**, *164*, 428−432.
(77) Xu, W.; Xue, W.; Huang, H.; Wang, J.; Zhong, C.; Mei, D. Morphology controlled synthesis of α-Fe_2O_{3-x} with benzimidazole-modified Fe-MOFs for enhanced photo-Fenton-like catalysis. *Appl. Catal., B* **2021**, *291*, 120129.
(78) González, C. M. O.; Morales, E. M. C.; Tellez, A. d. M. N.; Quezada, T. E. S.; Kharissova, O. V.; Méndez-Rojas, M. A. CO_2 Capture by MOFs. *Handbook of Greener Synthesis of Nanomaterials and Compounds*; Elsevier, 2021; pp 407−448.
(79) Kumar, V.; Mohapatra, T.; Dharmadhikari, S.; Ghosh, P. A Review Paper on Heterogeneous Fenton Catalyst: Types of Preparation, Modification Techniques, Factors Affecting the Synthesis, Characterization, and Application in the Wastewater Treatment. *Bull. Chem. React. Eng. Catal.* **2020**, *15* (1), 1−34.
(80) Chen, X.; Li, Q.; Zhang, M.; Li, J.; Cai, S.; Chen, J.; Jia, H. MOF-Templated Preparation of Highly Dispersed Co/Al_2O_3 Composite as the Photothermal Catalyst with High Solar-to-Fuel Efficiency for CO_2 Methanation. *ACS Appl. Mater. Interfaces* **2020**, *12* (35), 39304−39317.
(81) Ghosh, M. K.; Pathak, S.; Ghorai, T. K. Synthesis of Two Mononuclear Schiff Base Metal (M = Fe, Cu) Complexes: MOF Structure, Dye Degradation, H_2O_2 Sensing, and DNA Binding Property. *ACS Omega* **2019**, *4* (14), 16068−16079.
(82) Murinzi, T. W.; Hosten, E.; Watkins, G. M. Synthesis and characterization of a cobalt-2,6-pyridinedicarboxylate MOF with potential application in electrochemical sensing. *Polyhedron* **2017**, *137*, 188−196.
(83) Hindelang, K.; Vagin, S. I.; Anger, C.; Rieger, B. Tandem post-synthetic modification for functionalized metal-organic frameworks via epoxidation and subsequent epoxide ring-opening. *Chem. Commun. (Camb)* **2012**, *48* (23), 2888−90.
(84) Vakili, R.; Xu, S.; Al-Janabi, N.; Gorgojo, P.; Holmes, S. M.; Fan, X. Microwave-assisted synthesis of zirconium-based metal organic frameworks (MOFs): Optimization and gas adsorption. *Microporous Mesoporous Mater.* **2018**, *260*, 45−53.
(85) Chen, X.; Zhu, H. Catalysis by supported gold nanoparticles. *Comprehensive nanoscience and technology* **2011**, 1−10.
(86) Mu, X.; Jiang, J.; Chao, F.; Lou, Y.; Chen, J. Ligand modification of UiO-66 with an unusual visible light photocatalytic behavior for RhB degradation. *Dalton Trans* **2018**, *47* (6), 1895−1902.
(87) Zhang, Y.; Zhou, J.; Chen, X.; Feng, Q.; Cai, W. MOF-derived C-doped ZnO composites for enhanced photocatalytic performance under visible light. *J. Alloys Compd.* **2019**, *777*, 109−118.
(88) Dong, H.; Zhang, X.; Lu, Y.; Yang, Y.; Zhang, Y.-P.; Tang, H.-L.; Zhang, F.-M.; Yang, Z.-D.; Sun, X.; Feng, Y. Regulation of metal ions in smart metal-cluster nodes of metal-organic frameworks with open metal sites for improved photocatalytic CO_2 reduction reaction. *Appl. Catal., B* **2020**, *276*, 119173.
(89) Zhao, X.; Wu, W.; Jing, G.; Zhou, Z. Activation of sulfite autoxidation with $CuFe_2O_4$ prepared by MOF-templated method for abatement of organic contaminants. *Environ. Pollut.* **2020**, *260*, 114038.
(90) Li, Y.; Xia, Y.; Liu, K.; Ye, K.; Wang, Q.; Zhang, S.; Huang, Y.; Liu, H. Constructing Fe-MOF-Derived Z-Scheme Photocatalysts with Enhanced Charge Transport: Nanointerface and Carbon Sheath Synergistic Effect. *ACS Appl. Mater. Interfaces* **2020**, *12* (22), 25494−25502.
(91) Xiong, C.; Zhang, T.; Kong, W.; Zhang, Z.; Qu, H.; Chen, W.; Wang, Y.; Luo, L.; Zheng, L. ZIF-67 derived porous Co_3O_4 hollow nanopolyhedron functionalized solution-gated graphene transistors for simultaneous detection of glucose and uric acid in tears. *Biosens. Bioelectron.* **2018**, *101*, 21−28.
(92) Chen, W.; Wang, C.; Su, S.; Wang, H.; Cai, D. Synthesis of ZIF-9(III)/Co LDH layered composite from ZIF-9(I) based on controllable phase transition for enhanced electrocatalytic oxygen evolution reaction. *Chem. Eng. J.* **2021**, *414*, 128784.
(93) Pan, Y.-T.; Wan, J.; Zhao, X.; Li, C.; Wang, D.-Y. Interfacial growth of MOF-derived layered double hydroxide nanosheets on graphene slab towards fabrication of multifunctional epoxy nanocomposites. *Chem. Eng. J.* **2017**, *330*, 1222−1231.
(94) Zhou, J.-J.; Li, K.; Wang, W.; Lei, Y.; Wu, J.; Zhou, C.; Zhang, P.; Liu, J.; Hua, Z.; Chen, L.; Han, L. Boosting Specific Capacity for Supercapattery by In Situ Formation of Amorphous Ni−Co−Borate on MOF-Derived Ni−Co−LDH Nanosheet Array. *ACS Appl. Energy Mater.* **2020**, *3* (12), 12046−12053.

https://doi.org/10.1021/acsomega.2c05030
ACS Omega 2022, 7, 38158−38192

(95) Gong, H.; Zhang, X.; Wang, G.; Liu, Y.; Li, Y.; Jin, Z. Dodecahedron ZIF-67 anchoring ZnCdS particles for photocatalytic hydrogen evolution. *Mol. Catal.* **2020**, *485*, 110832.
(96) Shao, W.; Chen, Y. R.; Xie, F.; Zhang, H.; Wang, H. T.; Chang, N. Facile construction of a ZIF-67/AgCl/Ag heterojunction via chemical etching and surface ion exchange strategy for enhanced visible light driven photocatalysis. *RSC Adv.* **2020**, *10* (63), 38174−38183.
(97) Qiu, B.; Yang, C.; Guo, W.; Xu, Y.; Liang, Z.; Ma, D.; Zou, R. Highly dispersed Co-based Fischer−Tropsch synthesis catalysts from metal−organic frameworks. *J. Mater. Chem. A* **2017**, *5* (17), 8081−8086.
(98) Abrori, S. A.; Septiani, N. L. W.; Hakim, F. N.; Maulana, A.; Suyatman, S.; Nugraha, S.; Anshori, I.; Yuliarto, B. Non-Enzymatic Electrochemical Detection for Uric Acid Based on a Glassy Carbon Electrode Modified With MOF-71. *IEEE Sensors Journal* **2020**, *21* (1), 170−177.
(99) Xiang, L.; Sheng, L.; Wang, C.; Zhang, L.; Pan, Y.; Li, Y. Amino-functionalized ZIF-7 nanocrystals: improved intrinsic separation ability and interfacial compatibility in mixed-matrix membranes for CO_2/CH_4 separation. *Adv. Mater.* **2017**, *29* (32), 1606999.
(100) Li, P.; Li, J. J.; Feng, X.; Li, J.; Hao, Y.; Zhang, J.; Wang, H.; Yin, A.; Zhou, J.; Ma, X.; Wang, B. Metal-organic frameworks with photocatalytic bactericidal activity for integrated air cleaning. *Nat. Commun.* **2019**, *10* (1), 2177.
(101) Wu, Y.; Li, X.; Zhao, H.; Yao, F.; Cao, J.; Chen, Z.; Wang, D.; Yang, Q. Core-shell structured Cu_2O@HKUST-1 heterojunction photocatalyst with robust stability for highly efficient tetracycline hydrochloride degradation under visible light. *Chem. Eng. J.* **2021**, *426*, 131255.
(102) Cao, Y.; Wang, G.; Liu, H.; Li, Y.; Jin, Z.; Ma, Q. Regular octahedron Cu-MOFs modifies $Mn_{0.05}Cd_{0.95}S$ nanoparticles to form a S-scheme heterojunction for photocatalytic hydrogen evolution. *Int. J. Hydrogen Energy* **2021**, *46* (10), 7230−7240.
(103) Shi, C.; Zhou, X.; Liu, D.; Li, L.; Xu, M.; Sakiyama, H.; Muddassir, M.; Wang, J. A new 3D high connection Cu-based MOF introducing a flexible tetracarboxylic acid linker: Photocatalytic dye degradation. *Polyhedron* **2021**, *208*, 115441.
(104) Li, G.; Li, F.; Liu, J.; Fan, C. Fe-based MOFs for photocatalytic N2 reduction: Key role of transition metal iron in nitrogen activation. *J. Solid State Chem.* **2020**, *285*, 121245.
(105) Dao, X.-Y.; Xie, X.-F.; Guo, J.-H.; Zhang, X.-Y.; Kang, Y.-S.; Sun, W.-Y. Boosting Photocatalytic CO_2 Reduction Efficiency by Heterostructures of NH_2-MIL-101(Fe)/g-C_3N_4. *ACS Appl. Energy Mater.* **2020**, *3* (4), 3946−3954.
(106) Nguyen, H. L.; Gandara, F.; Furukawa, H.; Doan, T. L.; Cordova, K. E.; Yaghi, O. M. A Titanium-Organic Framework as an Exemplar of Combining the Chemistry of Metal- and Covalent-Organic Frameworks. *J. Am. Chem. Soc.* **2016**, *138* (13), 4330−3.
(107) Jiang, W.; Li, Z.; Liu, C.; Wang, D.; Yan, G.; Liu, B.; Che, G. Enhanced visible-light-induced photocatalytic degradation of tetracycline using BiOI/MIL-125(Ti) composite photocatalyst. *J. Alloys Compd.* **2021**, *854*, 157166.
(108) Kaur, R.; Rana, A.; Singh, R. K.; Chhabra, V. A.; Kim, K.-H.; Deep, A. Efficient photocatalytic and photovoltaic applications with nanocomposites between CdTe QDs and an NTU-9 MOF. *RSC Adv.* **2017**, *7* (46), 29015−29024.
(109) Yu, Y.; Li, S.; Huang, L.; Yu, J.; Zhang, H.; Song, S.; Zeng, T. Solar-driven CO2 conversion promoted by MOF − on − MOF homophase junction. *Catal. Commun.* **2021**, *150*, 106270.
(110) Yuan, S.; Qin, J. S.; Xu, H. Q.; Su, J.; Rossi, D.; Chen, Y.; Zhang, L.; Lollar, C.; Wang, Q.; Jiang, H. L.; Son, D. H.; Xu, H.; Huang, Z.; Zou, X.; Zhou, H. C. $[Ti_8Zr_2O_{12}(COO)_{16}]$ Cluster: An Ideal Inorganic Building Unit for Photoactive Metal-Organic Frameworks. *ACS. Cent. Sci.* **2018**, *4* (1), 105−111.
(111) Xu, H.; Xiao, R.; Huang, J.; Jiang, Y.; Zhao, C.; Yang, X. In situ construction of protonated g-C_3N_4/Ti_3C_2 MXene Schottky heterojunctions for efficient photocatalytic hydrogen production. *Chin. J. Catal.* **2021**, *42* (1), 107−114.
(112) Zhang, L.; Yang, J.; Xie, T.; Feng, S.; Xu, L. Boosting visible-light-driven photocatalytic activity of $BiPO_4$ via constructing Schottky junction with Ti_3C_2 MXene. *Materials & Design* **2020**, *192*, 108772.
(113) Li, J.; Li, J.; Wu, C.; Li, Z.; Cai, L.; Tang, H.; Zhou, Z.; Wang, G.; Wang, J.; Zhao, L.; Wang, S. Crystalline carbon nitride anchored on MXene as an ordered Schottky heterojunction photocatalyst for enhanced visible-light hydrogen evolution. *Carbon* **2021**, *179*, 387−399.
(114) Fajrina, N.; Tahir, M. A critical review in strategies to improve photocatalytic water splitting towards hydrogen production. *Int. J. Hydrogen Energy* **2019**, *44* (2), 540−577.
(115) Ding, M.; Xiao, R.; Zhao, C.; Bukhvalov, D.; Chen, Z.; Xu, H.; Tang, H.; Xu, J.; Yang, X. Evidencing Interfacial Charge Transfer in 2D CdS/2D MXene Schottky Heterojunctions toward High-Efficiency Photocatalytic Hydrogen Production. *Solar RRL* **2021**, *5* (2), 2000414.
(116) Alhabeb, M.; Maleski, K.; Anasori, B.; Lelyukh, P.; Clark, L.; Sin, S.; Gogotsi, Y. Guidelines for Synthesis and Processing of Two-Dimensional Titanium Carbide ($Ti_3C_2T_x$ MXene). *Chem. Mater.* **2017**, *29* (18), 7633−7644.
(117) Tahir, M.; Sherryna, A.; Mansoor, R.; Khan, A. A.; Tasleem, S.; Tahir, B. Titanium Carbide MXene Nanostructures as Catalysts and Cocatalysts for Photocatalytic Fuel Production: A Review. *ACS Appl. Nano Mater.* **2022**, *5* (1), 18−54.
(118) Anasori, B.; Gogotsi, Y. *Metal Carbides and Nitrides (MXenes) Structure, Properties and Applications*; Springer Nature Switzerland AG: Cham, Switzerland, 2019.
(119) Naguib, M.; Mashtalir, O.; Carle, J.; Presser, V.; Lu, J.; Hultman, L.; Gogotsi, Y.; Barsoum, M. W. Two-Dimensional Transition Metal Carbides. *ACS Nano* **2012**, *6*, 1322−1331.
(120) Feng, A.; Yu, Y.; Wang, Y.; Jiang, F.; Yu, Y.; Mi, L.; Song, L. Two-dimensional MXene Ti_3C_2 produced by exfoliation of Ti_3AlC_2. *Materials & Design* **2017**, *114*, 161−166.
(121) Khan, A. A.; Tahir, M. Well-designed 2D/2D $Ti_3C_2T_{A/R}$ MXene coupled g-C_3N_4 heterojunction with in-situ growth of anatase/rutile TiO_2 nucleates to boost photocatalytic dry-reforming of methane (DRM) for syngas production under visible light. *Appl. Catal., B* **2021**, *285*, 119777.
(122) Ghidiu, M.; Lukatskaya, M. R.; Zhao, M. Q.; Gogotsi, Y.; Barsoum, M. W. Conductive two-dimensional titanium carbide 'clay' with high volumetric capacitance. *Nature* **2014**, *516* (7529), 78−81.
(123) Liu, F.; Zhou, A.; Chen, J.; Jia, J.; Zhou, W.; Wang, L.; Hu, Q. Preparation of Ti_3C_2 and Ti_2C MXenes by fluoride salts etching and methane adsorptive properties. *Appl. Surf. Sci.* **2017**, *416*, 781−789.
(124) Kvashina, T. S.; Uvarov, N. F.; Korchagin, M. A.; Krutskiy, Y. L.; Ukhina, A. V. Synthesis of MXene Ti_3C_2 by selective etching of MAX-phase Ti_3AlC_2. *Materials Today: Proceedings* **2020**, *31*, 592−594.
(125) Mashtalir, O.; Naguib, M.; Dyatkin, B.; Gogotsi, Y.; Barsoum, M. W. Kinetics of aluminum extraction from Ti_3AlC_2 in hydrofluoric acid. *Mater. Chem. Phys.* **2013**, *139* (1), 147−152.
(126) Yang, S.; Zhang, P.; Wang, F.; Ricciardulli, A. G.; Lohe, M. R.; Blom, P. W. M.; Feng, X. Fluoride-Free Synthesis of Two-Dimensional Titanium Carbide (MXene) Using A Binary Aqueous System. *Angew. Chem., Int. Ed.* **2018**, *57* (47), 15491−15495.
(127) Lukatskaya, M. R.; Halim, J.; Dyatkin, B.; Naguib, M.; Buranova, Y. S.; Barsoum, M. W.; Gogotsi, Y. Room-temperature carbide-derived carbon synthesis by electrochemical etching of MAX phases. *Angew. Chem., Int. Ed.* **2014**, *53* (19), 4877−80.
(128) Sun, W.; Shah, S. A.; Chen, Y.; Tan, Z.; Gao, H.; Habib, T.; Radovic, M.; Green, M. J. Electrochemical etching of Ti_2AlC to Ti_2CTx (MXene) in low-concentration hydrochloric acid solution. *J. Mater. Chem. A* **2017**, *5* (41), 21663−21668.
(129) Li, T.; Yao, L.; Liu, Q.; Gu, J.; Luo, R.; Li, J.; Yan, X.; Wang, W.; Liu, P.; Chen, B.; Zhang, W.; Abbas, W.; Naz, R.; Zhang, D. Fluorine-Free Synthesis of High-Purity $Ti_3C_2T_x$ (T = OH, O) via Alkali Treatment. *Angew. Chem. Int. Ed.* **2018**, *57* (21), 6115−6119.
(130) Carey, M.; Hinton, Z.; Natu, V.; Pai, R.; Sokol, M.; Alvarez, N. J.; Kalra, V.; Barsoum, M. W. Dispersion and Stabilization of

https://doi.org/10.1021/acsomega.2c05030
ACS Omega 2022, 7, 38158−38192

Alkylated 2D MXene in Nonpolar Solvents and Their Pseudocapacitive Behavior. *Cell Reports Physical Science* **2020**, *1* (4), 100042.
(131) Halim, J.; Lukatskaya, M. R.; Cook, K. M.; Lu, J.; Smith, C. R.; Naslund, L. A.; May, S. J.; Hultman, L.; Gogotsi, Y.; Eklund, P.; Barsoum, M. W. Transparent Conductive Two-Dimensional Titanium Carbide Epitaxial Thin Films. *Chem. Mater.* **2014**, *26* (7), 2374−2381.
(132) Zhao, X.; Radovic, M.; Green, M. J. Synthesizing MXene Nanosheets by Water-free Etching. *Chem.* **2020**, *6* (3), 544−546.
(133) Lee, Y.; Kim, S. J.; Kim, Y.-J.; Lim, Y.; Chae, Y.; Lee, B.-J.; Kim, Y.-T.; Han, H.; Gogotsi, Y.; Ahn, C. W. Oxidation-resistant titanium carbide MXene films. *J. Mater. Chem. A* **2020**, *8* (2), 573−581.
(134) Li, M.; Lu, J.; Luo, K.; Li, Y.; Chang, K.; Chen, K.; Zhou, J.; Rosen, J.; Hultman, L.; Eklund, P.; Persson, P. O. A.; Du, S.; Chai, Z.; Huang, Z.; Huang, Q. Element Replacement Approach by Reaction with Lewis Acidic Molten Salts to Synthesize Nanolaminated MAX Phases and MXenes. *J. Am. Chem. Soc.* **2019**, *141* (11), 4730−4737.
(135) Anasori, B.; Lukatskaya, M. R.; Gogotsi, Y. 2D metal carbides and nitrides (MXenes) for energy storage. *Nat. Rev. Mater.* **2017**, *2*, 16098.
(136) Li, Y.; Shao, H.; Lin, Z.; Lu, J.; Liu, L.; Duployer, B.; Persson, P. O. A.; Eklund, P.; Hultman, L.; Li, M.; Chen, K.; Zha, X. H.; Du, S.; Rozier, P.; Chai, Z.; Raymundo-Pinero, E.; Taberna, P. L.; Simon, P.; Huang, Q. A general Lewis acidic etching route for preparing MXenes with enhanced electrochemical performance in non-aqueous electrolyte. *Nat. Mater.* **2020**, *19* (8), 894−899.
(137) Natu, V.; Pai, R.; Sokol, M.; Carey, M.; Kalra, V.; Barsoum, M. W. 2D $Ti_3C_2T_z$ MXene Synthesized by Water-free Etching of Ti_3AlC_2 in Polar Organic Solvents. *Chem.* **2020**, *6* (3), 616−630.
(138) Su, T.; Hood, Z. D.; Naguib, M.; Bai, L.; Luo, S.; Rouleau, C. M.; Ivanov, I. N.; Ji, H.; Qin, Z.; Wu, Z. Monolayer $Ti_3C_2T_x$ as an Effective Co-catalyst for Enhanced Photocatalytic Hydrogen Production over TiO_2. *ACS Appl. Energy Mater.* **2019**, *2* (7), 4640−4651.
(139) Tahir, M. Investigating the Influential Effect of Etchant Time in Constructing 2D/2D HCN/MXene Heterojunction with Controlled Growth of TiO_2 NPs for Stimulating Photocatalytic H_2 Production. *Energy Fuels* **2021**, *35* (8), 6807−6822.
(140) My Tran, N.; Thanh Hoai Ta, Q.; Noh, J.-S. Unusual synthesis of safflower-shaped TiO_2/Ti_3C_2 heterostructures initiated from two-dimensional Ti_3C_2 MXene. *Appl. Surf. Sci.* **2021**, *538*, 148023.
(141) Song, T.; Hou, L.; Long, B.; Ali, A.; Deng, G. J. Ultrathin MXene "bridge" to accelerate charge transfer in ultrathin metal-free 0D/2D black phosphorus/g-C_3N_4 heterojunction toward photocatalytic hydrogen production. *J. Colloid Interface Sci.* **2021**, *584*, 474−483.
(142) Qin, J.; Liu, B.; Lam, K.-H.; Song, S.; Li, X.; Hu, X. 0D/2D MXene Quantum Dot/Ni-MOF Ultrathin Nanosheets for Enhanced N_2 Photoreduction. *ACS Sustainable Chem. Eng.* **2020**, *8* (48), 17791−17799.
(143) Qin, X.; Cao, R.; Gong, W.; Luo, L.; Shi, G.; Ji, L.; Zhu, A. Hydrothermal growth of ZnCdS/TiO_2 nanoparticles on the surface of the Ti_3C_2 MXene sheet to enhance photocatalytic performance under visible light. *J. Solid State Chem.* **2022**, *306*, 122750.
(144) Zuo, G.; Wang, Y.; Teo, W. L.; Xie, A.; Guo, Y.; Dai, Y.; Zhou, W.; Jana, D.; Xian, Q.; Dong, W.; Zhao, Y. Enhanced photocatalytic water oxidation by hierarchical 2D-Bi_2MoO_6@2D-MXene Schottky junction nanohybrid. *Chem. Eng. J.* **2021**, *403*, 126328.
(145) Kim, Y.-J.; Kim, S. J.; Seo, D.; Chae, Y.; Anayee, M.; Lee, Y.; Gogotsi, Y.; Ahn, C. W.; Jung, H.-T. Etching Mechanism of Monoatomic Aluminum Layers during MXene Synthesis. *Chem. Mater.* **2021**, *33* (16), 6346−6355.
(146) Zhang, T.; Pan, L.; Tang, H.; Du, F.; Guo, Y.; Qiu, T.; Yang, J. Synthesis of two-dimensional $Ti_3C_2T_x$ MXene using HCl+LiF etchant: Enhanced exfoliation and delamination. *J. Alloys Compd.* **2017**, *695*, 818−826.
(147) Zhang, Q.; He, J.; Fu, X.; Xie, S.; Fan, R.; Lai, H.; Cheng, W.; Ji, P.; Sheng, J.; Liao, Q.; Zhu, W.; Li, H. Fluorine-free strategy for hydroxylated Ti_3C_2/Ti_3AlC_2 catalysts with enhanced aerobic oxidative desulfurization and mechanism. *Chem. Eng. J.* **2022**, *430*, 132950.
(148) Khan, U.; Luo, Y.; Kong, L. B.; Que, W. Synthesis of fluorine free MXene through lewis acidic etching for application as electrode of proton supercapacitors. *J. Alloys Compd.* **2022**, *926*, 166903.
(149) Xiao, R.; Zhao, C.; Zou, Z.; Chen, Z.; Tian, L.; Xu, H.; Tang, H.; Liu, Q.; Lin, Z.; Yang, X. In situ fabrication of 1D CdS nanorod/2D Ti_3C_2 MXene nanosheet Schottky heterojunction toward enhanced photocatalytic hydrogen evolution. *Appl. Catal., B* **2020**, *268*, 118382.
(150) Su, T.; Hood, Z. D.; Naguib, M.; Bai, L.; Luo, S.; Rouleau, C. M.; Ivanov, I. N.; Ji, H.; Qin, Z.; Wu, Z. 2D/2D heterojunction of Ti_3C_2/g-C_3N_4 nanosheets for enhanced photocatalytic hydrogen evolution. *Nanoscale* **2019**, *11* (17), 8138−8149.
(151) Zhuang, Y.; Liu, Y.; Meng, X. Fabrication of TiO_2 nanofibers/MXene Ti_3C_2 nanocomposites for photocatalytic H_2 evolution by electrostatic self-assembly. *Appl. Surf. Sci.* **2019**, *496*, 143647.
(152) Wang, W.-T.; Batool, N.; Zhang, T.-H.; Liu, J.; Han, X.-F.; Tian, J.-H.; Yang, R. When MOFs meet MXenes: superior ORR performance in both alkaline and acidic solutions. *J. Mater. Chem. A* **2021**, *9* (7), 3952−3960.
(153) Munir, S.; Rasheed, A.; Rasheed, T.; Ayman, I.; Ajmal, S.; Rehman, A.; Shakir, I.; Agboola, P. O.; Warsi, M. F. Exploring the Influence of Critical Parameters for the Effective Synthesis of High-Quality 2D MXene. *ACS Omega* **2020**, *5* (41), 26845−26854.
(154) Xie, Y.; Rahman, M. M.; Kareem, S.; Dong, H.; Qiao, F.; Xiong, W.; Liu, X.; Li, N.; Zhao, X. Facile synthesis of CuS/MXene nanocomposites for efficient photocatalytic hydrogen generation. *CrystEngComm* **2020**, *22* (11), 2060−2066.
(155) Yang, Y.; Zhang, D.; Fan, J.; Liao, Y.; Xiang, Q. Construction of an Ultrathin S-Scheme Heterojunction Based on Few-Layer g-C_3N_4 and Monolayer $Ti_3C_2T_x$ MXene for Photocatalytic CO_2 Reduction. *Solar RRL* **2021**, *5* (2), 2000351.
(156) Zeng, Z.; Yan, Y.; Chen, J.; Zan, P.; Tian, Q.; Chen, P. Boosting the Photocatalytic Ability of Cu_2O Nanowires for CO_2 Conversion by MXene Quantum Dots. *Adv. Funct. Mater.* **2019**, *29* (2), 1806500.
(157) Du, X.; Zhao, T.; Xiu, Z.; Xing, Z.; Li, Z.; Pan, K.; Yang, S.; Zhou, W. $BiVO_4$@$ZnIn_2S_4$/Ti_3C_2 MXene quantum dots assembly all-solid-state direct Z-Scheme photocatalysts for efficient visible-light-driven overall water splitting. *Applied Materials Today* **2020**, *20*, 100719.
(158) Liu, L.; Ying, G.; Wen, D.; Li, Y.; Zhang, K.; Min, H.; Hu, C.; Sun, C.; Wang, C. High-performance copper-matrix materials reinforced by nail board-like structure 2D Ti_3C_2T MXene with in-situ TiO_2 particles. *Materials Science and Engineering: A* **2022**, *832*, 142392.
(159) Zhao, S.; Pan, D.; Liang, Q.; Zhou, M.; Yao, C.; Xu, S.; Li, Z. Ultrathin NiAl-Layered Double Hydroxides Grown on 2D $Ti_3C_2T_x$ MXene to Construct Core−Shell Heterostructures for Enhanced Photocatalytic CO_2 Reduction. *J. Phys. Chem. C* **2021**, *125* (19), 10207−10218.
(160) Zhao, M.; Huang, Y.; Peng, Y.; Huang, Z.; Ma, Q.; Zhang, H. Two-dimensional metal-organic framework nanosheets: synthesis and applications. *Chem. Soc. Rev.* **2018**, *47* (16), 6267−6295.
(161) Zhuang, L.; Ge, L.; Liu, H.; Jiang, Z.; Jia, Y.; Li, Z.; Yang, D.; Hocking, R. K.; Li, M.; Zhang, L.; et al. and Scalable General Strategy for Synthesizing Ultrathin Two-Dimensional Metal-Organic Framework Nanosheets for the Oxygen Evolution Reaction. *Angew. Chem., Int. Ed. Engl.* **2019**, *58* (38), 13565−13572.
(162) Yuan, M.; Wang, R.; Sun, Z.; Lin, L.; Yang, H.; Li, H.; Nan, C.; Sun, G.; Ma, S. Morphology-Controlled Synthesis of Ni-MOFs with Highly Enhanced Electrocatalytic Performance for Urea Oxidation. *Inorg. Chem.* **2019**, *58* (17), 11449−11457.
(163) Sarawade, P.; Tan, H.; Polshettiwar, V. Shape- and Morphology-Controlled Sustainable Synthesis of Cu, Co, and In Metal Organic Frameworks with High CO_2 Capture Capacity. *ACS Sustainable Chem. Eng.* **2013**, *1* (1), 66−74.

https://doi.org/10.1021/acsomega.2c05030
ACS Omega 2022, 7, 38158−38192

(164) Wan, H.; Wang, Y.; Chen, J.; Meng, H. M.; Li, Z. 2D Co-MOF nanosheet-based nanozyme with ultrahigh peroxidase catalytic activity for detection of biomolecules in human serum samples. *Mikrochim. Acta* **2021**, *188* (4), 130.
(165) Niu, Y.; Yuan, Y.; Zhang, Q.; Chang, F.; Yang, L.; Chen, Z.; Bai, Z. Morphology-controlled synthesis of metal-organic frameworks derived lattice plane-altered iron oxide for efficient trifunctional electrocatalysts. *Nano Energy* **2021**, *82*, 105699.
(166) Mateo, D.; Morlanes, N.; Maity, P.; Shterk, G.; Mohammed, O. F.; Gascon, J. Efficient Visible-Light Driven Photothermal Conversion of CO2 to Methane by Nickel Nanoparticles Supported on Barium Titanate. *Adv. Funct. Mater.* **2021**, *31*, 2008244.
(167) Song, C.; Liu, X.; Xu, M.; Masi, D.; Wang, Y.; Deng, Y.; Zhang, M.; Qin, X.; Feng, K.; Yan, J.; Leng, J.; Wang, Z.; Xu, Y.; Yan, B.; Jin, S.; Xu, D.; Yin, Z.; Xiao, D.; Ma, D. Photothermal Conversion of CO2 with Tunable Selectivity Using Fe-Based Catalysts: From Oxide to Carbide. *ACS Catal.* **2020**, *10* (18), 10364−10374.
(168) Chen, G.; Gao, R.; Zhao, Y.; Li, Z.; Waterhouse, G. I. N.; Shi, R.; Zhao, J.; Zhang, M.; Shang, L.; Sheng, G.; Zhang, X.; Wen, X.; Wu, L. Z.; Tung, C. H.; Zhang, T. Alumina-Supported CoFe Alloy Catalysts Derived from Layered-Double-Hydroxide Nanosheets for Efficient Photothermal CO_2 Hydrogenation to Hydrocarbons. *Adv. Mater.* **2018**, *30* (3), 1704663.
(169) Dhakshinamoorthy, A.; Li, Z.; Garcia, H. Catalysis and photocatalysis by metal organic frameworks. *Chem. Soc. Rev.* **2018**, *47* (22), 8134−8172.
(170) Wang, L.; Jin, P.; Duan, S.; She, H.; Huang, J.; Wang, Q. In-situ incorporation of Copper(II) porphyrin functionalized zirconium MOF and TiO2 for efficient photocatalytic CO2 reduction. *Sci. Bull.* **2019**, *64* (13), 926−933.
(171) Zhang, H.; Wei, J.; Dong, J.; Liu, G.; Shi, L.; An, P.; Zhao, G.; Kong, J.; Wang, X.; Meng, X.; Zhang, J.; Ye, J. Efficient Visible-Light-Driven Carbon Dioxide Reduction by a Single-Atom Implanted Metal-Organic Framework. *Angew. Chem., Int. Ed. Engl.* **2016**, *55* (46), 14310−14314.
(172) Zhao, Z.-W.; Zhou, X.; Liu, Y.-N.; Shen, C.-C.; Yuan, C.-Z.; Jiang, Y.-F.; Zhao, S.-J.; Ma, L.-B.; Cheang, T.-Y.; Xu, A.-W. Ultrasmall Ni nanoparticles embedded in Zr-based MOFs provide high selectivity for CO2 hydrogenation to methane at low temperatures. *Catal. Sci. Technol.* **2018**, *8* (12), 3160−3165.
(173) Li, S.; Ji, K.; Zhang, M.; He, C.; Wang, J.; Li, Z. Boosting the photocatalytic CO_2 reduction of metal-organic frameworks by encapsulating carbon dots. *Nanoscale* **2020**, *12* (17), 9533−9540.
(174) Shi, H.; Zhang, P.; Liu, Z.; Park, S.; Lohe, M. R.; Wu, Y.; Shaygan Nia, A.; Yang, S.; Feng, X. Ambient-Stable Two-Dimensional Titanium Carbide (MXene) Enabled by Iodine Etching. *Angew. Chem., Int. Ed.* **2021**, *60* (16), 8689−8693.
(175) Wan, Y.-J.; Rajavel, K.; Li, X.-M.; Wang, X.-Y.; Liao, S.-Y.; Lin, Z.-Q.; Zhu, P.-L.; Sun, R.; Wong, C.-P. Electromagnetic interference shielding of Ti_3C_2T MXene modified by ionic liquid for high chemical stability and excellent mechanical strength. *Chem. Eng. J.* **2021**, *408*, 127303.
(176) Cao, F.; Zhang, Y.; Wang, H.; Khan, K.; Tareen, A. K.; Qian, W.; Zhang, H.; Agren, H. Recent Advances in Oxidation Stable Chemistry of 2D MXenes. *Adv. Mater.* **2022**, *34* (13), 2107554.
(177) Seredych, M.; Shuck, C. E.; Pinto, D.; Alhabeb, M.; Precetti, E.; Deysher, G.; Anasori, B.; Kurra, N.; Gogotsi, Y. High-Temperature Behavior and Surface Chemistry of Carbide MXenes Studied by Thermal Analysis. *Chem. Mater.* **2019**, *31* (9), 3324−3332.
(178) Zhong, C.; Shang, Z.; Zhao, C.; Luo, H. a.; Cao, Y.; Yan, D.; You, K. Co-Catalyst $Ti_3C_2T_X$ MXene-Modified ZnO Nanorods Photoanode for Enhanced Photoelectrochemical Water Splitting. *Top. Catal.* **2022**, DOI: 10.1007/s11244-022-01619-0.
(179) Almusattar, W.; Tahir, M.; Madi, M.; Tahir, B. Fabricating Ti_3C_2 MXene cocatalyst supported NiAl-LDH/g-C3N4 ternary nanocomposite for stimulating solar photocatalytic H_2 production. *J. Environ. Chem. Eng.* **2022**, *10* (4), 108010.
(180) Ma, Y.; Xu, D.; Chen, W.; Tang, Y.; Wang, X.; Li, L.; Wang, J. Oxygen-vacancy-embedded 2D/2D NiFe-LDH/MXene Schottky heterojunction for boosted photodegradation of norfloxacin. *Appl. Surf. Sci.* **2022**, *572*, 151432.
(181) Zhong, Q.; Li, Y.; Zhang, G. Two-dimensional MXene-based and MXene-derived photocatalysts: Recent developments and perspectives. *Chem. Eng. J.* **2021**, *409*, 128099.
(182) Bao, Y.; Liu, Y.; Pan, J.; Chen, P.; Liu, X.; Li, Y.; Tang, X.; Zhang, W.; Liu, B.; Liu, J. Constructing 2D layered PCN/Ti_3C_2/Bi_2MoO_6 heterojunction with MXene as charge mediator for enhanced photocatalytic performance. *Appl. Surf. Sci.* **2022**, *589*, 152883.
(183) Liu, Q.; Tan, X.; Wang, S.; Ma, F.; Znad, H.; Shen, Z.; Liu, L.; Liu, S. MXene as a non-metal charge mediator in 2D layered CdS@Ti_3C_2@TiO_2 composites with superior Z-scheme visible light-driven photocatalytic activity. *Environmental Science: Nano* **2019**, *6* (10), 3158−3169.
(184) Zhou, Y.; Yu, M.; Zhan, R.; Wang, X.; Peng, G.; Niu, J. Ti_3C_2 MXene-induced interface electron separation in g-C_3N_4/Ti_3C_2 MXene/$MoSe_2$ Z-scheme heterojunction for enhancing visible light-irradiated enoxacin degradation. *Sep. Purif. Technol.* **2021**, *275*, 119194.
(185) Yang, J.-X.; Yu, W.-B.; Li, C.-F.; Dong, W.-D.; Jiang, L.-Q.; Zhou, N.; Zhuang, Z.-P.; Liu, J.; Hu, Z.-Y.; Zhao, H.; Li, Y.; Chen, L.; Hu, J.; Su, B.-L. PtO nanodots promoting Ti_3C_2 MXene in-situ converted Ti_3C_2/TiO_2 composites for photocatalytic hydrogen production. *Chem. Eng. J.* **2021**, *420*, 129695.
(186) Khan, A. A.; Tahir, M.; Bafaqeer, A. Constructing a Stable 2D Layered Ti_3C_2 MXene Cocatalyst-Assisted TiO_2/g-C_3N_4/Ti_3C_2 Heterojunction for Tailoring Photocatalytic Bireforming of Methane under Visible Light. *Energy Fuels* **2020**, *34* (8), 9810−9828.
(187) Huang, K.; Li, C.; Meng, X. In-situ construction of ternary Ti_3C_2 MXene@TiO_2/$ZnIn_2S_4$ composites for highly efficient photocatalytic hydrogen evolution. *J. Colloid Interface Sci.* **2020**, *580*, 669−680.
(188) Fang, J.; Xie, K.; Kang, Q.; Gou, Y. Facile fabrication of g-C_3N_4/CdS heterojunctions with enhanced visible-light photocatalytic degradation performances. *Journal of Science: Advanced Materials and Devices* **2022**, *7* (1), 100409.
(189) Dong, W.-W.; Jia, J.; Wang, Y.; An, J.-R.; Yang, O.-Y.; Gao, X.-J.; Liu, Y.-L.; Zhao, J.; Li, D.-S. Visible-light-driven solvent-free photocatalytic CO_2 reduction to CO by Co-MOF/Cu_2O heterojunction with superior selectivity. *Chem. Eng. J.* **2022**, *438*, 135622.
(190) Wang, L.; Jin, P.; Huang, J.; She, H.; Wang, Q. Integration of Copper(II)-Porphyrin Zirconium Metal−Organic Framework and Titanium Dioxide to Construct Z-Scheme System for Highly Improved Photocatalytic CO_2 Reduction. *ACS Sustainable Chem. Eng.* **2019**, *7* (18), 15660−15670.
(191) Xiao, L.; Zhang, Q.; Chen, P.; Chen, L.; Ding, F.; Tang, J.; Li, Y.-J.; Au, C.-T.; Yin, S.-F. Copper-mediated metal-organic framework as efficient photocatalyst for the partial oxidation of aromatic alcohols under visible-light irradiation: Synergism of plasmonic effect and schottky junction. *Appl. Catal., B* **2019**, *248*, 380−387.
(192) Wu, Y.; Li, X.; Yang, Q.; Wang, D.; Yao, F.; Cao, J.; Chen, Z.; Huang, X.; Yang, Y.; Li, X. Mxene-modulated dual-heterojunction generation on a metal-organic framework (MOF) via surface constitution reconstruction for enhanced photocatalytic activity. *Chem. Eng. J.* **2020**, *390*, 124519.
(193) Tahir, M.; Sherryna, A.; Khan, A. A.; Madi, M.; Zerga, A. Y.; Tahir, B. Defect Engineering in Graphitic Carbon Nitride Nanotextures for Energy Efficient Solar Fuels Production: A Review. *Energy Fuels* **2022**, *36* (16), 8948−8977.
(194) Syzgantseva, M. A.; Ireland, C. P.; Ebrahim, F. M.; Smit, B.; Syzgantseva, O. A. Metal Substitution as the Method of Modifying Electronic Structure of Metal-Organic Frameworks. *J. Am. Chem. Soc.* **2019**, *141* (15), 6271−6278.
(195) MS, R.; Shanmuga Priya, S.; Freudenberg, N. C.; Sudhakar, K; Tahir, M. Metal-organic framework-based photocatalysts for carbon dioxide reduction to methanol: A review on progress and application. *J. CO2 Util.* **2021**, *43*, 101374.

(196) Gomez Alvarez, E.; Wortham, H.; Strekowski, R.; Zetzsch, C.; Gligorovski, S. Atmospheric photosensitized heterogeneous and multiphase reactions: from outdoors to indoors. *Environ. Sci. Tehcnol.* **2012**, *46* (4), 1955−1963.
(197) Mu, Q.; Su, Y.; Wei, Z.; Sun, H.; Lian, Y.; Dong, Y.; Qi, P.; Deng, Z.; Peng, Y. Dissecting the interfaces of MOF-coated CdS on synergized charge transfer for enhanced photocatalytic CO_2 reduction. *J. Catal.* **2021**, *397*, 128−136.
(198) Karmakar, S.; Barman, S.; Rahimi, F. A.; Maji, T. K. Covalent grafting of molecular photosensitizer and catalyst on MOF-808: effect of pore confinement toward visible light-driven CO_2 reduction in water. *Energy Environ. Sci.* **2021**, *14* (4), 2429−2440.
(199) Tahir, M.; Tahir, B. 2D/2D/2D O-C_3N_4/Bt/$Ti_3C_2T_x$ heterojunction with novel MXene/clay multi-electron mediator for stimulating photo-induced CO_2 reforming to CO and CH_4. *Chem. Eng. J.* **2020**, *400*, 125868.
(200) Liu, Y.; He, Y.; Vargun, E.; Plachy, T.; Saha, P.; Cheng, Q. 3D Porous Ti_3C_2 MXene/NiCo-MOF Composites for Enhanced Lithium Storage. *Nanomaterials (Basel)* **2020**, *10* (4), 695.
(201) Zheng, S.; Zhou, H.; Xue, H.; Braunstein, P.; Pang, H. Pillared-layer Ni-MOF nanosheets anchored on Ti_3C_2 MXene for enhanced electrochemical energy storage. *J. Colloid Interface Sci.* **2022**, *614*, 130−137.
(202) Long, R.; Yu, Z.; Tan, Q.; Feng, X.; Zhu, X.; Li, X.; Wang, P. Ti_3C_2 MXene/NH_2-MIL-88B(Fe): Research on the adsorption kinetics and photocatalytic performance of an efficient integrated photocatalytic adsorbent. *Appl. Surf. Sci.* **2021**, *570*, 151244.
(203) Luo, X.; Abazari, R.; Tahir, M.; Fan, W. K.; Kumar, A.; Kalhorizadeh, T.; Kirillov, A. M.; Amani-Ghadim, A. R.; Chen, J.; Zhou, Y. Trimetallic metal−organic frameworks and derived materials for environmental remediation and electrochemical energy storage and conversion. *Coord. Chem. Rev.* **2022**, *461*, 214505.
(204) Huang, R.; Liao, D.; Chen, S.; Yu, J.; Jiang, X. A strategy for effective electrochemical detection of hydroquinone and catechol: Decoration of alkalization-intercalated Ti_3C_2 with MOF-derived N-doped porous carbon. *Sens. Actuators, B* **2020**, *320*, 128386.
(205) Jiang, G.; Zheng, N.; Chen, X.; Ding, G.; Li, Y.; Sun, F.; Li, Y. In-situ decoration of MOF-derived carbon on nitrogen-doped ultrathin MXene nanosheets to multifunctionalize separators for stable Li-S batteries. *Chem. Eng. J.* **2019**, *373*, 1309−1318.
(206) Chen, W.; Han, B.; Xie, Y.; Liang, S.; Deng, H.; Lin, Z. Ultrathin Co-Co LDHs nanosheets assembled vertically on MXene: 3D nanoarrays for boosted visible-light-driven CO_2 reduction. *Chem. Eng. J.* **2020**, *391*, 123519.
(207) Hu, L.; Xiao, R.; Wang, X.; Wang, X.; Wang, C.; Wen, J.; Gu, W.; Zhu, C. MXene-induced electronic optimization of metal-organic framework-derived CoFe LDH nanosheet arrays for efficient oxygen evolution. *Appl. Catal., B* **2021**, *298*, 120599.
(208) Li, S.; Wu, F.; Lin, R.; Wang, J.; Li, C.; Li, Z.; Jiang, J.; Xiong, Y. Enabling photocatalytic hydrogen production over Fe-based MOFs by refining band structure with dye sensitization. *Chem. Eng. J.* **2022**, *429*, 132217.
(209) Li, N.; Liu, J.; Liu, J. J.; Dong, L. Z.; Xin, Z. F.; Teng, Y. L.; Lan, Y. Q. Adenine Components in Biomimetic Metal-Organic Frameworks for Efficient CO_2 Photoconversion. *Angew. Chem., Int. Ed. Engl.* **2019**, *58* (16), 5226−5231.
(210) Liao, W. M.; Zhang, J. H.; Wang, Z.; Lu, Y. L.; Yin, S. Y.; Wang, H. P.; Fan, Y. N.; Pan, M.; Su, C. Y. Semiconductive Amine-Functionalized Co(II)-MOF for Visible-Light-Driven Hydrogen Evolution and CO_2 Reduction. *Inorg. Chem.* **2018**, *57* (18), 11436−11442.
(211) Saeed, A.; Chen, W.; Shah, A. H.; Zhang, Y.; Mehmood, I.; Liu, Y. Enhancement of photocatalytic CO_2 reduction for novel $Cd_{0.2}Zn_{0.8}S$@Ti_3C_2 (MXenes) nanocomposites. *J. CO2 Util.* **2021**, *47*, 101501.
(212) Najam, T.; Shah, S. S. A.; Peng, L.; Javed, M. S.; Imran, M.; Zhao, M.-Q.; Tsiakaras, P. Synthesis and nano-engineering of MXenes for energy conversion and storage applications: Recent advances and perspectives. *Coord. Chem. Rev.* **2022**, *454*, 214339.
(213) Yu, L.; Liu, B.; Wang, Y.; Yu, F.; Ma, J. Recent progress on MXene-Derived material and its' application in energy and environment. *J. Power Sources* **2021**, *490*, 229250.
(214) Sharma, K.; Hasija, V.; Patial, S.; Singh, P.; Nguyen, V.-H.; Nadda, A. K.; Thakur, S.; Nguyen-Tri, P.; Nguyen, C. C.; Kim, S. Y. Recent progress on MXenes and MOFs hybrids: Structure, synthetic strategies and catalytic water splitting. *Int. J. Hydrogen Energy* **2022**, DOI: 10.1016/j.ijhydene.2022.01.004.
(215) Tian, P.; He, X.; Zhao, L.; Li, W.; Fang, W.; Chen, H.; Zhang, F.; Huang, Z.; Wang, H. Ti_3C_2 nanosheets modified Zr-MOFs with Schottky junction for boosting photocatalytic HER performance. *Sol. Energy* **2019**, *188*, 750−759.
(216) Tian, P.; He, X.; Zhao, L.; Li, W.; Fang, W.; Chen, H.; Zhang, F.; Huang, Z.; Wang, H. Enhanced charge transfer for efficient photocatalytic H_2 evolution over UiO-66-NH_2 with annealed $Ti_3C_2T_x$ MXenes. *Int. J. Hydrogen Energy* **2019**, *44* (2), 788−800.
(217) Li, Y.; Liu, Y.; Wang, Z.; Wang, P.; Zheng, Z.; Cheng, H.; Dai, Y.; Huang, B. In-situ growth of Ti_3C_2@MIL-NH_2 composite for highly enhanced photocatalytic H_2 evolution. *Chem. Eng. J.* **2021**, *411*, 128446.
(218) Zhao, J.-H.; Liu, L.-W.; Li, K.; Li, T.; Liu, F.-T. Conductive Ti_3C_2 and MOF-derived CoS_x boosting the photocatalytic hydrogen production activity of TiO_2. *CrystEngComm* **2019**, *21* (14), 2416−2421.
(219) Shi, L.; Wu, C.; Wang, Y.; Dou, Y.; Yuan, D.; Li, H.; Huang, H.; Zhang, Y.; Gates, I. D.; Sun, X.; Ma, T. Rational Design of Coordination Bond Connected Metal Organic Frameworks/MXene Hybrids for Efficient Solar Water Splitting. *Adv. Funct. Mater.* **2022**, *32* (30), 2202571.
(220) Sherryna, A.; Tahir, M. Role of Surface Morphology and Terminating Groups in Titanium Carbide MXenes ($Ti_3C_2T_x$) Cocatalysts with Engineering Aspects for Modulating Solar Hydrogen Production: A Critical Review. *Chem. Eng. J.* **2022**, *433*, 134573.
(221) Tahir, M. Binary Ni_2P/Ti_3C_2 Multilayer Cocatalyst Anchored TiO_2 Nanocomposite with Etchant/Oxidation Grown TiO_2 NPs for Enhancing Photocatalytic H_2 Production. *Energy Fuels* **2021**, *35* (17), 14197−14211.
(222) Afroz, K.; Moniruddin, M.; Bakranov, N.; Kudaibergenov, S.; Nuraje, N. A heterojunction strategy to improve the visible light sensitive water splitting performance of photocatalytic materials. *J. Mater. Chem. A* **2018**, *6* (44), 21696−21718.
(223) Schultz, T.; Frey, N. C.; Hantanasirisakul, K.; Park, S.; May, S. J.; Shenoy, V. B.; Gogotsi, Y.; Koch, N. Surface Termination Dependent Work Function and Electronic Properties of $Ti_3C_2T_x$ MXene. *Chem. Mater.* **2019**, *31* (17), 6590−6597.
(224) Tahir, M.; Sherryna, A.; Zakaria, Z. Y. Facile Synthesis of MAX Modified Graphitic Carbon Nitride Nanocomposite for Stimulating Hydrogen Production Through Photocatalytic Water Splitting. *Chem. Eng. Trans.* **2021**, *89*, 571−576.
(225) Tasleem, S.; Tahir, M.; Zakaria, Z. Y. Fabricating structured 2D Ti_3AlC_2 MAX dispersed TiO_2 heterostructure with Ni_2P as a cocatalyst for efficient photocatalytic H_2 production. *J. Alloys Compd.* **2020**, *842*, 155752.
(226) Sherryna, A.; Tahir, M. Recent developments in layered double hydroxide structures with their role in promoting photocatalytic hydrogen production: A comprehensive review. *Int. J. Energy Res.* **2022**, *46*, 2093−2140.